

**framatome**

---

**Incorporation of Chromia-Doped  
Fuel Properties in AREVA  
Approved Methods**

ANP-10340NP-A  
Revision 0

Topical Report

May 2018

Framatome Inc.

---

(c) 2018 Framatome Inc.

**Copyright © 2018**

**Framatome Inc.  
All Rights Reserved**





UNITED STATES  
NUCLEAR REGULATORY COMMISSION  
WASHINGTON, D.C. 20555-0001

May 23, 2018

Mr. Gary Peters, Director  
Licensing and Regulatory Affairs  
Framatome Inc.  
3315 Old Forest Road  
Lynchburg, VA 24501

SUBJECT: FINAL SAFETY EVALUATION FOR FRAMATOME INC. TOPICAL REPORT  
ANP-10340P, REVISION 0, "INCORPORATION OF CHROMIA-DOPED FUEL  
PROPERTIES IN AREVA APPROVED METHODS" (CAC NO. MF7707;  
EPID L-2016-TOP-0004)

Dear Mr. Peters:

By letter dated April 29 2016 (Agencywide Documents Access and Management System (ADAMS) Accession No. ML16124B091), Framatome, Inc. (Framatome, formerly AREVA, Inc.) submitted Topical Report (TR) ANP-10340P, Revision 0, "Incorporation of Chromia-Doped Fuel Properties in AREVA Approved Methods," to the U.S. Nuclear Regulatory Commission (NRC) staff for review and approval. By letter dated April 26, 2018 (ADAMS Accession No. ML18100B020), an NRC draft safety evaluation (SE) regarding our approval of TR ANP-10340P, Revision 0, was provided for your review and comment. By letter dated May 1, 2018 (ADAMS Accession No. ML18123A355), Framatome provided comments on the draft SE. The NRC staff's disposition of the Framatome comments on the draft SE are discussed in the attachment (ADAMS Accession No. ML18129A025) to the final SE enclosed with this letter.

The NRC staff has found that TR ANP-10340P, Revision 0, is acceptable for referencing in licensing applications for nuclear power plants to the extent specified and under the limitations and conditions delineated in the TR and in the enclosed final SE. The final SE defines the basis for our acceptance of the TR.

Our acceptance applies only to material provided in the subject TR. We do not intend to repeat our review of the acceptable material described in the TR. When the TR appears as a reference in licensing action requests, our review will ensure that the material presented applies to the specific plant involved. Requests for licensing actions that deviate from this TR will be subject to a plant-specific review in accordance with applicable review standards.

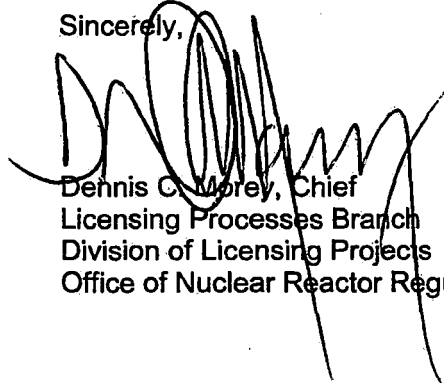
In accordance with the guidance provided on the NRC website, we request that Framatome publish approved proprietary and non-proprietary versions of TR ANP-10340P, Revision 0, within 3 months of receipt of this letter. The approved versions shall incorporate this letter and the enclosed final SE after the title page. Also, they must contain historical review information, including NRC requests for additional information and your responses. The approved versions shall include an "-A" (designating approved) following the TR identification symbol.

As an alternative to including the RAIs and RAI responses behind the title page, if changes to the TR were provided to the NRC staff to support the resolution of RAI responses, and if the NRC staff reviewed and approved those changes as described in the RAI responses, there are two ways that the accepted version can capture the RAIs:

1. The RAIs and RAI responses can be included as an Appendix to the accepted version.
2. The RAIs and RAI responses can be captured in the form of a table (inserted after the final SE) which summarizes the changes as shown in the approved version of the TR. The table should reference the specific RAIs and RAI responses which resulted in any changes, as shown in the accepted version of the TR.

If future changes to the NRC's regulatory requirements affect the acceptability of this TR, Framatome will be expected to revise the TR appropriately or justify its continued applicability for subsequent referencing. Licensees referencing this TR would be expected to justify its continued applicability or evaluate their plant using the revised TR.

Sincerely,



Dennis C. Morey, Chief  
Licensing Processes Branch  
Division of Licensing Projects  
Office of Nuclear Reactor Regulation

Project No. 728  
Docket No. 99902041

Enclosure:  
Final Safety Evaluation

FINAL SAFETY EVALUATION BY THE OFFICE OF NUCLEAR REACTOR REGULATION

TOPICAL REPORT ANP-10340P, REVISION 0,

"INCORPORATION OF CHROMIA-DOPED FUEL PROPERTIES IN

AREVA APPROVED METHODS"

PROJECT NO. 99902041

1.0 INTRODUCTION AND BACKGROUND

By letter dated April 29, 2016 (Agencywide Documents Access and Management System (ADAMS) Accession No. ML16124B091), Framatome Inc. (Framatome, formerly AREVA Inc.) submitted for U.S. Nuclear Regulatory Commission (NRC) staff review and approval Topical Report (TR) ANP-10340P, Revision 0, "Incorporation of Chromia-Doped Fuel Properties in AREVA Approved Methods" (Reference 1). Framatome desires to introduce chromia-doped fuel pellets to Framatome boiling water reactor (BWR) fuel products to increase fuel reliability and operational flexibility. The scope of this TR focuses on relevant fuel material properties and in-core behavioral characteristics that are affected by the addition of chromia to the uranium dioxide (UO<sub>2</sub>) fuel. Material properties of the doped fuel such as melting, density, thermal expansion, thermal conductivity, grain size and grain strength, stored thermal energy, creep yield strength, elastic modulus, strain hardening coefficient and tangent modulus, plastic Poisson's ratio, and swelling are treated using the RODEX4 thermal-mechanical code (Reference 2). Additionally, certain models are also included in the AURORA-B methodology to predict the dynamic response of BWR fuel during transient, postulated accident, and beyond design-basis accident (DBA) scenarios.

The TR describes the proposed introduction of chromia-doped fuel pellets into normal core reloads. A nominal value of [ ] weight parts per million (wppm) ([ ] weight percent (wt %)) of chromia (Cr<sub>2</sub>O<sub>3</sub>) is to be introduced in a UO<sub>2</sub> pellet. This safety evaluation (SE) refers only to the dopant concentration range detailed in Section 3.1.1 of this SE.

During this review, a regulatory audit was conducted (References 2 and 3). After conclusion of the audit, a round of request for additional information (RAI) questions were issued (Reference 4) and responses were received (Reference 5).

This SE is largely ordered parallel to the submitted TR. Section 2.0 covers the regulatory evaluation, Section 3.0 covers the technical evaluation, and makes up the bulk of the document. Section 4.0 contains the limitations and conditions. Section 5.0 contains the conclusions. References are found in Section 6.0. The technical evaluation includes material properties in Section 3.1, behavioral assessment in Section 3.2, the operating experience and qualification dataset in Section 3.3, qualification of RODEX4 in Section 3.4, qualification of AURORA-B in Section 3.5, license criteria in Section 3.6, and finally power maneuvering guidelines in Section 3.7.

**Enclosure**

## 2.0 REGULATORY EVALUATION

The NRC staff used the guidance in Standard Review Plan (SRP), NUREG-0800, Section 4.2, "Fuel System Design," for the review of ANP-10340P, Revision 0. SRP Section 4.2 acceptance criteria are based on meeting the requirements of General Design Criteria (GDC) 10 of Appendix A of Title 10 of the *Code of Federal Regulations* (10 CFR) Part 50, "Reactor Design."

GDC 10 states:

The reactor core and associated coolant, control, and protection systems shall be designed with the appropriate margin to assure that specified acceptable fuel design limits are not exceeded during any condition of normal operation, including the effects of anticipated operational occurrences.

In accordance with SRP Section 4.2, the objectives of the fuel system safety review are to provide assurance that:

- a. The fuel system is not damaged as a result of normal operation and anticipated operational occurrences (AOOs),
- b. Fuel system damage is never so severe as to prevent control rod insertion when it is required,
- c. The number of fuel rod failures is not underestimated for postulated accidents, and
- d. Coolability is always maintained.

The NRC staff reviewed ANP-10340P, Revision 0 to: (1) ensure that the material properties and in-core behavioral characteristics of chromia-doped fuel, as analyzed using the RODEX4 and AURORA-B codes, are capable of accurately (or conservatively) ensuring the fuel system safety criteria, (2) identify any limitations on the behavioral characteristics of the additive fuel, and (3) ensure compliance of fuel design criteria with licensing requirements of fuel designs.

## 3.0 TECHNICAL EVALUATION

### 3.1 Chromia-doped Fuel Material Properties

The chromia-doped fuel material properties are addressed in this section. These properties are used in RODEX4 and AURORA-B and describe behavior during normal operation, AOOs, and accidents.

#### 3.1.1 Microstructure

While not a material property itself, microstructure can have an effect on other properties of the fuel. The primary effect of chromia doping on microstructure is the enhancement of the fuel grain size. This enhances the viscoplasticity of the fuel and has an effect on the fission gas release (FGR) from the fuel. The chromia concentration ([       ] wppm) has been selected such that the chromia is [       ]. This leads to an

average grain size of [ ] This is [ ]  
] than standard  $\text{UO}_2$ .

The NRC staff asked RAI-1a, which asked for clarification on manufacturing specification limits on chromia content as well as Framatome's quality assurance procedure to ensure the fuel produced is within those limits. Framatome responded that chromium content will be maintained within a range of [ ] microgram chromium per gram of uranium ( $\mu\text{gCr/gU}$ ) for each pellet lot. The nominal value corresponds with [ ] wppm of  $\text{Cr}_2\text{O}_3$  as defined in the TR. Framatome will use Inductively Coupled Plasma-Mass Spectrometry to analyze chromia content, and sample several individual pellets in each lot.

The NRC staff finds the response to RAI-1a acceptable. The manufacturing tolerances will be included in the conditions and limitations in Section 4.0 of this SE.

### 3.1.2 Theoretical Density

In the original TR submittal (Reference 1), Framatome stated that chromium mostly occupies interstitial positions in the  $\text{UO}_2$  ceramic matrix, and provided equations for determining the theoretical density of the doped fuel. Details of this section were discussed at the regulatory audit, and RAI-2 was asked to address remaining questions. RAI-2a requested clarification on the description of the location of the added chromium ions within the uranium sub-lattice. Framatome clarified that the chromium (Cr) is primarily a [ ], and has amended the description in the TR accordingly. (Amended pages are included with the RAI responses in Reference 5). The NRC finds this explanation acceptable.

RAI-2b requested clarification on the method for calculating theoretical density of chromia-doped fuel, given the changing explanation of lattice location expected in response to RAI-2a. Framatome responded that the method of calculation is appropriate independent of the location of the dopant in the uranium sub-lattice. As this method has been previously approved for use with gadolinia dopants in RODEX4, the NRC finds this explanation, and the method for calculating theoretical density, to be acceptable.

RAI-2c noted a typographical error in equation 4-4. Framatome has corrected the error.

RAI-3 requested clarification on the statement that the stoichiometry of doped and standard  $\text{UO}_2$  is similar, and requested information on any impact on the fuel properties due to any difference in stoichiometry. Framatome responded that doped and standard  $\text{UO}_2$  have the same manufacturing specifications for stoichiometry. Framatome states that, as there are no significant differences in oxygen to uranium ratio between standard and doped fuel, there are also no differences in fuel properties as a result of stoichiometry. The NRC staff finds this response to be acceptable.

### 3.1.3 Thermal Expansion

Thermal expansion of the fuel pellet is important primarily to the determination of the pellet-clad gap, which has a large effect on heat transfer. As  $\text{UO}_2$  thermal expansion has been shown to experience only minor changes with much higher levels of impurities, Framatome states that the small percentage of chromia added will have a negligible effect on the thermal expansion of the fuel. Therefore, Framatome will be using the thermal expansion coefficient for standard  $\text{UO}_2$ .

The NRC staff finds Framatome's treatment of thermal expansion to be acceptable.

RAI-6 was asked to clarify a point in this section of the TR, which stated that the chromia level was in the range of impurity content in the fuel pellet. Framatome clarified that the statement was in reference to the total impurity limit, rather than a statement that chromia could be treated as an impurity. The NRC staff finds the explanation acceptable.

#### 3.1.4 Specific Heat and Enthalpy

Specific heat is a property used in the calculation of fuel stored energy during transients. It is also used in the calculation of thermal conductivity.

Framatome states that the specific heat of un-irradiated  $\text{UO}_2$  and chromia-doped fuel was measured using differential scanning calorimetry, with an estimated uncertainty of 7 percent. The results of this measurement show that the doped fuel experiences a small increase in specific heat. Framatome has stated that this difference is negligible and the doped fuel will be analyzed using the same specific heat formulation as un-doped  $\text{UO}_2$ . This result has been extrapolated to higher temperatures [ ] as well.

The NRC finds this treatment of specific heat to be acceptable based on the experimental evidence provided and the theoretical explanation for extrapolating this data.

#### 3.1.5 Thermal Conductivity

Fuel thermal conductivity is essential to the modeling of both steady state and transient phenomena, as it directly impacts fuel temperature and stored energy. Generally speaking, higher thermal conductivity results in lower fuel temperatures and less stored energy in the fuel.

Framatome states that laser flash diffusivity measurements were performed on chromia-doped  $\text{UO}_2$  and gadolinia fuels as well as standard  $\text{UO}_2$ . These tests subject a thin disc specimen to a high-intensity, short duration radiant energy pulse. This energy is absorbed by one side of the specimen, and the subsequent temperature rise over time is measured on the opposite side. From these results thermal diffusivity can be calculated. Thermal conductivity is then simply the product of thermal diffusivity and volumetric heat capacity.

Framatome conducted two in-house thermal diffusivity measurement campaigns, one each in 2006 and 2015. In both cases Framatome also sent a sub-set of samples to the Joint Research Center-Institute for Transuranium Elements (JRC-ITU) for confirmation and complementary measurements. [ ]

]

The thermal conductivity correlation developed for chromia-doped fuel is discussed in Section 3.4.1 in the context of qualification of RODEX4.

### 3.1.6 Grain Size and Growth

Increased grain size drives many of the property and behavior differences between standard and chromia-doped fuel. As grain size is an input into many properties calculated in RODEX4, NRC staff asked RAI-1b: "Please define the manufacturing specification limits on grain size, and describe AREVA's quality assurance procedures to ensure that the fuel produced remains within these limits."

Framatome responded by stating that the specification for chromia-doped pellets indicates a [ ]. This is consistent with the grain size data that has been previously collected. Framatome will sample pellets to calculate the 95 percent LCL value and update the RODEX4 input distribution annually, as described in the RODEX4 TR. As the NRC has previously approved this approach, this is found to be acceptable for use with chromia-doped fuel.

Framatome states that grain growth is not expected due to the already-large grain size present in doped  $\text{UO}_2$ . [

]. Given the evidence provided that [ ], the NRC finds this acceptable.

### 3.1.7 Elastic Moduli

Elastic Moduli can impact cladding strain analyses for AOO events; however, Framatome states that the elastic properties of the fuel are not of fundamental importance to predicting fuel behavior under normal operation or abnormal conditions (such as AOOs or accident conditions).

Framatome refers to literature to indicate that additives cause only a minor change to these properties, with a significant addition (10-20 wt%) of gadolinium or plutonium resulting in a small change to Young's Modulus, and no change in Poisson's ratio. Given the much smaller percentage of chromia, Framatome states that they will continue to use the models for standard  $\text{UO}_2$  for these properties. The NRC staff has reviewed this justification and finds it acceptable.

### 3.1.8 Tensile Fracture Strength

Tensile fracture strength is important to understanding the fuel pellet cracking behavior under thermal stress. This is effected by fuel porosity, pore size, and grain size. Un-irradiated fuels testing were performed by Framatome [

] These differences are accounted for by the increased grain size of the doped fuel. As these results are consistent with expected behavior, and contribute to pellet cladding interaction (PCI) performance benefits, the NRC staff finds Framatome's treatment of tensile fracture strength acceptable.

### 3.1.9 Creep and Plastic Deformation

Creep and plastic deformation are important material properties for understanding fuel behavior under compressive stress. This stress occurs later in life, when the fuel pellet and cladding are

in contact due to a combination of clad creep-down and fuel pellet swelling. Increased creep rate and plastic deformation of the fuel allow the pellet to adjust to these stresses without damaging the clad, leading to reduced occurrence of pellet-clad mechanical interaction (PCMI) fuel damage.

Framatome states that uniaxial mechanical compression tests were performed to assess creep and plastic deformation of chromia-doped fuel. [

] Given the experimental data presented, the NRC staff finds the treatment of creep and plastic deformation to be acceptable.

### 3.1.10 Fuel Pellet Cracking

Accurate understanding of fuel pellet cracking behavior is important to the prediction of fuel pellet deformation and PCMI. Fuel pellets crack radially due to thermal stresses. Framatome states that at the beginning of life the power must exceed [ ] to initiate radial cracking.

While chromia-doped fuel has a different tensile strength, as described in Section 3.1.8 of this SE, the cracking mechanism for doped and standard  $\text{UO}_2$  fuel during steady-state operation appears fundamentally the same. The chromia-doped fuel does, however, behave differently under power ramp conditions.

[

]

The NRC staff finds the treatment of fuel pellet cracking under steady state power ramp conditions to be acceptable.

### 3.1.11 In-reactor Densification

When first irradiated,  $\text{UO}_2$  fuel undergoes a densification process due to a combination of increased temperature and the fission process. This densification is important to the calculation of the fuel pellet diameter, and therefore the fuel-to-cladding gap. This densification is a result of a reduction in micron-scale pores. In-reactor densification is commonly simulated using out-of-pile resinter tests, which also lead to a reduction of these small pores.

Framatome states that the chromia-doped fuel was tested using a 24-hour out-of-reactor thermal stability test at 1700 degrees Celsius ( $^{\circ}\text{C}$ ). Framatome states that the fuel is [

]



The NRC staff finds Framatome's treatment of in-reactor densification to be acceptable.

### 3.1.12 Effect of Additive on the High Burnup Fuel Pellet Rim Structure

Irradiation of fuel to high burnup results in changes to the structure of  $\text{UO}_2$  pellets. These changes begin when the local burnup exceeds approximately 60 gigawatt-days per metric ton of uranium (GWd/MTU) and occur in the lower temperature region or near the periphery of the pellet and result in a structure known as the high burnup structure (HBS) or rim structure. Formation of the HBS is attributed to recrystallization which starts at grain boundaries and propagates into the affected grains and to the formation of small pores on and within grains.

RAI-14 asked for additional explanation and data regarding the formation of the HBS. Framatome clarified that the post-irradiation examination (PIE) data used in the analysis provided in the TR was on chromia-doped fuel with a chromia concentration outside of the proposed specification range. Framatome was able to share additional data from a PIE performed on doped fuel that is more representative of the product Framatome intends to produce.

Data collected on standard  $\text{UO}_2$  HBS has a very large spread when plotted against burnup. While large grain size should hinder the formation of the HBS, and this has been observed in some PIEs. Framatome states that the chromia-doped fuel examined is within this spread and, therefore, no changes to the HBS models are needed.

The NRC staff finds this explanation acceptable, as HBS data presented appear to be within the uncertainty of non-doped  $\text{UO}_2$ . It is also noted that this treatment is likely conservative, but the quantity of data is insufficient to draw further conclusions.

## 3.2 Behavioral Assessment

The use of chromia-doped fuel could potentially impact the following in-reactor fuel behaviors: fuel washout as a result of fuel clad failure, lower fuel melting limits, and performance during loss-of-coolant accidents (LOCAs) and reactivity initiated accidents (RIAs).

### 3.2.1 Washout Characteristics

Washout behavior occurs after failure of the fuel cladding. Water is introduced into the fuel rod interior and interacts with the fuel pellet. In BWR conditions, water is mildly corrosive to  $\text{UO}_2$ . Corrosivity depends on multiple factors but primarily is dependent on the grain structure of the fuel.

Framatome used thermogravimetry to achieve a greater understanding of the underlying phenomena by measuring the mass change of unirradiated standard and chromia-doped fuel pellets with varied grain size in an oxidizing environment at 380 °C. This test indicated that the larger grain-size chromia-doped pellets experienced up to a 50 percent increase in oxidation resistance, while the small grain size chromia performed comparably to undoped  $\text{UO}_2$ .

A second study was performed investigating corrosion behavior of unirradiated fuel in autoclave leaching tests under BWR conditions. These showed that the chromia-doped fuel [

] in comparison with undoped fuel.

Framatome states that this trend will remain valid in irradiated fuel.

The NRC staff finds that Framatome has provided sufficient evidence that chromia-doped fuel washout characteristics are bounded by undoped UO<sub>2</sub>, and therefore, finds Framatome's explanation to be acceptable.

### 3.2.2 Fuel Melting

Framatome has measured the melting point of standard  $\text{UO}_2$ , chromia-doped  $\text{UO}_2$ , and chromia-doped  $(\text{U-Gd})\text{O}_2$  fuel using laser heating and fast multi-channel pyrometry at JRC-ITU. Framatome reported that the melting temperature for chromia-doped fuel is [ ] over the entire burnup range. Gadolia-doped fuel melting temperature [ ]

The NRC staff asked RAI-4a to better understand if and how this [ ] melting temperature was incorporated into RODEX4 and downstream safety analyses. Framatome responded that the melting point [ ] can be applied either within RODEX4 or as part of the post-processing of results. Framatome clarified that, while either approach is appropriate, RODEX4 has been updated to include the [ ] melting temperature for chromia-doped fuel. The NRC staff finds this explanation to be satisfactory. Framatome also clarified in this response that RODEX4's melting temperature model is not burnup dependent, but instead uses the expected minimum fuel melting temperature. By [ ], they are capturing the results from the JRC-ITU experiment. The NRC staff finds this acceptable.

RAI-4b asked for clarification on the statistical approach used by Framatome to calculate the [ ] for melting temperature from the JRC-ITU experiments. Framatome responded with a detailed description of their treatment of uncertainty for these experiments. Uncertainty is a result of data dispersion, uncertainty in the emissivity of the fuel sample, and pyrometer calibration. These have been geometrically combined and adjusted for sample size to determine one-sided 95/95 values. The NRC staff agrees with this approach and finds it to be acceptable as it accounts for uncertainties appropriately.

### 3.2.3 Doped Neutron-Absorber Fuel Rods

Framatome is also requesting approval of chromia-doped neutron-absorber fuel (NAF). NAF is  $\text{UO}_2$  with gadolinia dopant added, and is alternatively referred to as gadolinia-doped fuel. Framatome included data collected for chromia-doped NAF thermal conductivity and melting temperature, which the NRC staff reviewed and found acceptable.

RAI-11 asked Framtome to disposition the remaining properties for chromia-doped NAF; a summary of the response follows:

- Microstructure and grain size are relatively unchanged between normal NAF and chromia-doped NAF, as the effect of the much larger quantity of gadolinia dopant exceeds that of the chromia.
- In-reactor densification is assessed during fabrication, and behaves the same as normal NAF

- Creep behavior was assessed for chromia-doped gadolinia fuel. This test found the samples to fall on a logarithmic curve. The creep rate for the chromia-doped NAF falls between the creep rates for standard  $\text{UO}_2$  and chromia-doped  $\text{UO}_2$ .
- Washout behavior of chromia-doped NAF was studied in autoclave experiments under BWR conditions. Doped NAF fuel performs [ ] at 290 °C, and shows [ ] at 360 °C.
- NAF is more resistant to PCI than  $\text{UO}_2$ . This is not expected to change with chromia doping.
- The remaining properties included in the RIA (tensile fracture strength, fuel pellet cracking, HBS formation, performance under LOCA, and performance under RIA) are expected to be equivalent to un-doped NAF fuel.

Due to the evidence and theoretical arguments provided, the NRC staff finds the use of undoped NAF properties to be acceptable for analysis of chromia-doped NAF.

### 3.2.4 Behavior During Accident Conditions

#### 3.2.4.1 Loss-of-Coolant Accidents

The performance of the emergency core cooling system is judged relative to the performance of the reactor fuel under postulated LOCA conditions. 10 CFR 50.46 and Appendix K provide analytical requirements and prescriptive limits (e.g., 2200 degrees Fahrenheit (°F) peak cladding temperature (PCT), 17 percent ECR maximum cladding oxidation (MLO)) applicable to  $\text{UO}_2$  fuel pellets within cylindrical zircaloy or ZIRLO cladding. These analytical limits preserve a coolable rod bundle array by ensuring adequate post-quench cladding ductility. The introduction of chromia-doped fuel pellets does not directly alter the applicability of the 10 CFR 50.46 analytical requirements and prescriptive limits associated with maintaining adequate cladding ductility; however, changes in fuel properties and performance may alter the accident progression and influence PCT and MLO calculation. In addition to 10 CFR 50.46, fuel performance may impact the LOCA radiological consequence assessment (often bounded by the maximum hypothetical accident). The following fuel properties and performance metrics were evaluated with respect to chromia-doped fuel:

- Fuel thermal conductivity and stored energy
- Fission gas release, rod internal pressure, and rod ballooning
- Fuel-to-cladding bond layer and oxygen ingress
- Fuel pellet fragmentation, relocation, and dispersal
- Fission gas release and accident source term

A change in fuel thermal conductivity will impact the amount of stored energy in the fuel pellet. Section 4.5 of ANP-10340P describes the impact of chromia addition on fuel thermal conductivity and Section 7.1 describes changes in the RODEX4 thermal conductivity model. See Section 3.4.1 of this SE for further assessment of fuel thermal conductivity. In general, the addition of chromia reduces fuel thermal conductivity which tends to increase fuel stored energy. This potential impact is being explicitly addressed in the RODEX4 calculated stored energy and initial fuel conditions (input) to the downstream LOCA calculations.

A change in FGR will impact rod internal pressure which, in turn, will impact the probability of fuel rod ballooning and rupture. Section 7.2 of ANP-10340P describes the validation of the RODEX4 FGR model for chromia-doped fuel. See Section 3.4.2 of this SE for further assessment of FGR. In general, the addition of chromia increases the grain size which increases the diffusion path; however, the lower thermal conductivity tends to increase the rate of diffusion. An increase in FGR would lead to higher rod internal pressures and increase the likelihood of fuel rod ballooning and rupture. These potential impacts are being explicitly addressed in the RODEX4 initial fuel conditions (input) to the downstream LOCA calculations.

The 10 CFR 50.46c rulemaking identified a new cladding degradation mechanism involving oxygen ingress from the fuel-to-cladding bonding layer, which reduces the time-at-temperature to nil ductility. A change in fuel irradiation swelling or pellet microstructure, which impacts the formation of the fuel-to-cladding bond layer, may change the timing (BU) at which point 2-sided oxidation must be considered. As 10 CFR 50.46c has not been finalized, this potential effect will not be considered in this SE.

A change in pellet microstructure or fission gas retention may impact the susceptibility to fuel fragmentation or the resulting fragmentation size distribution. Section 5.3.1 of ANP-10340P describes impact of chromia addition to fuel fragmentation under LOCA conditions. Citing a technical paper presented at TopFuel 2013, Framatome states that the susceptibility to fine fragmentation is highly correlated to the formation of the high burnup structure (HBS). Framatome concludes that (1) pellet cracking pattern, (2) fuel-to-cladding interface bonding, and (3) HBS formation and evolution are comparable to that of  $\text{UO}_2$ .

RAI-12 requested supporting evidence for the statement in the TR that cracking and pellet-clad interface behavior in chromia-doped pellets is very similar to that in standard  $\text{UO}_2$ . Framatome provided data from the post-irradiation annealing test for standard and chromia-doped pellets, conducted by the Nuclear Fuel Industry Research (NFIR) Program from various fuel types irradiated in IFA-649 at the Halden Reactor Project (Halden). The data provided supports the conclusion that chromia-doped and standard  $\text{UO}_2$  behavior is similar. Therefore, the NRC staff finds the treatment of pellet cracking and pellet-clad interface to be acceptable.

Any interaction between chromia dopant and fission products may alter the amount or chemical species of releases during Design Basis Accidents or Severe Accidents. While Framatome did not include a discussion in the TR, the source term released from the fuel during postulated accidents was questioned in RAI-13. Framatome responded that the dopant does not modify the isotope inventories. Given this and the negligible impact on neutron flux-spectrum, Framatome plans to use NUREG-1465 to determine the alternate source term (AST) for chromia-doped fuel as it does undoped  $\text{UO}_2$ . The NRC staff finds Framatome's treatment of AST acceptable.

#### 3.2.4.2 Reactivity Initiated Accidents

The regulation at 10 CFR Part 50, Appendix A, GDC 28 requires reactivity control systems to be designed with appropriate limits on potential amount and rate of reactivity increase to assure that the effects of postulated reactivity accidents can neither (1) result in damage to the reactor coolant pressure boundary greater than local yielding nor (2) sufficiently disturb the core, its support structures, or other reactor pressure vessel internals to impair significantly the capability to cool the core. For BWRs, the postulated control rod drop accident (CRDA) is the limiting RIA.

The following fuel properties and performance metrics were evaluated with respect to chromia-doped fuel:

- Control blade worth and reactor kinetics
- Fuel transient thermal expansion and gaseous swelling
- Fuel melting temperature
- Fission gas release, rod internal pressure, and rod ballooning
- Fuel pellet fragmentation, relocation, and dispersal
- Transient fission gas release and accident source term

Section 9.3 of ANP-10340P describes the impact of chromia addition to nuclear design requirements and reactor kinetics. There is no impact on reactor physics calculations because chromium and oxygen cross sections are included in the nuclear data library of the CASMO-4 lattice code. Additions of chromia to the fuel will require no changes to existing neutronics codes or methodologies. Hence, any impact of chromia addition on core physics predictions will be explicitly accounted for.

Section 7.3 of ANP-10340P describes the new RODEX4 intragranular gaseous swelling model. PIE data on chromia-doped fuel rods show larger cladding deformation following both steady-state and power ramp irradiations, which indicates an increased fuel pellet deformation in comparison to standard fuel. Measured cladding strain was used to validate the new RODEX4 model. Section 5.3.2 of ANP-10340P describes the potential impact of chromia addition on fuel performance under RIA conditions. Framatome states that [

].

RAI-7b and RAI-7c requested additional evidence on fuel swelling and fragmentation, respectively. The RAIs also suggested the Nuclear Safety Research Reactor (NSRR) as a possible source for RIA performance data on fuel pellets different than standard  $\text{UO}_2$ . As no data from NSRR exists for chromia-doped fuel, Framatome discussed performance of other fuels with similar properties, such as gadolinia doped, large-grain undoped, and niobia-doped fuel, which has similar intragranular swelling features. Framatome states that all of these tests showed similar outcome during RIA pulse testing as standard  $\text{UO}_2$ , and assert that gadolinia doped fuel is bounding, and as gadolinia fuel is included in DG-1327, it is expected that the draft guide would be similarly applicable to chromia-doped fuel.

Similarly, Framatome states that niobia-doped fuel should bound the fuel fragmentation performance of chromia-doped fuel, as the intragranular gaseous swelling is larger for niobia doped fuel. They further point to NFIR post-irradiation annealing tests that indicate that FGR is lower for doped fuel than standard  $\text{UO}_2$ . This test also found that fuel fragment size was a factor of burnup, but that no fine-fragmentation was found during the anneal testing on any standard or doped  $\text{UO}_2$ , nor mixed oxide (MOX), between 40 and 48 GWd/tHM. Framatome asserts that the fission gas residing within the grains in intragranular bubbles will decrease the FGR during RIA, as fission gas reaches the gap primarily through a process of cracking along the grain boundary.

The Organization for Economic Co-operation and Development/Nuclear Energy Agency (OECD/NEA) State-of-the-Art report, "Nuclear Fuel Behaviour Under Reactivity-initiated

Accident (RIA) Conditions," make the following observation (Section A.5.1.4) (Reference 6) with respect to fuel grain size on RIA fuel performance:

It should be remarked that rod OI-10 showed exceptionally low fission gas release and cladding residual deformation. From the peak fuel enthalpy in this test, it is expected that film-boiling occurred during the transient [ ]. Yet, the cladding peak residual hoop strain is merely 0.7%, and the transient fission gas release is only 2.6%. These unusually low values are probably a consequence of the large grain (~28  $\mu\text{m}$ ) UO<sub>2</sub> fuel that was used in the OI-10 test rod. Due to the large grain size, there is less fission gas accumulated in grain boundary bubbles, and the transient fission gas release is lower than from fuel pellets with normal grain size (~10  $\mu\text{m}$ ).

This observation supports Framatome's claim regarding less transient FGR under RIA conditions.

After review of the additional information submitted by Framatome, the NRC staff finds the description of chromia-doped fuel's RIA performance, from the standpoints of fuel pellet swelling and fragmentation to be acceptable.

A change in fuel melting temperature may impact the allowable amount of deposited energy (coolability criterion), predicted number of failed fuel rods, and radiological source term. Section 5.2 of ANP-10340P describes the impact of chromia addition on fuel melting temperature. In general, the addition of chromia [ ] the fuel melting temperature. Changes were experimentally determined and will be explicitly accounted for in the approved methodology. With respect to fuel performance under RIA conditions, Section 5.3.2 of ANP-10340P concludes that the limited amount of chromia will not induce significant changes in fuel specific heat, thermal conductivity, or fuel melting point. As such, the radial average fuel enthalpy threshold for incipient melting of chromia-doped fuel is not significantly different than standard UO<sub>2</sub> fuel.

RAI-7a requested clarification of a statement made in the TR which indicated that the change in margin to fuel melt is negligible between doped and standard UO<sub>2</sub>. Framatome was asked to explain how the changes to fuel conductivity and melting point would affect allowable peak radial average fuel enthalpy and predicted number of fuel rod failures due to fuel melt. Framatome responded by stating that thermal-mechanical and thermal-hydraulic methodologies calculated each reload cycle would both include the new properties, and therefore any change to the average fuel enthalpy threshold for incipient melting would be explicitly accounted for. They additionally pointed to the example calculation provided in ANP-10340P, which indicated that there is generally a minimal impact to margin to fuel melt. The NRC staff finds the explicit calculation of fuel melt margin using the new thermal conductivity and melting temperature to be acceptable.

During the regulatory audit, Framatome indicated that, under certain conditions, chromium [ ] through some other process, and [ ]. The NRC staff asked RAI-5 to gather additional information and understanding of this behavior. This discussion is included in this section of the SE, as fuel centerline temperature is seen as the primary driver of the phenomenon, and RIA results in increased fuel centerline temperature.

Framatome described the solubility of chromia and other chromium species inside the pellet qualitatively as a function of temperature and burnup. In response to RAI-5a, which requested a description of the change in chromia content in the pellet with increased temperature, Framatome stated that:

During power ramps, some chromia will reduce, causing the liberation of oxygen. This oxygen is expected to migrate to oxidize the inside of the cladding, which has the effect of counteracting stress corrosion cracking (SCC). The chromium remaining in the pellet is converted to a metallic precipitate, and it is expected that this would restore the thermal conductivity to that of undoped  $\text{UO}_2$ .

In response to RAI-5b, which requested any data from hot-cell examinations that would confirm this behavior, Framatome described the change in [ ] in the pellet center, and showed x-ray cartography data that provides experimental evidence for this behavior.

In response to RAI-5c, which asked if chromia migration might lead to an increase FGR, Framatome clarified that the chromium does not leave the [ ], and thus would not precipitate in such a way to negatively impact FGR, but rather that the oxygen may migrate under certain conditions.

The NRC staff has reviewed these responses, and the data contained within, and find them to be acceptable.

A change in FGR will impact rod internal pressure which, in turn, will impact the probability of fuel rod ballooning and rupture. Section 7.2 of ANP-10340P describes the validation of the RODEX4 FGR model for chromia-doped fuel. See Section 3.4.2 of this SE for further assessment of FGR. In general, the addition of chromia increases the grain size which increases the diffusion path; however, the lower thermal conductivity tends to increase the rate of diffusion. An increase in FGR would lead to higher rod internal pressures and increase the likelihood of fuel rod ballooning and rupture. These potential impacts are being explicitly addressed in the RODEX4 initial fuel conditions (input) to downstream safety analyses, including RIA calculations.

A change in pellet microstructure or fission gas retention may impact the susceptibility to fuel fragmentation or the resulting fragmentation size distribution. Section 5.3.2 of ANP-10340P describes the potential impact of chromia addition to fuel fragmentation under RIA conditions. Citing microstructural examinations of irradiated fuel, Framatome concludes that chromia-doped fuel has a [ ].

Any interaction between chromia dopant and fission products may alter the amount or chemical species of releases under RIA conditions. Citing microstructural examinations of irradiated fuel, Framatome concludes that chromia-doped fuel has a [ ]

under RIA conditions. Additionally, in the response to RAI-7a, Framatome stated that the impact on source term due to a change in melting temperature will be taken into account when AST analyses are performed.

In a recent review of Global Nuclear Fuel-Americas, LLC additive fuel pellets for BWR applications, the NRC staff evaluated the impacts on fuel performance under RIA conditions. Results presented from NSRR RIA tests on fuel rod segments with different additive compositions and concentrations exhibited similar behavior and failure thresholds as standard

UO<sub>2</sub> rods. These results support the discussion above which refers to tests with niobium-doped, gadolinia, large grain standard, and MOX fuel.

The RIA empirical database which forms the technical bases for the soon to be published regulatory guidance and acceptance criteria in DG-1327 is comprised of over 150 prompt pulse tests performed at several research reactors on a large variation of fuel rod designs, including non-standard UO<sub>2</sub> fuel pellets. While no explicit RIA tests were conducted on chromia-doped fuel, tests conducted on other non-standard UO<sub>2</sub> fuel strongly suggest that the concentrations of chromia requested in this TR (and the known impacts on fuel properties) are unlikely to significantly or negatively impact fuel performance under RIA conditions.

One potential unintended consequence of eliminating fuel designs with the natural or low alloy zirconium liner cladding (with the substitution of chromia-doped fuel) is the change in the initial, pre-transient cladding hydrogen distribution. The barrier liner acts as a sponge for hydrogen absorbed through waterside corrosion. The barrier effectively removes significant amounts of hydrogen and the detrimental effects of hydrides from the base metal. Out-of-pile mechanical testing on irradiated cladding segments suggest that the zirconium liner, even after significant irradiation and hydride precipitation, remains ductile. Since the presence of a barrier liner depletes hydrogen from the base metal and remains ductile, a barrier lined fuel rod will likely exhibit more ductility than a non-lined fuel rod at the same hydrogen level.

As a result of this phenomenon, a potential inconsistency exists with recrystallized annealed (RXA) Zry-2 cladding. A majority of the NSRR prompt power test results used to develop the PCMI cladding failure threshold for RXA cladding are based on RXA Zry-2 fuel rod segments with a zirconium liner. Application of these test results to RXA Zry-2 fuel rod designs without a liner may be non-conservative. Future applicants should carefully consider the applicability of these cladding failure curves to non-lined RXA Zry-2 fuel rod designs.

The NRC staff finds the performance of chromia-doped fuel under RIAs acceptable.

### 3.3 Operating Experience and Qualification Data

Framatome has conducted [ ] steady-state lead fuel assembly (LFA) campaigns in pressurized water reactor (PWR) and BWR reactors using chromia-doped UO<sub>2</sub> fuel pellets, beginning in 1997. These have included enrichments up to 4.95 percent U<sup>235</sup>, and densities of from [ ]. Cladding for these pellets has included [ ]

Maximum rod burn-up of approximately [ ] has been obtained. This includes a LFA program in a domestic BWR.

Rods irradiated as part of the LFA campaigns have been used for ramp testing, as described in Section 3.3.2 of this SE, and Section 6.2 of the TR. Framatome states that most of the ramped fuel rods were irradiated to burnup levels that are typically most limiting with respect to PCI failures. In addition, high-burnup rods were also tested, to assess the impact of hydrogen uptake.



### 3.3.1 Steady State Dataset

The range of burnup achieved in commercial reactors at steady-state is summarized in Table 3.3-1 below, taken from the TR. These were irradiated in the following cladding materials:

[ ],  
[ ]

Fuel rod designs included in the database are:

[ ],  
[ ].

Following irradiation, PIE measurements of the following were conducted:

[ ].

Some rods were full-length, while others were rodlets used for ramp testing after base irradiation was achieved. [ ].

Temperature measurements were also collected for separate effects testing of high burnup fuel (~50 MWd/kgU). A rod that had accumulated burnup was refabricated and instrumented with a central thermocouple and irradiated in a test reactor with on-line temperature measurement.  
[ ]

[ ]

### 3.3.2 Ramp Dataset

The range of burnup achieved for the ramp dataset is summarized in Table 3.3-1, taken from the TR. The ramp dataset is used to justify the ramp rates discussed in Section 3.7 of this SE.

The following cladding materials were used in this dataset:

[ ],

[ ]

Fuel rod designs included in the database are:

[ ],

[ ].

Following irradiation, PIE measurements of the following were conducted:

[ ].

For the BWR program [

]

The NRC staff concludes that Framatome has provided sufficient operating experience for chromia-doped fuel for use within the bounds of the conditions and limitations included in this SE.

### 3.4 Qualification of RODEX4

RODEX4 is Framatome's fuel thermal-mechanical code approved for BWR fuel design and licensing analyses with standard  $\text{UO}_2$  and gadolinia-doped  $\text{UO}_2$ . The following sections of this report detail changes made to RODEX4 to accommodate the properties and behavior of chromia-doped fuel.

Validation and verification of these changes was carried out by comparing the data described in Section 3.3 of this SE and Section 6 of the TR. This data includes [

].

#### 3.4.1 Thermal Conductivity Model

Thermal conductivity is measured experimentally by determining the thermal diffusivity and the specific heat capacity of the material. Thermal diffusivity measurements were taken during the JRC-ITU 1999 campaign, as well as "in-house" campaigns conducted by Framatome in 2006 and 2015. A subset of samples from these in-house campaigns was sent to JRC-ITU for

complementary measurements. Thermal conductivity is also described in Section 3.1.5 of this SE.

#### 3.4.1.1 Adaptation of RODEX4 thermal conductivity model to unirradiated chromia-doped fuel

JRC-ITU data used either measured specific heat, or a known specific heat correlation. As Framatome is not intending to modify the specific heat correlation used for standard  $\text{UO}_2$  and [ ] for use with chromia-doped fuel, the thermal conductivity of the samples was recalculated using the MATPRO correlation used in RODEX4. This change resulted in lower uncertainty and a better match with the data.

During the 2015 campaign Framatome tested a number of different chromia concentrations and found that conductivity decreases with increasing chromia concentration, [ ].

Using this experimental data, a new thermal conductivity model was developed for chromia-doped fuel. This model is specified in the TR, Section 7.1.1 and [ ]

]

#### 3.4.1.2 Validation of RODEX4 thermal conductivity model to irradiated chromia-doped fuel

Standard  $\text{UO}_2$  fuel experiences degradation of thermal conductivity with increased burnup. To validate that this effect is also present in chromia-doped fuel, Framatome benchmarked RODEX4 to the REMORA2 test, where a pellet centerline temperature was measured online using thermocouples after achieving a burnup of around 62 MWd/kgU. This showed good agreement when applying the same thermal conductivity degradation effect to chromia-doped fuel as is applied to standard  $\text{UO}_2$ .

Due to the experimental measurements and satisfactory benchmarking of RODEX4, the NRC staff finds Framatome's thermal conductivity models for chromia-doped fuel and chromia-doped NAF to be acceptable.

#### 3.4.2 Fission Gas Release Model

Framatome states that the FGR model in RODEX4 remains unchanged. This is due to competing effects: larger grain size reduces FGR by slowing the diffusion to grain boundaries, but the reduction in grain boundary area leads to decreased fission gas retention at these boundaries. Framatome provides a plot of calculated versus measured FGR from a number of lead assemblies.

Framatome discounts the impact that chromia has on the diffusion rate of fission products through the fuel matrix. A plot is presented in the TR showing predicted versus measured FGR from a database of 48 doped samples and 13 undoped control samples paired with data in the doped set. These data show a relatively wide degree of variability, but generally are in agreement with the predicted values.

The NRC staff requested, in RAI-9, that Framatome model test IFA-716 from the Halden experimental reactor using RODEX4. This experiment measured FGR from chromia-doped fuel as well as standard and large-grain undoped  $\text{UO}_2$ . Framatome submitted this as well as the results from modeling IFA-677, which was similar to IFA-716 but contained standard  $\text{UO}_2$  as well as fuel pellets with a different dopant. Tables 3.4-1 and 3.4-2 below summarize the important results from these test rods. For the purposes of evaluating the FGR in chromia-doped fuel, there are a total of 3 rods of interest containing standard  $\text{UO}_2$  (677-2, 677-6, 716-2), and 2 rods with chromia dopant (716-1 and 716-6). All of these rods except 716-2 had online FGR calculated from online rod internal pressure, and 677-6 and 716-6 both were also subjected to PIE FGR measurements using puncture testing.

RODEX4 very slightly overpredicted FGR for the two standard  $\text{UO}_2$  rods for which there is data. The two chromia-doped rods, on the other hand, were underpredicted by the code. It is worth noting that the total FGR for these two rods is still small, where the standard  $\text{UO}_2$  has typically also had a relatively large spread of data.

The NRC staff also requested the data used to generate this plot in RAI-8a. This data was provided with additional information, such as grain size and chromia content, that was not in the original submittal. This data was examined to determine if any of the other parameters correlated with FGR calculational errors. No trends were found. Framatome also submitted a plot of FGR, replicated below, using the 95/95 bound for diffusion coefficient and LHGR. This additional plot provided assurance that the FGR dataset is representative of the doped fuel under review, and that the FGR correlation in RODEX 4 does a satisfactory job of predicting the experimental data. For these reasons, the NRC staff finds the FGR model acceptable for use with chromia-doped  $\text{UO}_2$ .

Framatome also requested that the grain size restriction (for standard  $\text{UO}_2$ ) imposed by the SE for RODEX4 (Reference 7) be lifted. The primary stated reason for that restriction was the limited FGR data for undoped fuel with grain size above 20  $\mu\text{m}$  MLI. To better disposition this request, the NRC staff requested additional FGR data to support the use of large-grain standard  $\text{UO}_2$  in RAI-10a, and requested that Framatome model a Halden test (Halden-716) which studied the behavior of both chromia-doped as well as large grain undoped  $\text{UO}_2$  fuel.

Framatome's response to RAI-10a provided a total of 9 data points for FGR from standard  $\text{UO}_2$  with grain size over 20  $\mu\text{m}$ . Framatome's response to RAI-9 demonstrated underprediction of FGR from large grain undoped  $\text{UO}_2$ .

The NRC staff has determined that this is insufficient evidence to warrant removing the restriction on grain size for standard  $\text{UO}_2$ . Although this is not a new limitation or condition, for clarity this will be included in the limitations and conditions in Section 4 of this SE.

Table 3.4-1 Salient Features and Measured Data for Modelled rods of IFA 677  
(From Reference 5, Table 9-1)

Rod	677-1	677-2	677-6
Fuel type	(Cr-Al) <sub>2</sub> O <sub>3</sub> doped	Standard	Standard
Grain size (MLI)	37.3	11	7.8
Stoichiometry	2.002	2.004	2.002
Fill gas pressure (bar)	13.5	13.5	13.5
FGR from online pressure (%)	22	19.7	19.1
FGR from PIE (%)	N/A	N/A	19
Calculated FGR (%)	16.2	21.8	20.1

Table 3.4-2: Salient Features and Measured Data for Modelled rods of IFA 716  
(From Reference 5, Table 9-2)

Rod	716-1	716-2	716-4	716-5	716-6
Fuel type	Cr <sub>2</sub> O <sub>3</sub> doped	Standard	Large grain, non-doped	Large grain, non-doped	Cr <sub>2</sub> O <sub>3</sub> doped
Grain size (MLI)	50 (70)	11	45	45 (55)	50 (59)
Stoichiometry	2.005	2.001	2.005	2.006	2.002
Fill gas pressure (bar)	10	10	10	10	10
FGR from online pressure (%)	5.71	N/A	6.75	6.6	7.84
FGR from PIE (%)	N/A	N/A	N/A	4.32	5.73
Calculated FGR (%)	2.4	3.1	1	4.1	1.8

Figure 3.4-1: FGR Results for the Chromia-Doped Database with LHGR and Diffusion Coefficient Biased to the 95/95 Upper Bounds (From Reference 5, Figure 8-1)



### 3.4.3 Intragranular Gaseous Swelling Model

In standard  $\text{UO}_2$ , fission gases collect and may form bubbles along the grain boundary, known as intergranular bubbles. As chromia-doped fuel has larger grains and enhanced creep and plasticity it has a propensity for forming intragranular bubbles instead, as the gases collect inside the grain instead of along the grain boundary. These bubbles lead to increased fuel pellet and cladding deformation, especially following a power ramp.

To accurately capture this phenomenon, Framatome has added an intragranular swelling (IGSW) model to RODEX4. After using PIE ceramography to calibrate the parameters of this model, Framatome presented data showing good agreement between measured and calculated fuel clad strain from the chromia-doped fuel database. Given the validation data provided, NRC staff finds this model acceptable for modeling fission gas swelling in chromia-doped fuel.

During the regulatory audit, NRC staff asked if the intergranular model is turned off for chromia-doped fuel pellets. Framatome responded that the model reduces IGSW with increased grain size, and therefore does not need to be adjusted for chromia-doped fuel. The NRC staff finds this acceptable.

RAI-10b requested additional information regarding how the IGSW model will be applied to standard UO<sub>2</sub>. In response, Framatome states that the model is only used if the grain size exceeds [ ] microns MLI. They also state that they would not expect standard UO<sub>2</sub> to exceed that value.

In their response to this RAI Framatome demonstrated that, for standard UO<sub>2</sub> below the 20 micron 3-D limit, including the IGSW model results in a small conservative change in the predicted strain increment during power ramps, a small change in the clad diameter change after steady-state irradiation, and a small non-conservative change in the FGR prediction. The NRC staff has reviewed this response and found it to be acceptable.

### 3.5 Qualification of AURORA-B

Framatome states that AURORA-B will include the use of RODEX4 and S-RELAP5, and that the thermal conductivity model described in Section 3.4.1 of this SE will be incorporated into S-RELAP5.

The NRC staff finds this acceptable. This does not over-ride or replace any conditions or limitations placed on the use of AURORA-B methodologies by the NRC staff in other safety evaluations.

### 3.6 Licensing Criteria Assessment

Framatome states that no fundamental changes are necessary in order to model chromia-doped fuel using RODEX4 or AURORA B methodologies, beyond changes to correlations discussed in Sections 1.0 and 8.0 of the TR, and covered in Sections 3.4 and 3.5 of this SE. Additionally, there is no change to any design or licensing criteria. Examples of the design analyses were performed with the chromia-doped option activated and the results of those analyses are discussed below.

These examples were examined in greater detail at the regulatory audit (References 2 and 3) conducted by NRC staff. No discrepancies were found.

#### 3.6.1 Steady State and AOO Analyses

Framatome repeated a recent ATRIUM 10XM reload steady-state calculation (performed with RODEX4) using the chromia-doped fuel model options activated, and the results were compared to the standard UO<sub>2</sub> cases. The outcome of this comparison shows that, compared to standard UO<sub>2</sub>, chromia-doped fuel exhibits:

- [ ]
- [ ]
- [ ]
- [ ]

[ ].

For the AOO analysis, Framatome calculated fast AOO setback factors for control rod withdrawal error, and flow run-up. Compared to standard  $\text{UO}_2$ , chromia-doped fuel exhibits:

- [ ]
- [ ]

[ ].

The NRC staff has examined the results of this analysis presented in the TR, as well as the detailed calculations made available at the regulatory audit. The results are acceptable, as they demonstrate expected behavior.

### 3.6.2 Safety Analyses

Framatome performed sample problems that cover AOOs, LOCA, and CRDA using AURORA-B. The AOO analysis performed with AURORA-B is separate from that performed with RODEX4, described in Section 3.6.1, and focuses primarily on thermal-hydraulic response rather than thermal-mechanical. The primary consequences of chromia-doped fuel over standard  $\text{UO}_2$ , for these analyses, are competing effects on energy stored in the fuel. On one hand, doped fuel closes the gap between the cladding and the pellet earlier, which results in lower thermal resistance between fuel and coolant. On the other hand, decreased fuel thermal conductivity has the opposite effect.

Framatome provided results for three AOOs: turbine trip-no bypass (TTNB), feedwater controller failure (FWCF), and anticipated transient without scram. Different figures of merit are of primary interest for different AOOs. For TTNB and FWCF, margin to boiling crisis (i.e., critical power ratio, or CPR) are of interest. As margin is reduced with increase thermal conductivity, the upper bound best estimate thermal conductivity correlation, described in Section 3.4.1.1 of this SE, was used to ensure conservatism. Framatome presents the results of these calculations in Table 9-4 of the TR, which indicates that, for these example calculations, chromia-doped fuel exhibits only small changes to CPR and maximum system pressure for these three transients.

For the remaining sample problems (large-break LOCA, small-break LOCA, and CRDA), the figure of merit is PCT. The results show that the doped fuel has very little effect on the results of the calculation, with only a very small increase in PCT, explained by a small increase in stored energy.



### 3.6.3 Impact on Nuclear Design Requirements

Framatome states that there is no impact on reactor physics calculations as cross sections for Cr and O are included in the CASMO-4 lattice code. Framatome further states that the change in reactivity is small, as the absorption cross section for chromium is small compared to that of the fuel and the small change of density is properly captured. Thus changes are small and will be captured by current analysis methods. The NRC staff finds this acceptable.

### 3.7 Power Maneuvering Guidelines

The movement of high worth control blades during BWR power maneuvering may result in a significant increase in local power. Depending on the initial pellet-to-clad gap width, fuel pellet thermal expansion may lead to an increase in cladding stress. Given the right combination of mechanical stress, chemical agent (e.g., iodine), and time, pellet cladding interaction – stress corrosion cracking (PCI-SCC) induced crack propagation may lead to cladding failure. PCI-SCC cladding failures during power maneuvering were a significant operational issue prior to the introduction of liner cladding (i.e., thin layer of natural or low alloy zirconium on cladding inside diameter) in combination with power maneuvering guidelines.

The regulation at 10 CFR Part 50 Appendix A GDC 10, *Reactor design*, requires that the reactor core and associated coolant, control, and protection systems shall be designed with appropriate margin to assure that specified acceptable fuel design limits are not exceeded during any condition of normal operation, including the effects of AOOs. In accordance with GDC 10, licensees should establish power maneuvering guidelines, based upon experimental data, which minimize the likelihood of fuel rod cladding failures. However, recognizing the low safety significance of a limited number of fuel rod failures, existing plant technical specification allowable limits on reactor coolant activity, and the ability of plant operators to identify and respond to fuel rod failures during power maneuvering, the NRC staff does not require specified, reviewed, and approved power maneuvering restrictions.

Section 10.2 of ANP-10340P describes ramp testing performed on irradiated chromia-doped  $\text{UO}_2$  fuel rod segments. The purpose of these ramp tests was to quantify the PCI-SCC performance of chromia-doped  $\text{UO}_2$  fuel and demonstrate it as an alternative to present liner cladding in terms of PCI-SCC protection for BWR applications. Figure 10-1 of ANP-10340P (reproduced below in Figure 3.7-1) provides the Framatome ramp test database as a function of conditioning power versus power increment. Further details were provided in response to RAI 8b (Reference 5).

Fuel rod design (e.g., rod diameter, initial gap size, cladding thickness, cladding microstructure) and operating history (e.g., power history, burnup, cladding corrosion) play an important role in quantifying PCI-SCC resistance and defining power maneuvering guidelines. Figure 3.7-2 illustrates the extent of the Framatome ramp test database for BWR fuel designs with chromia-doped fuel as a function of conditioning power and separately as a function of fuel burnup. The database is limited both in the total number of ramp tests (14), the number which experienced cladding failure (4), and the range of conditioning power and burnup.

To investigate Framatome's claim that chromia-doped  $\text{UO}_2$  fuel is a viable alternate to liner cladding in terms of PCI-SCC protection, the NRC staff reviewed the Studsvik Cladding Integrity Program (SCIP-I, SCIP-II) ramp testing empirical database. With over 180 ramp tests

conducted on BWR fuel rods with liner cladding, the SCIP database encompasses a much broader range of initial and test conditions. Figure 3.7-3 plots the SCIP test results along with the Framatome BWR database (failed versus survived as a function of conditioning power and power increment). The transition between failure and survival as a function of conditioning power is similar between chromia-doped fuel and liner cladding and certainly within the spread of the SCIP database.

Figure 3.7-4 plots only the tests which experienced cladding failure. Hundreds of earlier SCIP ramp tests with standard Zry-2 BWR cladding (unlined) have been added to investigate the relative benefit of both chromia-doped and liner cladding. Examination of this figure reveals significant improvements in PCI-SCC resistance for both chromia-doped and liner cladding, especially at higher conditioning powers.

Figure 3.7-5 adds the cladding liner fuel rod failure threshold and proposed chromia-doped fuel rod failure threshold to the SCIP and Framatome database depicted earlier in Figure 3.7-3. Based on the limited chromia-doped ramp database and the spread in the broader SCIP BWR liner cladding database, the NRC staff is not convinced that the chromia-doped fuel offer superior PCI-SCC resistance relative to liner cladding. Both chromia-doped fuel and liner cladding exhibit significant improvements in PCI-SCC resistance relative to non-liner BWR cladding designs. As such, chromia-doped fuel is a viable alternate to liner cladding.

Licensees and their fuel vendors are responsible for establishing power maneuvering guidelines, which when combined with the beneficial PCI-SCC performance of either chromia-doped or barrier liner, provide a reasonable assurance of fuel rod cladding integrity during power maneuvering.

Figure 3.7-1:



Figure 3.7-2:

[

]

[

]

Figure 3.7-3:



Figure 3.7-4:



Figure 3.7-5:



#### 4.0 LIMITATIONS AND CONDITIONS

1. The limitation imposed on grain size of standard  $\text{UO}_2$  in the RODEX4 TR SE (Reference 7) is unchanged.
2. Chromia-doped fuel is licensed to the same currently approved rod-average burnup limit as standard  $\text{UO}_2$ : 62 GWd/MTU.
3. Chromia concentration shall be limited to the range specified in the response to RAI-1a: [ ]  $\mu\text{gCr/gU}$ . This limit shall also apply to chromia-doped NAF.

#### 5.0 CONCLUSIONS

Framatome has presented data and analyses to support their request for approval of chromia-doped  $\text{UO}_2$  fuel for use in BWRs, where the dopant is within the range [ ]  $\mu\text{gCr/gU}$ . Material property changes have been implemented in both the RODEX-4 thermal-mechanical code and the AURORA-B transient analysis methodology. The impact of the chromia dopant on in-reactor fuel performance (such as washout characteristics, RIA behavior, LOCA behavior, and FGR) has been adequately analyzed.

The NRC staff concludes that thermal-mechanical performance of the proposed fuel is adequately addressed in the Framatome submittal with the application of the RODEX4 fuel performance code. Fuel melt temperature and thermal conductivity are found to be affected by the chromia dopant in excess of any expected effect from grain size. Additional properties are affected by grain size, such as fuel swelling and steady state fragmentation. FGR is found to be adequately predicted using the existing correlation in RODEX4, for which grain size is an input.

Additionally, the NRC staff found chromia-doped NAF fuel to be well represented by existing gadolinia-doped fuel properties, with the exception of thermal conductivity and fuel melt temperature which were directly measured.

The NRC staff's SE of chromia-doped fuel is subject to the limitations and conditions listed in Section 4.0.

#### 6.0 REFERENCES

1. ANP-10340P/NP, Revision 0, "Incorporation of Chromia-Doped Fuel Properties in AREVA Approved Methods," AREVA, April 2016 (Agencywide Documents Access and Management System (ADAMS) Accession Nos. ML16124B092 (Public) and ML16124B093 (Non-Public)).
2. "Plan for Audit Supporting NRC Review of ANP-10340P, Revision 0," February 28, 2017 (ADAMS Accession No. ML17045A530).
3. "Audit Report to Support the Review of AREVA Inc. Topical Report ANP-10340P, Revision 0," August 1, 2017 (ADAMS Accession Nos. ML17179A399 (Public) and ML17179A405 (Non-Public)).



4. "Request for Additional Information Regarding AREVA Inc. Topical Report ANP-10340P, Revision 0," August 4, 2017 (ADAMS Accession No. ML17179A345).
5. Additional Information Regarding ANP-10340, "Incorporation of Chromia-Doped Fuel Properties in AREVA Approved Methods," Framatome, March 28, 2018 (ADAMS Accession Nos. ML18092A601 (Public) and ML18092A602 (Non-Public))
6. NEA/CSNI/R(2010)1, "Nuclear Fuel Behaviour Under Reactivity-initiated Accident (RIA) Conditions, State-of-the-art Report", 2010,  
<https://www.oecd-neo.org/nsd/docs/2010/csni-r2010-1.pdd>
7. BAW-10247PA/NPA, Revision 0, "Realistic Thermal-Mechanical Fuel Rod Methodology for Boiling Water Reactors", April 30, 2008 (ADAMS Accession Nos. ML081340208 (Public), ML081340383, and ML081340385 (Non-Public))

Attachment: Comment Resolution Table

Principle Contributors: Joshua Whitman, NRR/DSS  
Paul Clifford, NRR/DSS

Date:



April 29, 2016  
NRC:16-010

U.S. Nuclear Regulatory Commission  
Document Control Desk  
11555 Rockville Pike  
Rockville, MD 20852

**Request for Review and Approval of ANP-10340P, Revision 0 "Incorporation of Chromia-Doped Fuel Properties in AREVA Approved Methods"**

AREVA Inc. (AREVA) requests the NRC's review and approval of the topical report ANP-10340P, Revision 0 "Incorporation of Chromia-Doped Fuel Properties in AREVA Approved Methods," dated April 2016, for referencing in licensing actions.

This topical report addresses the method of analysis changes necessary to implement the use of chromia-doped fuel into AREVA's suite of BWR licensing methods. Many of the topical reports which make up AREVA's suite of BWR methods are currently being reviewed for approval by the NRC. Topical report ANP-10340P is an integral part of the BWR suite of methods. The use of chromia-doped fuel has the goal of enhancing safe operation at BWR plants by reducing PCI failures.

In support of the Office of Nuclear Reactor Regulation's prioritization efforts, the Topical Report Prioritization Scheme is included as an enclosure with this letter.

AREVA would appreciate the NRC approval of this topical report by the end of the fourth quarter of calendar year 2017.

AREVA considers some of the material contained in the enclosed document to be proprietary. As required by 10 CFR 2.390(b), an affidavit is enclosed to support the withholding of the information from public disclosure. A proprietary version and a non-proprietary version of the report are enclosed.

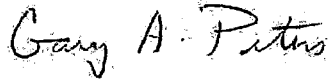
There are no commitments within this letter or its enclosures.

**AREVA INC.**

3315 Old Forest Road, Lynchburg, VA 24501  
Tel.: 434 832 3000 - [www.aveva.com](http://www.aveva.com)

If you have any questions related to this information, please contact Mr. Morris E. Byram, Product Licensing Manager, by telephone at (434) 832-4665, or by e-mail at [Morris.Byram@areva.com](mailto:Morris.Byram@areva.com).

Sincerely,



Gary A. Peters, Director  
Licensing & Regulatory Affairs  
AREVA Inc.

cc: J. G. Rowley  
Project 728

Enclosures:

1. Proprietary copy of topical report ANP-10340, Revision 0, "Incorporation of Chromia-Doped Fuel Properties in AREVA Approved Methods"
2. Non-Proprietary copy of topical report ANP-10340, Revision 0, "Incorporation of Chromia-Doped Fuel Properties in AREVA Approved Methods"
3. ANP-10340, Revision 0 Priority Form
4. Notarized Affidavit

TR Prioritization Scheme			
Title: ANP-10340P, Rev. 0 "Incorporation of Chromia-Doped Fuel Properties in AREVA Approved Methods"			
Expect submitting FY	TAC	PM	Today's Date: 4/29/2015
Technical Review Division(s)		Technical Review Branch(s)	
<b>Factors</b>	<b>Select the Criteria That the TR satisfies</b>	<b>Points can be Assigned for Each Criteria</b>	<b>Assigned Points</b>
<b>TR Classification</b> (Select one only)	Resolve Generic Safety Issue (GSI)	6	2
	Emergent NRC Technical Issue	3	
	New technology improves safety	2	
	TR Revision reflecting current requirements or analytical methods.	2	
	Standard TR	1	
<b>TR Applicability</b> (Select one only)	Potential industry-wide applications	3	2
	Potentially applicable to entire groups of licensees.	2	
	Intended for only partial groups of licensees.	1	
<b>TR Implementation Certainty</b> (Select one only)	Industry-wide Implementation expected	3	1
	Expected implementation by an entire group of licensees (BWROG, PWROG, BWRVIP, etc.) who sponsored the TR.	2	
	Docketed intent by U.S. plant(s) but no formal LAR schedule yet	1	
	No US plants have indicated strong intent on docket to implement yet.	0	
<b>Tie to a LAR</b> (Select if applicable)	A SE is requested by a certain date (less than two years) to support a licensing activity or renewal date (note it in Comments)	3	3
<b>Review Progress</b> (Points are cumulative as applicable)	Accepted for review	0.3	
	RAI issued	0.5	
	RAI responded	1.2	
	SE Drafted	2.0	
<b>Management (LT/ET) discretion adjustment</b>		-3 to +3	
<b>Total Points (Add the total points from each factor and total here):</b>			<b>8</b>
<b>Comments: Request Approval by December 2017 for LAR Reference.</b>			

## AFFIDAVIT

COMMONWEALTH OF VIRGINIA    )  
  ) ss.  
CITY OF LYNCHBURG            )

1. My name is Morris Byram. I am Manager, Product Licensing, for AREVA Inc. (AREVA) and as such I am authorized to execute this Affidavit.

2. I am familiar with the criteria applied by AREVA to determine whether certain AREVA information is proprietary. I am familiar with the policies established by AREVA to ensure the proper application of these criteria.

3. I am familiar with the AREVA information contained in the AREVA document ANP-10340P, Rev. 0, "Incorporation of Chromia-Doped Fuel Properties in AREVA Approved Methods," and referred to herein as "Document." Information contained in this Document has been classified by AREVA as proprietary in accordance with the policies established by AREVA Inc. for the control and protection of proprietary and confidential information.

4. This Document contains information of a proprietary and confidential nature and is of the type customarily held in confidence by AREVA and not made available to the public. Based on my experience, I am aware that other companies regard information of the kind contained in this Document as proprietary and confidential.

5. This Document has been made available to the U.S. Nuclear Regulatory Commission in confidence with the request that the information contained in this Document be withheld from public disclosure. The request for withholding of proprietary information is made in accordance with 10 CFR 2.390. The information for which withholding from disclosure is

requested qualifies under 10 CFR 2.390(a)(4) "Trade secrets and commercial or financial information."

6. The following criteria are customarily applied by AREVA to determine whether information should be classified as proprietary:

- (a) The information reveals details of AREVA's research and development plans and programs or their results.
- (b) Use of the information by a competitor would permit the competitor to significantly reduce its expenditures, in time or resources, to design, produce, or market a similar product or service.
- (c) The information includes test data or analytical techniques concerning a process, methodology, or component, the application of which results in a competitive advantage for AREVA.
- (d) The information reveals certain distinguishing aspects of a process, methodology, or component, the exclusive use of which provides a competitive advantage for AREVA in product optimization or marketability.
- (e) The information is vital to a competitive advantage held by AREVA, would be helpful to competitors to AREVA, and would likely cause substantial harm to the competitive position of AREVA.

The information in this Document is considered proprietary for the reasons set forth in paragraphs 6(b), 6(c) and 6(d) above.

7. In accordance with AREVA's policies governing the protection and control of information, proprietary information contained in this Document has been made available, on a limited basis, to others outside AREVA only as required and under suitable agreement providing for nondisclosure and limited use of the information.

8. AREVA policy requires that proprietary information be kept in a secured file or area and distributed on a need-to-know basis.

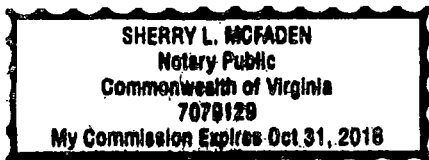
9. The foregoing statements are true and correct to the best of my knowledge,  
information, and belief.

Mario E. Benavente

SUBSCRIBED before me this 28<sup>th</sup>  
day of April, 2016.

Sherry L. McFaden

Sherry L. McFaden  
NOTARY PUBLIC, COMMONWEALTH OF VIRGINIA  
MY COMMISSION EXPIRES: 10/31/18  
Reg. # 7079129



Received 8/8/16

T4.12.1 - NRC-16-014



UNITED STATES  
NUCLEAR REGULATORY COMMISSION  
WASHINGTON, D.C. 20555-0001

July 29, 2016

Mr. Gary Peters, Director  
Licensing and Regulatory Affairs  
AREVA Inc.  
3315 Old Forest Road  
Lynchburg, VA 24501

SUBJECT: ACCEPTANCE FOR REVIEW OF AREVA INC. TOPICAL REPORT  
ANP-10340P, REVISION 0, "INCORPORATION OF CHROMIA-DOPED FUEL  
PROPERTIES IN AREVA APPROVED METHODS" (TAC NO. MF7707)

Dear Mr. Peters

By letter dated April 29, 2016 (Agencywide Documents Access and Management System Accession No. ML16124B091), AREVA Inc. (AREVA) submitted for U.S. Nuclear Regulatory Commission (NRC) staff review Topical Report (TR) ANP-10340P, Revision 0, "Incorporation of Chromia-Doped Fuel Properties in AREVA Approved Methods." The NRC staff has performed an acceptance review of TR ANP-10340P. We have found that the material presented is sufficient to begin our review. The NRC staff expects to issue its request for additional information by March 10, 2017, and issue its draft safety evaluation (SE) by September 29, 2017. This schedule information takes in consideration the NRC's current review priorities and available technical resources and may be subject to change. If modifications to these dates are deemed necessary, we will provide appropriate updates to this information. The NRC staff estimates that the review will require approximately 350 staff hours including project management and contractor time. The review schedule milestones and estimated review costs were discussed and agreed upon in a telephone conference between AREVA Product Licensing Manager, Morris Byram, and the NRC staff on July 5, 2016.

Section 170.21 of Title 10 of the *Code of Federal Regulations* requires that TRs are subject to fees based on the full cost of the review. You did not request a fee waiver; therefore, NRC staff hours will be billed accordingly.

As with all TRs, the SE will be reviewed by the NRC's Office of the General Counsel (OGC) to determine whether it falls within the scope of the Congressional Review Act (CRA). During the course of this review, OGC considers whether any endorsement or acceptance of a TR by the NRC amounts to a rule as defined in the CRA. If this initial review concludes that the SE, with its accompanying TR, may be a rule, the NRC will forward the package to the Office of Management and Budget (OMB) for further review and consideration. Any review by OMB would impact the schedule for the issuance of the final SE.



G. Peters

- 2 -

If you have questions regarding this matter, please contact Jonathan G. Rowley at (301) 415-4053.

Sincerely,

A handwritten signature in black ink, appearing to read "Kevin Hsueh". The signature is written in a cursive, flowing style.

Kevin Hsueh, Chief  
Licensing Processes Branch  
Division of Policy and Rulemaking  
Office of Nuclear Reactor Regulation

Project No. 728



UNITED STATES  
NUCLEAR REGULATORY COMMISSION  
WASHINGTON, D.C. 20555-0001

August 4, 2017

Mr. Gary Peters, Director  
Licensing and Regulatory Affairs  
AREVA Inc.  
3315 Old Forest Road  
Lynchburg, VA 24501

SUBJECT: REQUEST FOR ADDITIONAL INFORMATION RE: AREVA INC. TOPICAL  
REPORT ANP-10340P, REVISION 0, "INCORPORATION OF  
CHROMIA-DOPED FUEL PROPERTIES IN AREVA APPROVED METHODS"  
(CAC NO. MF7707)

Dear Mr. Peters:

By letter dated April 29, 2016 (Agencywide Documents Access and Management System Accession No. ML16124B091), AREVA Inc. (AREVA) submitted for U.S. Nuclear Regulatory Commission (NRC) staff review and approval Topical Report ANP-10340P, Revision 0, "Incorporation of Chromia-Doped Fuel Properties in AREVA Approved Methods." Upon review of the information provided, the NRC staff has determined that additional information is needed to complete the review. On June 27, 2017, Morris Byram, AREVA Licensing and Regulatory Affairs, and I agreed that the NRC staff will receive the response to the enclosed request for additional information (RAI) questions by October 27, 2017.

If you have any questions regarding the enclosed RAI questions, please contact me at 301-415-4053.

Sincerely,

A handwritten signature in cursive script, reading "Jonathan G. Rowley", is positioned above the typed name.

Jonathan G. Rowley, Project Manager  
Licensing Processes Branch  
Division of Policy and Rulemaking  
Office of Nuclear Reactor Regulation

Project No. 728

Enclosure:  
RAI Questions

REQUEST FOR ADDITIONAL INFORMATION  
RELATED TO TOPICAL REPORT ANP-10340P, REVISION 0,  
"INCORPORATION OF CHROMIA-DOPED FUEL PROPERTIES IN AREVA  
APPROVED METHODS"  
AREVA INC.  
CAC NO. MF7707

**RAI-1**

Section 4.0 of the topical report (TR) defines a target chromia ( $\text{Cr}_2\text{O}_3$ ) concentration and mentions manufacturing uncertainties on this target concentration. Section 4.1 describes the basis for the target  $\text{Cr}_2\text{O}_3$  concentration including the resultant range in uranium oxide ( $\text{UO}_2$ ) grain size.

- a. Please define the manufacturing specification limits on  $\text{Cr}_2\text{O}_3$  content, and describe AREVA's quality assurance procedures to ensure that the fuel produced remains within these limits.
- b. Please define the manufacturing specification limits on grain size, and describe AREVA's quality assurance procedures to ensure that the fuel produced remains within these limits.

**RAI-2**

Section 5.3.2 of the TR states that "[

].” Section 4.2 states that “: [

- a. During an audit on April 11 - 12, 2017, AREVA mentioned that additional clarification to these descriptions was necessary. Please provide the appropriate changes.
- b. Given this new description, provide justification for the calculational method for theoretical density.
- c. Equation 4-4 appears to contain an error or typo. Please provide a correction.

**RAI-3**

Section 4.2 of the TR states that final stoichiometry of  $\text{Cr}_2\text{O}_3$ -doped fuel is [

].

Enclosure

- a. Please describe the [ ] and any manufacturing specifications associated with stoichiometry.
- b. Please describe the impact of [ ].

**RAI-4**

Section 5.2 of the TR describes the impact of  $\text{Cr}_2\text{O}_3$  dopant on fuel melting point.

- a. Given that the melting temperature of  $\text{Cr}_2\text{O}_3$ -doped fuel [ ]  $\text{Cr}_2\text{O}_3$ -doped fuel melting point is not incorporated into RODEX4 and downstream safety analyses. Please provide justification.
- b. Please describe the statistical approach used to calculate the [ ] fuel melting temperature.

**RAI-5**

During an audit on April 11 - 12, 2017, AREVA stated that, at normal operating temperatures, chromium [ ], or some other process, and [ ].

- a. Please describe this phenomenon in greater detail.
- b. Please provide any data from hot-cell examinations describing the [ ].
- c. Section 4.1 of the TR states that "... $\text{Cr}_2\text{O}_3$  was also found to accelerate fission gas diffusion coefficients when added in quantities of approximately 5000 wppm [ ] (Reference 2), which led to dopant segregation on grain boundaries during irradiation." Does the migration of chromium during operation lead to this issue?

**RAI-6**

In Section 4.3 of the TR, AREVA concludes "Therefore, a  $\text{Cr}_2\text{O}_3$  dopant level that is in the range of impurity content has a negligible effect and the thermal expansion of this fuel will be the same as for standard  $\text{UO}_2$ ." However, the levels of chromia proposed in this TR exceed the impurity limit. Please explain what is meant by this statement, or correct the text of the TR.

**RAI-7**

Section 5.3.2 of the TR discusses the response of  $\text{Cr}_2\text{O}_3$ -doped fuel during a reactivity-initiated accident (RIA) with respect to standard  $\text{UO}_2$  fuel.

- a. The TR suggests that the change in margin to fuel melt is negligible between doped and standard  $\text{UO}_2$ . The TR includes a statement that "[

## 1.

- i. A change in [ ] would impact the allowable peak radial average fuel enthalpy as described in Section 7.2 of Draft Regulatory Guide 1327 (DG-1327). Please address the impact of these changes on future reload cores designed with  $\text{Cr}_2\text{O}_3$ -doped fuel.
- ii. A change in [ ] would impact the predicted number of fuel rod failures due to fuel melting as described in Section 3-3 of DG-1327. Please address the impact of these changes on future reload cores designed with  $\text{Cr}_2\text{O}_3$ -doped fuel.
- iii. A change in [ ] would impact the radiological source term (release attributed to fuel melting) as described in Appendix C of Regulatory Guide 1.183. Please address the impact of these changes on future reload cores designed with  $\text{Cr}_2\text{O}_3$ -doped fuel.

## b. The TR states that "[

]."

No data is provided to quantify the overall fuel swelling of the  $\text{Cr}_2\text{O}_3$ -doped fuel or justify the concluding remarks that on balance  $\text{Cr}_2\text{O}_3$ -doped fuel is anticipated to have the same behavior as standard  $\text{UO}_2$  under RIA conditions. Hundreds of prompt pulse tests have been conducted in research reactors such as the Nuclear Safety Research Reactor (NSRR) to evaluate the performance of irradiated fuel rods under RIA conditions. In these test programs, comparisons have been made between large grain and standard grain fuel rod performance (e.g., NSRR test OI-10 vs. OI-11). Tests have also been performed on a variety of different fuel compositions and doping agents. Please review the extensive RIA empirical database and compile data to characterize the fuel swelling of  $\text{Cr}_2\text{O}_3$ -doped fuel under RIA conditions.

## c. The TR states that "[

]."

No data is provided to quantify the fine fuel fragmentation or transient fission gas release of the  $\text{Cr}_2\text{O}_3$ -doped fuel or justify the concluding remarks that on balance  $\text{Cr}_2\text{O}_3$ -doped fuel is anticipated to have the same behavior as standard  $\text{UO}_2$  under RIA conditions. Hundreds of prompt pulse tests have been conducted in research reactors such as NSRR to evaluate the performance of irradiated fuel rods under RIA conditions. In these test programs, comparisons have been made between large grain and standard grain fuel rod performance (e.g., NSRR test OI-10 vs. OI-11). Tests have also been performed on a variety of different fuel compositions and doping agents. Please review the extensive RIA empirical database and compile data to characterize the fuel fragmentation and fission gas release of  $\text{Cr}_2\text{O}_3$ -doped fuel under RIA conditions. In addition, provide justification for the applicability of the transient fission gas release model described in Section 4 of DG-1327 to  $\text{Cr}_2\text{O}_3$ -doped fuel.

**RAI-8**

Some figures in the TR contain large and diverse datasets which NRC staff would like to examine in more detail.

- a. Please submit the data used to generate Plot 7-8, "Fission Gas Release Measured vs Calculated for Chromia-doped Database." Please include grain size and chromia content for each data point.
- b. Please submit the data used to generate Plot 10-1, "Ramp Test Data Showing Increased Fuel Failure Threshold for Chromia-Doped Fuel." Please include grain size and chromia content for each data point.

**RAI-9**

The Halden reactor is an instrumented heavy water moderated BWR used extensively to perform safety-focused research into materials and fuel behavior under prolonged irradiation programs. Halden instrumented fuel assembly 716 studied the behavior of large grain  $\text{Cr}_2\text{O}_3$ -doped fuel and large grain  $\text{UO}_2$  fuel. Please include the data generated from Halden-716 to validate the RODEX4 models.

**RAI-10**

During an audit on April 11 - 12, 2017, AREVA highlighted its request (as stated in the TR) to remove the NRC staff's limitation on analytical grain size placed on the approval of RODEX4. Section 2 of the TR states "The qualification of RODEX4 to chromia-doped fuel also justifies the removal of the grain size restriction imposed in the Safety Evaluation for Reference 20." The NRC staff needs additional information to evaluate the appropriateness of this change with respect to standard  $\text{UO}_2$ .

- a. Please submit supporting evidence for fission gas release, as well as any other properties which include grain size in RODEX4.
- b. The TR details the addition of a new intragranular swelling model for chromia-doped  $\text{UO}_2$ .
  - i. Will this model also be applied to standard  $\text{UO}_2$ ?
  - ii. If so, will it be applied to all standard  $\text{UO}_2$ , or will it only apply above a certain grain size threshold?
  - iii. Please show that existing swelling experimental data is correctly predicted using the configuration that is being requested for approval.

**RAI-11**

During an audit on April 11 - 12, 2017, AREVA clarified that approval for gadolinia (Gad) doped fuel with chromia dopant is being requested as well. The TR includes some discussion of Gad+Cr properties, but many properties of this fuel are not discussed. For the properties listed

below, please discuss if AREVA expects there to be a difference between Gad and Gad+Cr fuel pellets, the justification for this, and if a change will be made to licensing calculations.

- a. Microstructure – This plays a prominent part in many of the explanations in the TR; how does the addition of gadolinia dopant impact the microstructure of chromia-doped fuel?
- b. Grain size and growth – this section relies heavily on the microstructure of the fuel as a justification for the behavior.
- c. Tensile fracture strength
- d. Creep and plastic deformation
- e. Fuel pellet cracking
- f. In-reactor densification
- g. High Burnup Structure formation
- h. Washout behavior
- i. Performance under loss-of-coolant accident (LOCA) conditions
- j. Performance during a RIA
- k. PCI benefits

#### **RAI-12**

Section 5.3.1 discusses the performance of  $\text{Cr}_2\text{O}_3$ -doped fuel under LOCA conditions. The TR states “[

]” Please provide supporting evidence from the fuel examinations.

#### **RAI-13**

NUREG-1465 describes a more realistic estimate of the radiological species released to containment in the event of a severe reactor accident involving substantial meltdown of the core. That document describes the specific nuclide types, quantities, chemical form, phase, and timing of release into containment. Please provide justification for the applicability of NUREG-1465 to  $\text{Cr}_2\text{O}_3$ -doped fuel.

#### **RAI-14**

Section 4.12 of the TR discusses the effect of chromia dopant on the formation of the high burnup structure (HBS). The following questions refer to this section.

- a. During the discussion on HBS, the burnup levels which experience HBS formation are compared for doped and standard  $\text{UO}_2$ . The TR states “[

]” The data presented is illogical and does not support the conclusions. Please explain if this statement is in error.

- b. Please provide evidence from the hot-cell post irradiation examination studies supporting the statements for chromia-doped fuel regarding HBS.

# framatome

March 28, 2018

NRC:18:011

U.S. Nuclear Regulatory Commission  
Document Control Desk  
11555 Rockville Pike  
Rockville, MD 20852

## **Additional Information Regarding ANP-10340P, "Incorporation of Chromia-Doped Fuel Properties in AREVA Approved Methods"**

Ref. 1: Letter Gary A. Peters (AREVA Inc.) to Document Control Desk (NRC), "Request for Review and Approval of ANP-10340P, Revision 0, 'Incorporation of Chromia-Doped Fuel Properties in AREVA Approved Methods'," NRC:16:010, April 29, 2016.

Ref. 2: Letter, Letter Gary Peters (AREVA Inc.) to Document Control Desk (NRC), "Response to Request for Additional Information Regarding ANP-10340P, 'Incorporation of Chromia-Doped Fuel Properties in AREVA Approved Methods'," NRC:17:045, October 27, 2017.

Framatome Inc. (Framatome, formally AREVA Inc.) requested the NRC's review and approval of the topical report ANP-10340P, "Incorporation of Chromia-Doped Fuel Properties in AREVA Approved Methods" in Reference 1. A response to a Request for Additional Information (RAI) was provided in Reference 2.

The NRC provided an additional comment on ANP-10340P in an email on March 6, 2018. A response to the additional comment is provided in Revision 1 of the Response to Request for Additional Information.

Framatome considers some of the information contained in the enclosed documents to be proprietary. As required by 10 CFR 2.390(b) an affidavit is enclosed to support the withholding of the information from public disclosure. Proprietary and non-proprietary versions of the RAI responses are enclosed.

There are no commitments within this letter or its enclosures.

Framatome Inc.  
3315 Old Forest Road  
Lynchburg, VA 24501  
Tel: (434) 832-3000

[www.framatome.com](http://www.framatome.com)



If you have any questions related to this submittal please contact Ms. Gayle F. Elliott, (Product Licensing Manager). She may be reached by telephone at 434-832-3347 or by e-mail at [Gayle.Elliott@framatome.com](mailto:Gayle.Elliott@framatome.com)

Sincerely,



Gary Peters, Director  
Licensing & Regulatory Affairs  
Framatome, Inc.

cc: J. G. Rowley  
Project 728

Enclosures:

1. ANP-10340Q1P, Revision 1, Response to Request for Additional Information-ANP-10340
2. ANP-10340Q1NP, Revision 1, Response to Request for Additional Information-ANP-10340
3. Notarized Affidavit

## AFFIDAVIT

STATE OF WASHINGTON    )  
                                  ) ss.  
COUNTY OF BENTON        )

1. My name is Alan B. Meginnis. I am Manager, Product Licensing, for Framatome Inc. and as such I am authorized to execute this Affidavit.

2. I am familiar with the criteria applied by Framatome to determine whether certain Framatome information is proprietary. I am familiar with the policies established by Framatome to ensure the proper application of these criteria.

3. I am familiar with the Framatome information contained in the report ANP-10340Q1P, Revision 1, "Response to Request for Additional Information- ANP-10340 Incorporation of Chromia-Doped Fuel Properties in AREVA Approved Methods," dated March 2018 and referred to herein as "Document." Information contained in this Document has been classified by Framatome as proprietary in accordance with the policies established by Framatome for the control and protection of proprietary and confidential information.

4. This Document contains information of a proprietary and confidential nature and is of the type customarily held in confidence by Framatome and not made available to the public. Based on my experience, I am aware that other companies regard information of the kind contained in this Document as proprietary and confidential.

5. This Document has been made available to the U.S. Nuclear Regulatory Commission in confidence with the request that the information contained in this Document be withheld from public disclosure. The request for withholding of proprietary information is made in accordance with 10 CFR 2.390. The information for which withholding from disclosure is

requested qualifies under 10 CFR 2.390(a)(4) "Trade secrets and commercial or financial information."

6. The following criteria are customarily applied by Framatome to determine whether information should be classified as proprietary:

- (a) The information reveals details of Framatome's research and development plans and programs or their results.
- (b) Use of the information by a competitor would permit the competitor to significantly reduce its expenditures, in time or resources, to design, produce, or market a similar product or service.
- (c) The information includes test data or analytical techniques concerning a process, methodology, or component, the application of which results in a competitive advantage for Framatome.
- (d) The information reveals certain distinguishing aspects of a process, methodology, or component, the exclusive use of which provides a competitive advantage for Framatome in product optimization or marketability.
- (e) The information is vital to a competitive advantage held by Framatome, would be helpful to competitors to Framatome, and would likely cause substantial harm to the competitive position of Framatome.

The information in the Document is considered proprietary for the reasons set forth in paragraphs 6(b), 6(c), 6(d) and 6(e) above.

7. In accordance with Framatome's policies governing the protection and control of information, proprietary information contained in this Document have been made available, on a limited basis, to others outside Framatome only as required and under suitable agreement providing for nondisclosure and limited use of the information.

8. Framatome policy requires that proprietary information be kept in a secured file or area and distributed on a need-to-know basis.

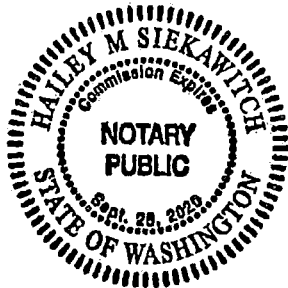
9. The foregoing statements are true and correct to the best of my knowledge,  
information, and belief.

Alan B. Mag...

SUBSCRIBED before me this 26<sup>th</sup>  
day of March, 2018.

Hailey M. Siekawitch

Hailey M Siekawitch  
NOTARY PUBLIC, STATE OF WASHINGTON  
MY COMMISSION EXPIRES: 9/28/2020



**Response to Request for Additional  
Information- ANP-10340**

ANP-10340Q1NP  
Revision 1

Incorporation of Chromia-Doped Fuel  
Properties in AREVA Approved Methods

Topical Report

March 2018

Framatome Inc.

---

**Copyright © 2018**

**Framatome Inc.  
All Rights Reserved**

**Nature of Changes**

Item	Section(s) or Page(s)	Description and Justification
1	8-7 to 8-9	Added a response to an additional comment from the NRC on the RODEX4 FGR model received in an email on March 6, 2018.

## Contents

	<u>Page</u>
1.0 RAI 1 .....	1-1
2.0 RAI 2 .....	2-1
3.0 RAI 3 .....	3-1
4.0 RAI 4 .....	4-1
5.0 RAI 5 .....	5-1
6.0 RAI 6 .....	6-1
7.0 RAI 7 .....	7-1
8.0 RAI 8 .....	8-1
9.0 RAI 9 .....	9-1
10.0 RAI 10 .....	10-1
11.0 RAI 11 .....	11-1
12.0 RAI 12 .....	12-1
13.0 RAI 13 .....	13-1
14.0 RAI 14 .....	14-1
15.0 REFERENCES .....	15-1
16.0 MARKUP PAGES .....	16-1



### List of Tables

Table 4—1	Summary of Melting Temperature Measurements .....	4-5
Table 7—1	Summary of Gadolinia Fuel RIA Tests in NSRR (Reference 7-3) .....	7-9
Table 8—1	FGR Database for Chromia-Doped Fuel .....	8-2
Table 8—2	FGR Dataset of Standard Non-Doped Fuel Associated with the Chromia-Doped Database .....	8-4
Table 8—3	Standard UO <sub>2</sub> Liner Fuel Rod Power Ramps – Low Burnup .....	8-5
Table 8—4	Standard UO <sub>2</sub> Liner Fuel Rod Power Ramps – High Burnup .....	8-5
Table 8—5	Standard UO <sub>2</sub> Liner Fuel Rod Power Ramps – Very High Burnup .....	8-6
Table 8—6	Chromia-Doped UO <sub>2</sub> Non-Liner Fuel Rod Power Ramps – BWR .....	8-6
Table 8—7	Chromia-Doped UO <sub>2</sub> Non-Liner Fuel Rod Power Ramps – PWR .....	8-6
Table 9—1	Salient Features and Measured Data for Modelled Rods of IFA-677 .....	9-9
Table 9—2	Salient Features and Measured Data for Modelled rods of IFA-716 .....	9-10

### List of Figures

Figure 4—1 Measured Melting (Freezing) Temperatures for Non-Doped and Chromia-Doped $\text{UO}_2$ .....	4-6
Figure 4—2 Measured Melting (Freezing) Temperatures for Non-Doped and Chromia-Doped 2 wt% Gad Fuel.....	4-7
Figure 4—3 Measured Melting (Freezing) Temperatures for Non-Doped and Chromia-Doped 5.5 wt% Gad Fuel.....	4-8
Figure 4—4 Measured Melting (Freezing) Temperatures for Non-Doped and Chromia-Doped 10 wt% Gad Fuel.....	4-9
Figure 5—1 Cr-O Phase Diagram vs O Potential and Conditions for Different Samples Used for Solubility Studies – Black Filled Circles from Reference 5-4, Circles from Reference 5-5 and Squares from Reference 5-1 .....	5-8
Figure 5—2 Variation of Cr Solubility vs Oxygen Partial Pressure for $T > 1651\text{ C}$ to the Left and $T < 1651\text{ C}$ to the Right (from Reference 5-1) .....	5-9
Figure 5—3 Cr Solubility in $\text{UO}_2$ as Function of Temperature: At Left Insoluble $\text{Cr}_2\text{O}_3$ and At Right Insoluble Phases CrO and Cr (from Reference 5-1) .....	5-10
Figure 5—4 EPMA Radial Profiles of Mo and Cr After a Power Ramp on Chromia-Doped Fuel .....	5-11
Figure 5—5 Elements Cartography on Power Ramped Chromia-Doped Fuel, Showing Metallic Precipitates in Pellet Center That Include Cr .....	5-12
Figure 5—6 Measured and Inferred Radial Cr Profile in a Power Ramped Chromia-Doped Fuel (from Reference 5-2) .....	5-13
Figure 5—7 Cr Solubility Variation after a Power Ramp in Two Ramped Rods to Different Terminal Power Levels (from Reference 5-2) .....	5-14
Figure 5—8 Derived O Potential during a Power Ramp on Chromia-Doped Fuel Based on Measured Cr Concentrations Shown in Figure 5-6 and 5-7 (Concentrations Shown on the Dash Lines) (from Reference 5-2) .....	5-15
Figure 7—1 Fission Gas Release During RIA Tests in NSRR .....	7-10
Figure 7—2 Fission Gas Release During Post-Irradiation Annealing Tests in NFIR .....	7-11
Figure 7—3 NFIR Slow TT on Very High Burnup Fuel .....	7-12
Figure 7—4 NFIR Stair-Case TT .....	7-13
Figure 8—1 FGR Results for the Chromia-Doped Database with LHGR and Diffusion Coefficient Biased to the 95%/95% Upper Bounds.....	8-9
Figure 9—1 Fuel Rods in the IFA-677 Rig (from Reference 9-1) .....	9-11

Figure 9—2 Fuel Rods in the IFA-716 Rig .....	9-12
Figure 9—3 Rod Pressure and FGR for Rod 677-1 .....	9-13
Figure 9—4 Center Temperature at Bottom T/C for Rod 677-1 .....	9-14
Figure 9—5 Center Temperature at Top T/C for Rod 677-1 .....	9-15
Figure 9—6 Rod Pressure and FGR for Rod 677-6 .....	9-16
Figure 9—7 Rod Pressure and FGR for Rod 677-2 .....	9-17
Figure 9—8 Rod Pressure and FGR for Rod 716-1 with 7% Power Uprate After 10 khr .....	9-18
Figure 9—9 Rod Pressure and FGR for Rod 716-6 Without 7% Power Uprate .....	9-19
Figure 9—10 Rod Pressure and FGR for Rod 716-5 with 7% Power Uprate .....	9-20
Figure 9—11 Center Temperature at Top T/C for Rod 716-1 with 7% Power Uprate After 10 khr .....	9-21
Figure 9—12 Center Temperature at Top T/C for Rod 716-6 with 7% Power Uprate .....	9-22
Figure 10—1 Grain Sizes for the Fuels Used in the FGR Chromia-Doped Database .....	10-6
Figure 10—2 IGSW RODEX4 vs. Standard RODEX4: Fission Gas Release .....	10-7
Figure 10—3 IGSW RODEX4 vs. Standard RODEX4: Strain Increment During Power Ramps .....	10-8
Figure 10—4 IGSW RODEX4 vs. Standard RODEX4: Clad Diameter Change After Steady-State Irradiation .....	10-9
Figure 11—1 Creep Behavior of Chromia-Doped Gadolinia Fuel .....	11-5
Figure 11—2 Washout Studies on Gd-Doped Fuel in High Pressure Steam for 5 Days .....	11-6
Figure 11—3 Washout Studies on Gd-Doped Fuel in High Pressure Steam (BWR Conditions) for 6 Days .....	11-7
Figure 11—4 Visual Aspect After 6 Days High Pressure Steam Wash-Out Studies .....	11-8
Figure 11—5 Incipient Cracks Arrested by Oxidation for Ramped Gd-Doped Fuel, (Slide 12 from SCIP Meeting, Nov 2013 Presentation "SCIP 2 Workshop: Oxygen Supply to Cladding") .....	11-9
Figure 12—1 Cracking Patterns During Steady-State Irradiation for Doped and Non-Doped Fuels .....	12-3
Figure 12—2 Cracking Patterns Following Power Ramps for Doped and Non- Doped Fuels .....	12-4
Figure 12—3 Evolution of Pellet-Cladding Bonding of Chromia-Doped Fuel .....	12-5

Figure 12—4 Fragment Size Histogram After NFIR Post-Irradiation Annealing Test for Standard Small and Large Grain Fuels .....	12-6
Figure 14—1 HBS Layer Width vs Pellet Average Burnup from Various Investigations .....	14-7
Figure 14—2 Total Porosity of Irradiated Disks as a Function of Burnup from JRC/ITU Studies.....	14-8
Figure 14—3 HBS Area Fraction of Irradiated Disks as a Function of Burnup from JRC/ITU Studies.....	14-9
Figure 14—4 Mean ECD of the HBS Pores as a Function of Burn up from JRC/ITU Studies.....	14-10
Figure 14—5 JRC/ITU Calculated Pressure in the HBS Pores as a Function of Burn up.....	14-11
Figure 14—6 HBS Porosity in CEA Studies .....	14-12
Figure 14—7 HBS Volume Fraction from CEA Studies.....	14-13
Figure 14—8 Ratio of Xe in Bubbles / Total Xe from SIMS Studies at CEA.....	14-14
Figure 14—9 HBS Nucleation Both on Grain Boundaries and Inside the Grain for Chromia-Doped Fuel .....	14-15

### Nomenclature

<b>Acronym</b>	<b>Definition</b>
AQL	Acceptable Quality Limit
AST	Alternative Source Term
ASTM	American Society for Testing and Materials
BR3	Belgian Reactor 3
BWR	Boiling Water Reactor
CEA	Commissariat a l'Energie Atomique
CRDA	Control Rod Drop Accident
ECD	Equivalent Circle Diameter
EHPG	Enlarged Halden Program Group
EPMA	Electron Probe Micro Analysis
EXAFS	Extended X-ray Absorption Fine Structure
FGR	Fission Gas Release
HBS	High Burnup Structure
ICP-MS	Inductively Coupled Plasma-Mass Spectrometry
IFA	Instrumented Fuel Assembly
IGSW	Intergranular Gaseous Swelling
JRC/ITU	Joint Research Centre / Institute for Transuranium Elements
LCL	Lower Confidence Limit
LHGR	Linear Heat Generation Rate
LOCA	Loss Of Coolant Accident
LTR	Licensing Topical Report
MLI	Mean Linear Intercept
NAF	Neutron Absorber Fuel
ND	Neutron Detector
NFIR	Nuclear Fuel Industry Research
NSE	Normal Spectral Emissivity
NSRR	Nuclear Safety Research Reactor
PCI	Pellet-Cladding Interaction

**Nomenclature (continued)**

<b>Acronym</b>	<b>Definition</b>
PCF	Power Conversion Factor
PCMI	Pellet-Cladding Mechanical Interaction
PIE	Post-Irradiation Examination
PWR	Pressurized Water Reactor
QIA	Quantitative Image Analysis
RIA	Reactivity Initiated Accident
SCC	Stress Corrosion Cracking
SCIP	Studsвик Cladding Improvement Program
T/C	Thermocouple
TR	Topical Report
TUI	Trans-Uranium Institute
XANES	X-ray Absorption Near-Edge Structure Spectroscopy

## **Introduction**

The United States Nuclear Regulatory Commission (NRC) provided a request for additional information (RAI) regarding the topical report ANP-10340P, Revision 0 (Reference 15.1) in Reference 15.2. A total of 14 questions were received from the NRC.

The following sections provide the responses to the NRC questions.

**1.0 RAI 1****Question:**

Section 4.0 of the LTR defines a target chromia concentration and mentions manufacturing uncertainties on this target concentration. Section 4.1 describes the basis for the target chromia concentration including the resultant range in  $\text{UO}_2$  grain size.

- a. Please define the manufacturing specification limits on chromia content, and describe AREVA's quality assurance procedures to ensure that the fuel produced remains within these limits.
- b. Please define the manufacturing specification limits on grain size, and describe AREVA's quality assurance procedures to ensure that the fuel produced remains within these limits.

**Response:**Response to RAI-1.a

The chromium content of the chromia-doped pellet product is controlled by specifying a range of [                    ]  $\mu\text{gCr/gU}$  for each pellet lot. This is the bounding range for the chromia-doped pellet chromium content.

The nominal value of  $1250 \mu\text{gCr/gU}$  corresponds to  $1600 \mu\text{gCr}_2\text{O}_3/\text{gUO}_2$  defined as nominal in ANP-10340P. The  $\mu\text{g/gU}$  unit for dopant concentration is controlled in the specification because this is what is measured in production by mass spectrometry. The initial powder blending stage uses  $\text{Cr}_2\text{O}_3$  in an amount that takes into account chromia [        ] during sintering in order to obtain the desired chromium concentration in the final as-sintered pellet.



The product specification's quality inspection sampling plan requires the analysis of chromium content of several individual pellets according to the Acceptable Quality Limit (AQL) adopted and each analysis result must meet the requirement for the lot to be acceptable (released).

The principal, but not only, method of analyzing chromium is Inductively Coupled Plasma-Mass Spectrometry (ICP-MS). The laboratory's standards program monitors the precision and accuracy of the ICP-MS test method and equipment.

Response to RAI-1.b

The chromia-doped pellet product specification states that [

]

This is consistent with the grain size range of the database, which consists of chromia-doped fuel rods with pellets having grain sizes centered on 50  $\mu\text{m}$ , as shown for the database used in code qualification in ANP-10340P and further illustrated in the response to RAI-10.

The product specification's quality inspection sampling plan requires analysis of grain size on several pellets (according to the AQL adopted) to calculate the 95% LCL value. Grain size is measured on longitudinally sectioned pellets as the mean linear intercept (MLI), according to the ASTM E112 standard.

As-manufactured chromia-doped grain size measurements, which are acquired continuously, will be evaluated annually and included in the yearly update of the manufacturing uncertainties per the approved RODEX4 topical report.

**2.0 RAI 2****Question:**

Section 5.3.2 of the LTR states that [

] Section 4.2 states that [

]

- a. During an audit on April 11-12, 2017, AREVA mentioned that additional clarification to these descriptions was necessary. Please provide the appropriate changes.
- b. Given this new description, provide justification for the calculational method for theoretical density.

Equation 4-4 appears to contain an error or typo. Please provide a correction.

**Response:**

Some earlier studies (References 2-1 and 2-2) concluded that Cr in solid solution in  $\text{UO}_2$  dissolves as interstitial. Reference 2-1 used this conclusion as support for the measured enhancement of diffusional release in chromia-doped fuel. Recent analytical studies clearly concluded that Cr is present mostly in substitution in the U sub-lattice (References 2-3 and 2-4).

The chromia-doped fuel studied in Reference 2-1 was manufactured in the laboratory and did not conform to AREVA's current sintering process; specifically, the Oxygen potential was not controlled during sintering of the experimental chromia doped fuel tested in Reference 2-1 and therefore, the Cr chemical state in the  $\text{UO}_2$  lattice is not representative of AREVA's chromia-doped fuel product. As described in ANP-10340P

and in response to RAI-5, a controlled combination of temperature and Oxygen potential are required during sintering for the specific dissolved Cr content in order to obtain the desired chromia-doped fuel properties. The chromia doped fuel in Reference 2-1 has a lower chromia content of 650 ppm and was sintered in reducing conditions; consequently, the chromia-doped fuel in Reference 2-1 did not have the desired microstructure.

#### Response to RAI-2.a

The correct characterization of chromia being in solid solution in  $\text{UO}_2$  is that, [

]

However, the exact location of Cr is not the classical random replacement of U atoms, but rather a small planar cluster of Cr atoms (Reference [2-3]). More details are provided in the response to RAI-5.

Mark up pages are provided to ANP-10340P in Section 16 of this document to modify the description of the Cr state in the  $\text{UO}_2$ .

#### Response to RAI-2.b

The calculation of the theoretical density of chromia-doped fuel, which has been described in Section 4.2 of ANP-10340P, is applicable to any pure or solid solution material because it is based on calculating the mass corresponding to the unit cell for the oxide with its specific composition and the volume of that unit cell. Therefore this calculational procedure is applicable to any form of solution, either substitutional or interstitial, the potential impact of the specific solute state being reflected in the lattice parameter of the solution.

This calculational approach was also used in the initial RODEX4 topical report (Reference 2-4) for non-doped and neutron absorber fuel (NAF) fuel types and it is also described in Reference 2-5.

Response to RAI-2.c

The formula in ANP-10340P Equation 4-4 is the fractional theoretical density of doped fuel with respect to the theoretical density of non-doped fuel; however, the symbol used on the left-hand side of Equation 4-4 represents the absolute density and the formula has to be corrected by adding on the right-hand side a multiplication by the theoretical density of non-doped fuel, as follows:

$$\rho_{th\ doped} = \frac{M_{ox\ doped}}{M_{ox}} \rho_{th\ non-doped}$$

A markup page to ANP-10340P is provided in Section 16 of this document to correct the equation.

**References for Response 2:**

- 2-1 S. Kashibe, K. Une, "Effect of additives ( $\text{Cr}_2\text{O}_3$ ,  $\text{Al}_2\text{O}_3$ ,  $\text{SiO}_2$ ,  $\text{MgO}$ ) on diffusional release of  $^{133}\text{Xe}$  from  $\text{UO}_2$  fuels," Jo. of Nucl. Mat. 254 (1998) 234-242.
- 2-2 A. Leenaers et al, "On the solubility of chromium sesquioxide in uranium dioxide fuel," Jo. of Nucl. Mat. 317 (2003) 62-68.
- 2-3 M. Fraczekiewicz, " Dopage au chrome du dioxyde d'uranium: modifications physiques induites," PhD Thesis, Universite de Grenoble, 2010.
- 2-4 BAW-10247-PA Revision 0, "Realistic Thermal-Mechanical Fuel Rod Methodology for Boiling Water Reactors," AREVA Inc., February 2008.
- 2-5 T. Cardinaels et al, "Chromia doped  $\text{UO}_2$  fuel: Investigation of the lattice parameter," JNM, 424 (2012) 252-260.

### 3.0 RAI 3

#### Question:

Section 4.2 of the LTR states that final stoichiometry of  $\text{Cr}_2\text{O}_3$ -doped fuel is [ ]

a. Please describe the [ ] and any manufacturing specifications associated with stoichiometry.

b. Please describe the impact of [ ]

#### Response:

##### Response to RAI-3.a

Both the standard and chromia-doped pellet product specifications state that stoichiometry, i.e., the oxygen-to-uranium ratio (O/U) shall be within the range of [ ] Product specification inspection sampling plans require O/U analysis of several individual pellets (according to the adopted AQL) and each analysis result must meet the requirement for the lot to be acceptable (released). Pellets analyzed for O/U come from the sample taken by quality inspection and are then submitted to the laboratory.

The laboratory measures the O/U of both pellet types by [ ]

[ ] The laboratory's standards program monitors the precision and accuracy of test methods and equipment.

There are no significant differences in O/U between standard and chromia-doped pellets. The average O/U from the recent [

] The O/U ratios of full-production scale chromia-doped pellets are expected to be consistent with standard pellet values.

Response to RAI-3.b

The response to item a, above, showed that there is no difference with regards to stoichiometry between standard and chromia-doped pellets. Therefore, there is no impact on the behavior of the standard and chromia-doped fuel types. The specific behavior of the dopant in operation is described in response to RAI-5.

#### 4.0 RAI 4

##### Question:

Section 5.2 of the LTR describes the impact of  $\text{Cr}_2\text{O}_3$ -dopant on fuel melting point.

a. Given that the melting temperature of  $\text{Cr}_2\text{O}_3$ -doped fuel [

]

$\text{Cr}_2\text{O}_3$ -doped fuel melting point is not incorporated into RODEX4 and downstream safety analyses. Please provide justification.

b. Please describe the statistical approach used to calculate the [

] fuel melting temperature.

##### Response:

##### Response to RAI-4.a

The fuel melting temperature for  $\text{UO}_2$  fuel in the RODEX4 methodology (References 4-1 and 4-2) is a constant that is not burnup dependent because it reflects the minimum value over the anticipated burnup range. The effect of the chromia dopant was determined to be a constant [ ] of the standard non-doped  $\text{UO}_2$  fuel melting temperature.

The verification of calculated centerline temperature compliance with the melting point criterion can then be made either inside RODEX4 or outside the fuel code, as part of the software that manages the set of required RODEX4 runs and post-processes the results. The latter option was chosen for the set of sample cases shown in ANP-10340P. RODEX4 has been updated to include the adjustment of the melting temperature for chromia-doped fuel. The [ ] in melting temperature for chromia-doped fuel is activated by the chromia-doped fuel input flag.

### Response to RAI-4.b

The results of the melting temperature measurements performed by JRC/ITU were available during the development of ANP-10340P as [

## 1 The

results have been summarized in Table 5.2 of ANP-10340P where the rightmost column contains the lower bound values calculated as described above and summarized below:

$$\left[ \begin{array}{c} (4-1) \\ (4-2) \end{array} \right]$$

The chromia-doped melting temperature adjustment term of [ ] was determined by calculating the difference between the lower bounds of melting temperatures of chromia-doped and non-doped UO<sub>2</sub> fuels (rightmost column values in Table 5.2 of ANP-10340P).

As mentioned in ANP-10340P, the description of the statistical method used to determine the total uncertainty was the same as the one documented in Reference 16 of ANP-10340P. The approach described above was chosen because the RODEX4 approach for the fuel melting temperature is to use a single lower bound value to represent the minimum fuel melt temperature over the allowed burnup range. A different approach would be necessary if the melting temperature were represented as a nominal fuel melting temperature as a function of burnup.



In order to obtain the total uncertainty value, JRC/ITU always used formula (3) of Reference 16 of ANP-10340P, which is the general formula for the independent error propagation law when the uncertainty sources are independent. Three main uncertainty sources have been considered in the analysis, as follows:

- 1) the "data dispersion" is the standard deviation of the experimental data points obtained for each individual fuel composition; this uncertainty contribution can be called  $dT_p$
- 2) The uncertainty due to the normal spectral emissivity value mentioned on page 8 of Reference 15 of ANP-10340P. For all samples an approximately constant value [

]

- 3) The third source of uncertainty is purely instrumental, and it is the uncertainty in the pyrometer calibration. At JRC/ITU the pyrometer was calibrated against a standard tungsten filament lamp, with an uncertainty indicated by the constructor and the calibration lab. The calibration uncertainty results in an approximately constant temperature uncertainty,  $dT_c$ , [ ] which is the value that we used for all samples.

Finally, the uncertainty values were obtained by using the formula:

$$dT_{tot} = \sqrt{dT_p^2 + dT_e^2 + dT_c^2} \quad (4-3)$$

The first uncertainty component above is derived as the statistical processing of a sample of finite size based on the raw data, which are presented in Table 4-1. The population sigma,  $dT_p$ , was obtained by using the corresponding Owen's adjustment factor (Reference 4-3) for the respective sample size, by the following formula:

$$\sigma(\text{population}) = \sigma(\text{sample}) * k(\text{sample size}) / k(\text{population})$$

In the above formula the k factors are one-sided 95/95 values, the one in the denominator being 1.645, the infinite-size sample value, hence applicable to the entire population.

With the above detailed statistical processing of the raw data and using the experimental uncertainties provided by JRC/ITU the total uncertainties were calculated according to Equation (4-3) and the standard deviations reported in Reference 16 of ANP-10340P were confirmed.

The raw data are illustrated in Figures 4-1 to 4-4 below and show that there is complete overlap between the non-doped and doped data sets for gadolinia fuels, while a small shift is noticed for the non-doped and chromia-doped  $\text{UO}_2$ .

Therefore, it was concluded that chromia doping does not affect gadolinia fuel melting temperature, which was the expected outcome considering that chromia content is 1-2 orders of magnitude lower than gadolinia content.

**Table 4—1 Summary of Melting Temperature Measurements**

--	--



**Figure 4—1 Measured Melting (Freezing) Temperatures for  
Non-Doped and Chromia-Doped  $\text{UO}_2$**



**Figure 4—2 Measured Melting (Freezing) Temperatures for  
Non-Doped and Chromia-Doped 2 wt% Gad Fuel**

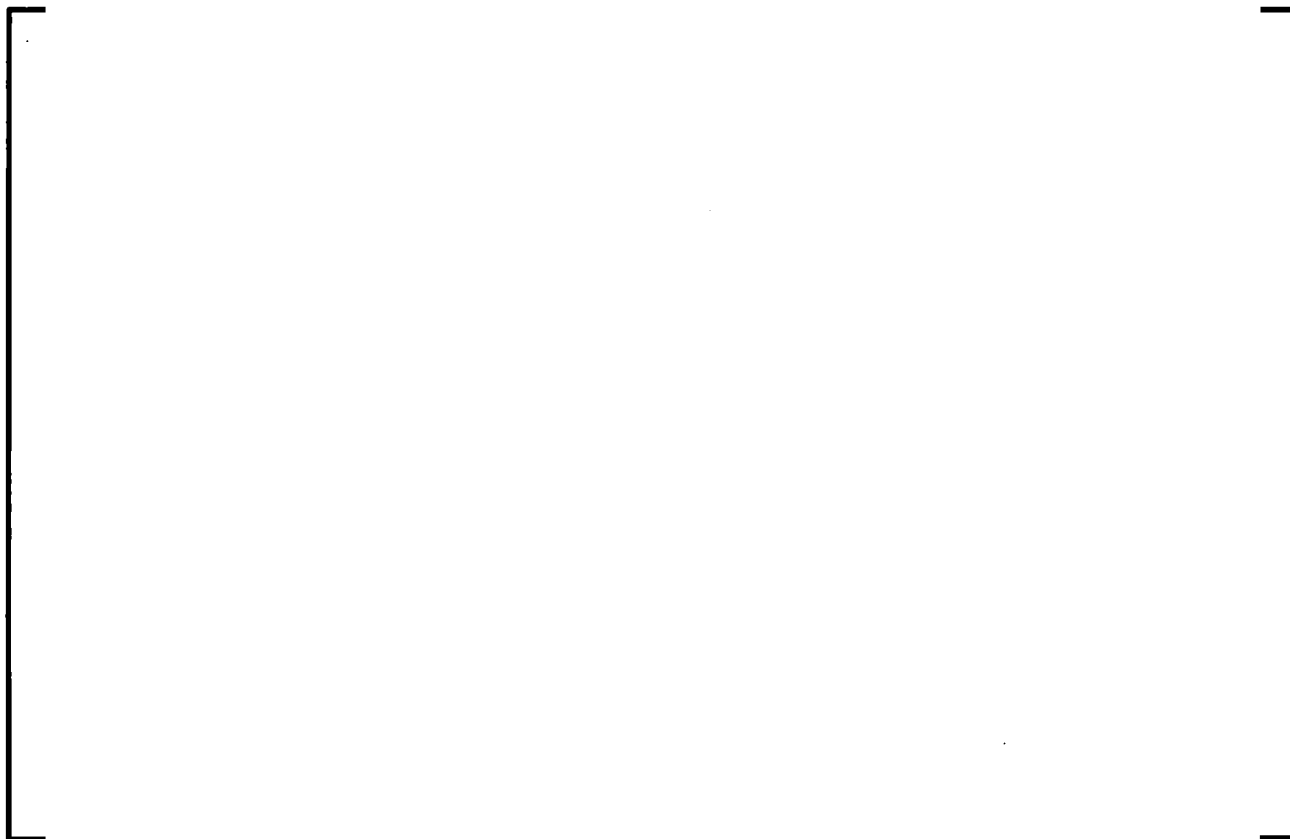


**Figure 4—3 Measured Melting (Freezing) Temperatures for  
Non-Doped and Chromia-Doped 5.5 wt% Gad Fuel**



**Figure 4—4 Measured Melting (Freezing) Temperatures for  
Non-Doped and Chromia-Doped 10 wt% Gad Fuel**

**References for Response 4:**

- 4-1 BAW-10247PA Revision 0, "Realistic Thermal-Mechanical Fuel Rod Methodology for Boiling Water Reactors," AREVA Inc., 2008.
- 4-2 EMF-2994(P), Revision 0, "RODEX4: Thermal-Mechanical Fuel Rod Performance Code Theory Manual," AREVA Inc., August 2004.
- 4-3 D. B. Owen "Factors for One-Sided Tolerance Limits and for Variable Sampling Plans," SCR-607, March 1963.

## 5.0 RAI 5

### Question:

During an audit, AREVA stated that, at normal operating temperatures, chromium

[ ] or some other process, and

[ ]

- a. Please describe this phenomenon in greater detail.
- b. Please provide any data from hot-cell examinations describing the [ ]
- c. Section 4.1 of the LTR states:  $\text{Cr}_2\text{O}_3$  was also found to accelerate fission gas diffusion coefficients when added in quantities of approximately 5000 wppm (Reference 2), which led to dopant segregation on grain boundaries during irradiation. Does the migration of chromium during operation lead to this issue?

### Response:

Chromia-doped pellets are manufactured by pressing and then sintering a blended powder with an addition of chromia [ ]

The sintering takes place in a controlled atmosphere with a given combination of oxygen potential and temperature in the hot region of the sintering furnace in order to establish the conditions for the Cr solubility state to be in the stability domain of CrO liquid phase (see the small triangular region to the right in Figure 5-1), which is conducive to enhanced grain growth and hence assures a large grain size doped pellet.

The solubility of chromia in the  $\text{UO}_2$  matrix is determined by the peak temperature and oxygen potential during sintering. The cooling rate is fast enough to freeze in the high-



temperature solution, by not allowing sufficient time for the equilibrium solute state at lower temperatures to be reached.

Generally, Cr content is slightly above the solubility limit. Thus, in the final product, the majority of the chromium content can be found as a soluble fraction in solid solution in  $\text{UO}_2$  and only a small part as an insoluble fraction in the form of separate Cr oxide precipitates. As shown in Figure 5-2 the nature of the initial solid Cr-O precipitates may change within nominal and off-nominal operating conditions, depending on fuel temperature and oxygen potential conditions.

The solubility of Cr in  $\text{UO}_2$  is dependent on three parameters, namely, temperature, oxygen potential and total Cr content. These three parameters are sufficient because at high temperatures (greater than  $1500^\circ\text{C}$ ), the fast kinetics of chemical reactions makes the system thermodynamically controlled, while at low temperatures the reaction kinetics is very slow and practically no change occurs.

Figure 5-1 illustrates the Cr solubility dependency on O potential, by showing the areas of stability of various Cr solid phases as a family of curves for different temperatures.

The solubility law of chromium in  $\text{UO}_2$  as a function of the oxygen partial pressure may be split into three linear sections:

- (i) of slope zero in the  $\text{Cr}_2\text{O}_3$  stability domain, the solid phase being of same stoichiometry as that of the soluble phase,
- (ii) of slope  $+1/4$  in the liquid CrO stability domain,
- (iii) of slope  $+3/4$  in the metallic Cr stability domain (Figure 5-2).

As the soluble chromium species in  $\text{UO}_2$  are oxygen-richer than the solid phases CrO(l) and Cr(s), the solubility increases as a function of the oxygen partial pressure in these two stability domains, as indicated by the positive value of the slopes, namely,  $+1/4$ ,  $+3/4$  for the solubility curves. Conversely, the slope of the solubility curve is zero inside

the stability area of  $\text{Cr}_2\text{O}_3(\text{s})$ , implying that chromium solubility is independent of the oxygen partial pressure in those conditions.

Based on previous data (reviewed in Reference 5-1) and on the recent studies reported in Reference 5-1, the dependency on temperature of Cr solubility in  $\text{UO}_2$  can be summarized as follows (illustrated in Figure 5-3):

- (i) the solubility of chromium increases with temperature in the  $\text{Cr}_2\text{O}_3$  stability range (Figure 5-3, left);
- (ii) the solubility of chromium decreases with temperature in the CrO and Cr stability areas (Figure 5-3, right);
- (iii) the solubility Cr metal in  $\text{UO}_2$  is much lower than that of the  $\text{Cr}_2\text{O}_3$  oxide.

This indicates that the solubility of chromium in  $\text{UO}_2$  at high temperature is highly dependent on oxygen potential conditions, which control both the soluble and insoluble forms of chromium in  $\text{UO}_2$ .

Solubility measurements collected in well-defined experimental conditions in the laboratory, which are shown on the right-hand side of Figure 5-1, were performed on hyper-stoichiometric  $\text{UO}_2$  pellets, initially doped with  $\text{Cr}_2\text{O}_3$  and then sintered for a few hours (~4 h) beyond 1700 °C under a controlled moistened atmosphere (pure  $\text{H}_2$  or  $\text{Ar}/\text{H}_2$ ). The gas moisture was maintained steady throughout the sintering process to ensure the oxygen partial pressure of the system remained constant (which also defines the chemical state of chromium during sintering). The partial pressure of water in the sintering atmosphere was controlled by measuring the dew point of the gas and the resulting oxygen potential was estimated with an empirical formula (Reference 5-1). The Cr in the matrix was determined by EPMA and in preliminary studies indirectly by the effect on grain size (Reference 5-1).

Qualitatively, the results show that the solubility of metallic chromium in  $\text{UO}_2$  is an increasing function of the oxygen partial pressure but a decreasing function of

temperature. However, the solubility of the chromium oxide ( $\text{Cr}_2\text{O}_3$ ) in  $\text{UO}_2$  increases with temperature. For all temperatures, the solubility of chromium in  $\text{UO}_2$  increases with the oxidation state of chromium in the solid phase, i.e.  $\text{Cr}^0 < \text{Cr}^{+2}\text{O} < \text{Cr}_2^{+3}\text{O}_3$ .

The precipitates observed in samples sintered under oxidizing conditions conducive to the CrO liquid phase stability domain, were consistent with a partial and incomplete disproportionation of the liquid CrO phase into  $1/3 \text{ Cr}$  and  $2/3 \text{ Cr}_2\text{O}_3$ . The former can associate with other metallic precipitates, while the latter remains associated with CrO and this explains the measured O/Cr ratio being slightly greater than unity.

The EPMA studies were complemented with X-ray absorption spectroscopy, using the XANES and EXAFS techniques (Reference 5-1). XANES studies reported in Reference 5-1 confirmed that Cr is in the +3 oxidation state in solution in  $\text{UO}_2$ , which corresponds to a solid solution with Cr in a quasi-substitutional state. EXAFS studies showed that a more complex state of solubilized Cr exists, in which Cr atoms are not uniformly dispersed as substitutional atoms in the U sub-lattice, but rather very small (sub-nanometric) clusters are present, which typically occupy regions of defects in the  $\text{UO}_2$  lattice. However, this Cr atom state is in equilibrium with the  $\text{UO}_2$  lattice and the condition can be characterized as quasi-substitutional with an increased lattice defect population.

#### Response to RAI-5.a

Depending on temperature and local oxygen potential during irradiation,  $\text{Cr}_2\text{O}_3$  can:

- remain dissolved as chromia in the low temperature region (below  $1400^\circ\text{C}$ ), which is characteristic of steady-state irradiations
- be reduced to Cr and evaporate, or remain in metallic precipitate – high temperature in central pellet zone during a power ramp (greater than  $1500^\circ\text{C}$ )
- be in either of the above states in a transition zone between  $1400^\circ\text{C}$  and  $1500^\circ\text{C}$

In non-doped fuel irradiated at moderate power during steady-state conditions, oxygen potential is generally set by the Mo/MoO<sub>2</sub> redox couple and the O/M of irradiated fuel remains stable, with slight decrease at higher burnups. However, at higher power levels, such as those experienced during power ramps, indications are that in the central region a reducing environment develops (Reference 5-2), which cause Cr<sub>2</sub>O<sub>3</sub> reduction that liberates oxygen in the process; the freed up oxygen most likely migrates and oxidizes the cladding inner surface, which counteracts SCC by blunting the tip of the cracks initiated after oxide cracking.

The process described above, whereby Cr<sub>2</sub>O<sub>3</sub> is reduced in the hot core of the pellet during either steady-state or transient conditions when the pellet temperature exceeds ~ 1500 C, has positive implications for fuel behavior. This is because the dopant is converted from a solubilized chromia to a metallic precipitate and therefore the thermal conductivity is restored to that of standard non-doped UO<sub>2</sub>.

The above is the combination of oxygen migration in a large temperature gradient that is set up during power ramps, or high steady-state power and the oxygen potential of the irradiated fuel that is set by the buffer elements Mo and potentially by dopants.

#### Response to RAI-5.b

The main experimental findings have been synthesized in the recently published Reference 5-2, which is the main source of the illustrations herein, together with some CEA reports.

In standard, non-doped UO<sub>2</sub>, Zr is detected in metallic precipitates at the pellet center; therefore, oxygen potential in the center of the pellet is set by the Zr/ZrO<sub>2</sub> redox couple. In chromia-doped fuel, Zr is not detected in metallic precipitates, but Cr is quasi-totally precipitated and thus oxygen potential is between that of the Zr and that of the Cr couples (at temperatures above 1500 °C).

After a power ramp, other couples than Mo/MoO<sub>2</sub> determine oxygen potential, which is set up at a lower value; this means oxygen leaves the center of the pellet.

[

]

The change in [ ] of Cr in the center of the pellet is evidenced by the x-ray cartography illustrated in Figure 5-5, in which the yellow circle shows [

]

The Cr radial profile after the power ramp is shown in Figure 5-6 based on the hot-cell examination of two ramped fuel rods. The radial profile is the same for the two rods, with a reduction in the center that starts at about the same temperature, although the power and centerline temperature were different.

This confirms the previous statement in the introduction that at high temperature (greater than 1500 °C) the state of Cr in terms of oxidation and presence as solute or metallic precipitate is thermodynamically established since the reaction kinetics are very fast. The radial profiles of the two fuel rods overlap over the common temperature range (up to 1460 °C) and the hotter one is a continuous extension of the other cooler rod (shown in Figure 5-7).

The evolution of Cr in the hot center is further illustrated in Figure 5-8.

#### Response to RAI-5.c

As stated above, Cr remains in the hot core of the pellet as part of the metallic precipitates. There is no evidence that [

]

[

] Therefore, the enhancement of the diffusion coefficient described in Reference 2 of ANP-10340P will not occur.

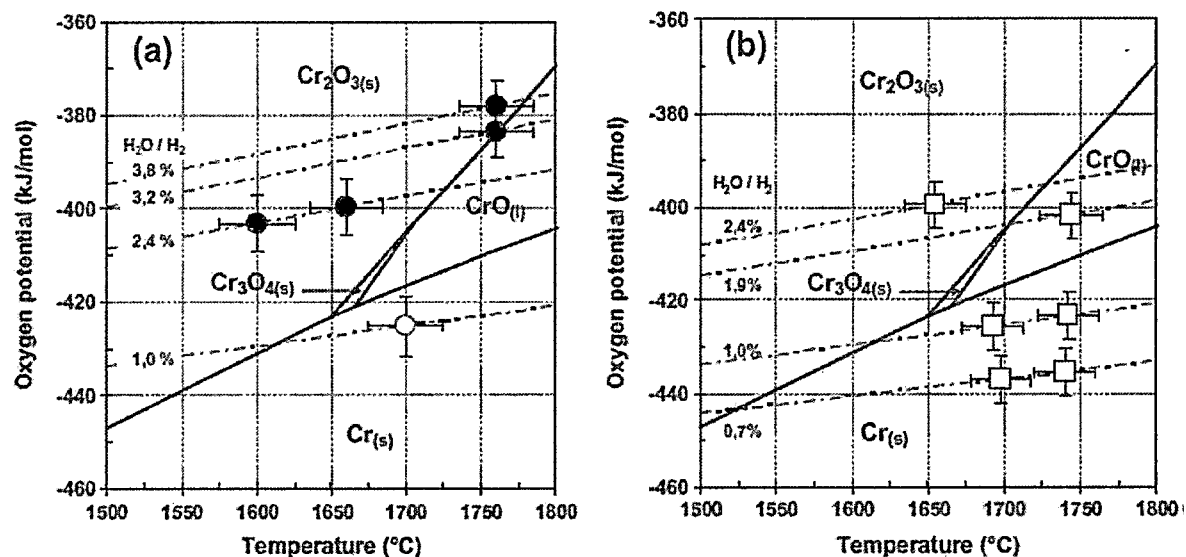


Figure 5—1 Cr-O Phase Diagram vs O Potential and Conditions for Different Samples Used for Solubility Studies – Black Filled Circles from Reference 5-4, Circles from Reference 5-5 and Squares from Reference 5-1

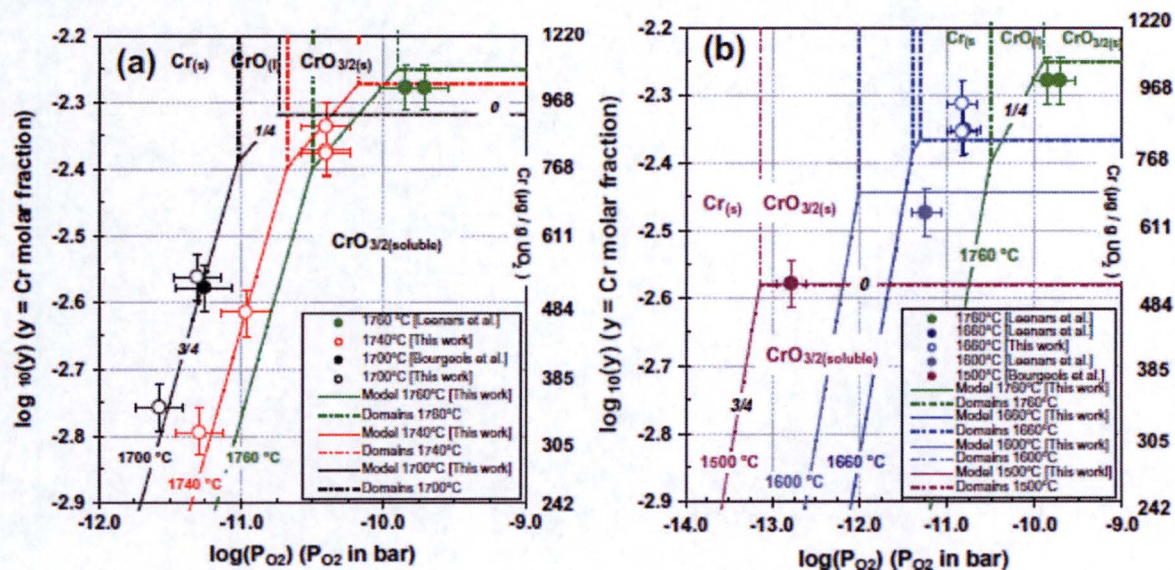


Figure 5—2 Variation of Cr Solubility vs Oxygen Partial Pressure for  
 T > 1651 C to the Left and T < 1651 C to the Right  
 (from Reference 5-1)



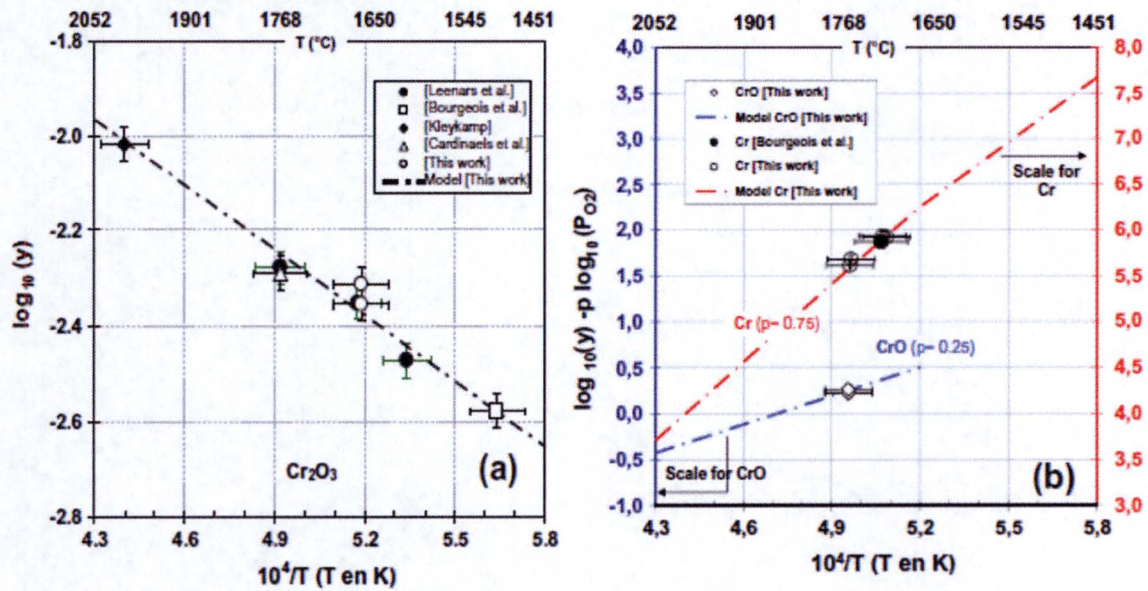


Figure 5—3 Cr Solubility in  $\text{UO}_2$  as Function of Temperature: At Left Insoluble  $\text{Cr}_2\text{O}_3$  and At Right Insoluble Phases CrO and Cr (from Reference 5-1)



**Figure 5—4 EPMA Radial Profiles of Mo and Cr After a Power Ramp  
on Chromia-Doped Fuel**



**Figure 5—5 Elements Cartography on Power Ramped Chromia-Doped Fuel, Showing Metallic Precipitates in Pellet Center That Include Cr**

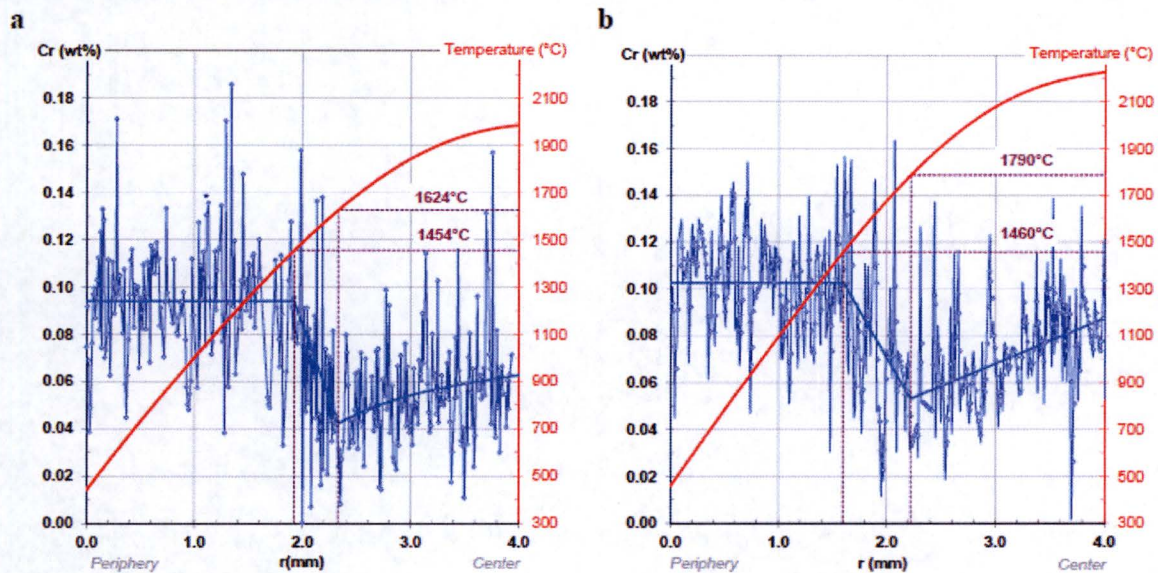


Figure 5—6 Measured and Inferred Radial Cr Profile in a Power Ramped Chromia-Doped Fuel (from Reference 5-2)



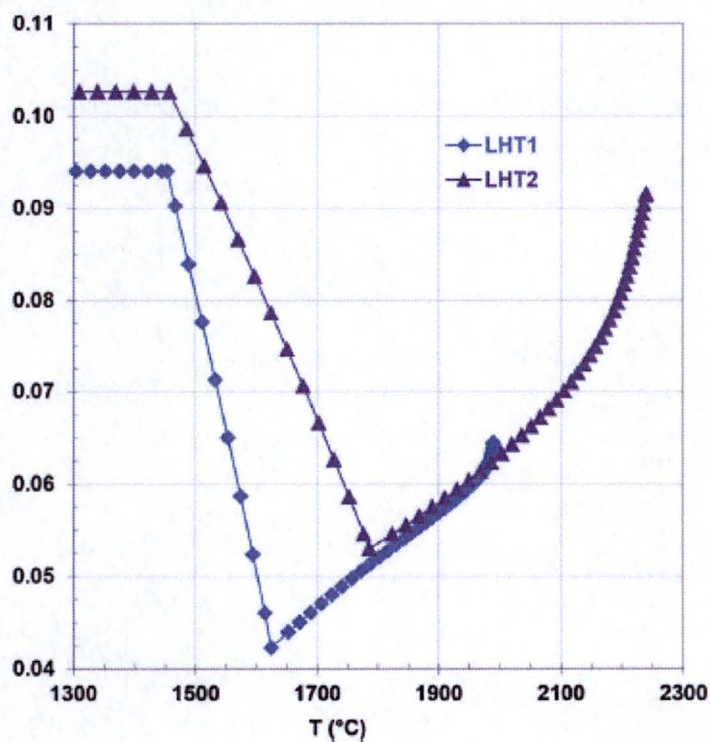


Figure 5—7 Cr Solubility Variation after a Power Ramp in Two Ramped Rods to Different Terminal Power Levels (from Reference 5-2)

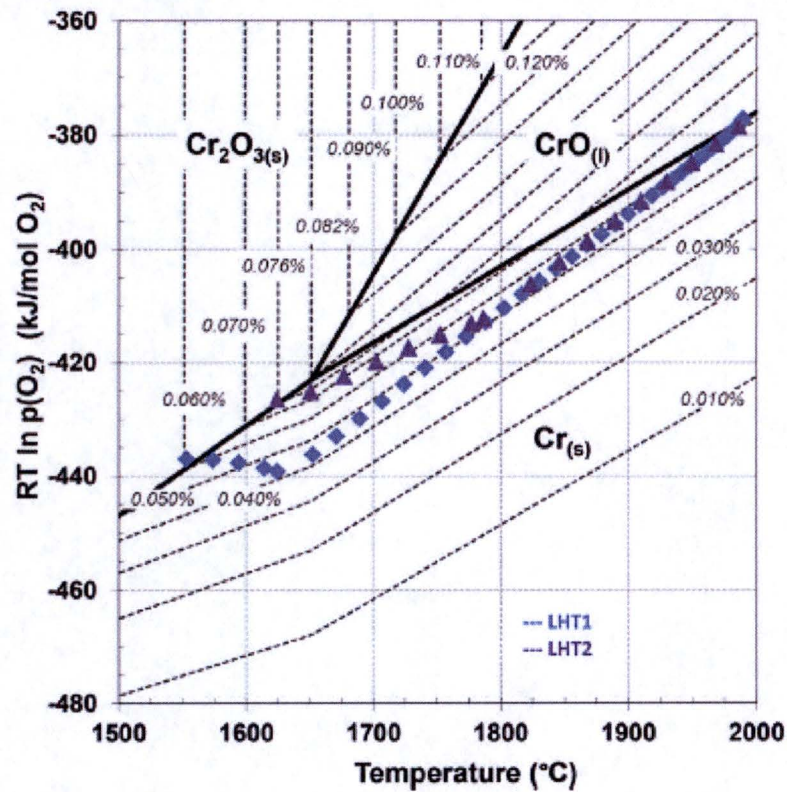


Figure 5—8 Derived O Potential during a Power Ramp on Chromia-Doped Fuel Based on Measured Cr Concentrations Shown in Figure 5-6 and 5-7 (Concentrations Shown on the Dash Lines) (from Reference 5-2)

**References for Response 5:**

- 5-1 Ch. Riglet-Martial et al, "Thermodynamics of chromium in  $\text{UO}_2$  fuel: A solubility model," Jo. of Nucl. Mat. 447 (2014) 63-72.
- 5-2 Ch. Riglet-Martial et al, "Experimental evidence of oxygen thermos-migration in PWR  $\text{UO}_2$  fuels during power ramps using in-situ oxido-reduction indicators," Jo. of Nucl. Mat. 480 (2016) 32-29.
- 5-3 V. Peres et al, "High temperature chromium volatilization from  $\text{Cr}_2\text{O}_3$  powder and  $\text{Cr}_2\text{O}_3$ -doped  $\text{UO}_2$  pellets in reducing atmospheres," Jo. of Nucl. Mat. 423 (2012) 93-101.
- 5-4 A. Leenaers, L. de Tollenaere, Ch. Delafoy, S. Van den Berghe, J. Nucl. Mater. 317 (2003) 62-68.
- 5-5 L. Bourgeois, Ph. Dehaudt, C. Lemaignan, A. Hammou, J. Nucl. Mater. 297 (2001) 313-326.

**6.0 RAI 6****Question:**

In Section 4.3 of the LTR, AREVA concludes "Therefore, a  $\text{Cr}_2\text{O}_3$  dopant level that is in the range of impurity content has a negligible effect and the thermal expansion of this fuel will be the same as for standard  $\text{UO}_2$ " However, the levels of chromia proposed in this LTR exceed the impurity limit. Please explain what is meant by this statement, or correct the text of the topical report.

**Response:**

The range of impurity content referred to in the quote from ANP-10340P, Section 4.3, is the total impurity level allowed by the ASTM specification for  $\text{UO}_2$  fuel, which is 1500  $\mu\text{g/gU}$ . This is greater than the upper bound of the Cr content, as defined in response to RAI-1. It is true that individual impurities are limited to a smaller concentration, such as the Cr limit of 250  $\mu\text{g/gU}$ . The statement Section 4.3 just emphasized the fact that elemental impurities in solution in the  $\text{UO}_2$  matrix do not affect thermal expansion, similar to Gadolinia fuel, in comparison to which the Cr concentration is one to two orders of magnitude lower than the Gadolinia concentration.



## 7.0 RAI 7

### Question:

Section 5.3.2 of the TR discusses the response of  $\text{Cr}_2\text{O}_3$ -doped fuel during a reactivity initiated accident (RIA) with respect to standard  $\text{UO}_2$  fuel.

- a. The TR suggests that the change in margin to fuel melt is negligible between doped and standard  $\text{UO}_2$ . The LTR includes a statement that: [

]

- i. A change in [ ] would impact the allowable peak radial average fuel enthalpy as described in Section 7.2 of DG-1327. Please address the impact of these changes on future reload cores designed with  $\text{Cr}_2\text{O}_3$ -doped fuel.
- ii. A change in [ ] would impact the predicted number of fuel rod failures due to fuel melting as described in Section 3.3 of DG-1327. Please address the impact of these changes on future reload cores designed with  $\text{Cr}_2\text{O}_3$ -doped fuel.
- iii. A change in [ ] would impact the radiological source term (release attributed to fuel melting) as described in Appendix C of RG 1.183. Please address the impact of these changes on future reload cores designed with  $\text{Cr}_2\text{O}_3$ -doped fuel.

b. The TR states that [

] No data is provided to quantify the

overall fuel swelling of the  $\text{Cr}_2\text{O}_3$ -doped fuel or justify the concluding remarks that on balance  $\text{Cr}_2\text{O}_3$ -doped fuel is anticipated to have the same behavior as standard  $\text{UO}_2$  under RIA conditions. Hundreds of prompt pulse tests have been conducted in research reactors such as the Nuclear Safety Research Reactor (NSRR) to evaluate the performance of irradiated fuel rods under RIA conditions. In these test programs, comparisons have been made between large grain and standard grain fuel rod performance (e.g., NSRR test OI-10 vs. OI-11). Tests have also been performed on a variety of different fuel compositions and doping agents. Please review the extensive RIA empirical database and compile data to characterize the fuel swelling of  $\text{Cr}_2\text{O}_3$ -doped fuel under RIA conditions.

c. The TR states that [

] No data is provided to quantify the fine

fuel fragmentation or transient fission gas release of the  $\text{Cr}_2\text{O}_3$ -doped fuel or justify the concluding remarks that on balance  $\text{Cr}_2\text{O}_3$ -doped fuel is anticipated to have the same behavior as standard  $\text{UO}_2$  under RIA conditions. Hundreds of prompt pulse tests have been conducted in research reactors such as NSRR to evaluate the performance of irradiated fuel rods under RIA conditions. In these test programs, comparisons have been made between large grain and standard grain fuel rod performance (e.g., NSRR test OI-10 vs. OI-11). Tests have also been performed on a variety of different fuel compositions and doping agents. Please review the extensive RIA empirical database and compile data to characterize the fuel fragmentation and fission gas release of  $\text{Cr}_2\text{O}_3$ -doped fuel under RIA conditions. In addition, provide justification for the applicability of the

transient fission gas release model described in Section 4 of DG-1327 to  $\text{Cr}_2\text{O}_3$ -doped fuel.

**Response:**

Question 7 addresses the features of the revised RIA guidance in DG-1327. It is noted that a separate topical report ANP-10333P (Reference 7-7) was submitted for the control rod drop accident (CRDA) methodology that uses RODEX4 in connection with AURORA-B and a sample case was included in the topical report ANP-10340P.

First, the Cr concentration in the chromia-doped fuel is orders of magnitude lower than Gadolinia concentration in NAF, e.g. nominal Cr concentration of  $1600 \mu\text{gCr}_2\text{O}_3/\text{gUO}_2$  compared to up to  $10,000 \mu\text{gGd}_2\text{O}_3/\text{gUO}_2$ . NAF is on the list of fuel types for which the new RIA regulation is applicable and therefore the chromia-doped fuel should also be included because the additive amount and its impact is bounded by NAF.

Second, both the thermal-mechanical and safety thermal-hydraulic methodologies are not generic and are applied for each reload and each cycle and the criteria are checked for the specific fuel type analyzed. Therefore, the impact of [

] is assessed for each reload/cycle.

Response to RAI-7.a

The thermal conductivity and melting point are [ ] for chromia-doped fuel in comparison to standard non-doped fuel, but considerably higher than those of NAF.

Response to RAI-7.a.i

This sub-question refers to Section 7.2 of DG-1327, in which two limits are specified for damaged core coolability; responses for the impact on the two limits are provided below:

- DG-1327 Section 7.2.1 Peak radial average fuel enthalpy below 230 cal/g

A [ ] thermal conductivity of chromia-doped fuel will slightly affect the margin for this limit, to a level similar to example provided ANP-10340P. Moreover, 230 cal/g deposited adiabatically and uniformly leads to ~ 2,300 °C temperature rise, which for CRDA is also the maximum temperature (T) during the RIA pulse; even with pellet edge power profile peak, T<sub>max</sub> is generally below T<sub>melt</sub> and the chromia-doped [ ] (see response to RAI-4).

Again, the analysis is performed for each reload so that the impact is always captured.

- DG-1327 Section 7.2.2 No, or limited central 10% melting

The impact of [ ] melting temperature for chromia-doped fuel is always taken into account because the analysis is carried out for each reload.

#### Response to RAI-7.a.ii

See the response to RAI-7.a.i.

#### Response to RAI-7.a.iii

The potential impact on the source term due to the [ ] melting temperature will be automatically taken into account when the AST analysis is performed.

The melting temperature and thermal conductivity [ ] of chromia-doped fuel are [ ] (bounded by) than that of Gadolinia fuel, which is accepted for both the current and the new RIA/LOCA and AST calculations.

#### Response to RAI-7.b

The comment made in the topical report in Section 5.3.2 is elaborated on, as follows. A distinctive feature of chromia-doped fuel is the development of a larger intragranular

bubble population, mostly during power ramps. These bubbles inside the grain are more numerous and larger in chromia-doped fuel than in standard non-doped fuel and have the potential to swell during a temperature transient, similar to the much larger pores of the HBS rim, but on a significantly smaller scale.

The kinetics of this additional transient gaseous swelling in chromia-doped fuel is not instantaneous, as it requires creep of the surrounding matrix and/or vacancy diffusion, both mechanisms requiring times significantly longer than the less than 1-2 second time scale of the first phase of a RIA pulse. The thermal expansion is instantaneous and dominates the first PCMI phase of the RIA pulse. There is no difference in the thermal expansion of chromia-doped fuel compared to standard non-doped fuel and therefore, it is anticipated that the behavior during a RIA pulse is similar.

In addition, there is a negative, self-limiting, feedback loop, whereby the additional transient gaseous swelling of intragranular bubbles increases the PCMI contact pressure between pellet and cladding, which implies a higher hydrostatic stress in the pellet, with the effect of restraining the bubble gaseous swelling. In addition, the enhanced viscoplasticity of chromia-doped fuel also helps to reduce the PCMI contact pressure by plastic deformation in the axial direction, similar to extrusion into dishing during normal operation power ramps.

The additional gaseous swelling of intragranular bubbles has another beneficial consequence: the transient FGR is restrained and delayed by the same negative feedback loop of enhanced PCMI contact pressure.

While, the in-reactor RIA-type pulse tests on chromia-doped fuel are not yet available, there have been some RIA tests in NSRR with Gadolinia and niobia-doped fuels and also a couple with large grain size standard fuel. The niobia-doped fuel has similar intragranular swelling features as chromia-doped fuel (Reference 7-1) and therefore it is relevant for chromia-doped fuel behavior during RIA transients. All these tests on fuel types with additives and standard non-doped but with large grain size, showed similar outcome during an RIA pulse as standard  $\text{UO}_2$ .

Eight RIA pulse tests in NSRR have been performed with Gadolinia fuel and the conclusions were as follows (Reference 7-2):

- 1) The failure mechanism of the  $\text{Gd}_2\text{O}_3\text{-UO}_2$  fuel rod is oxygen induced cladding embrittlement accompanied with wall thinning due to local melting of the cladding, which is same as that of  $\text{UO}_2$  fuel.
- 2) The failure threshold of the  $\text{Gd}_2\text{O}_3\text{-UO}_2$  fuel is between 265 and 275 cal/g- $\text{UO}_2$ , almost the same as that of  $\text{UO}_2$  fuel. In fact, the failure threshold for Gadolinia fuel was slightly higher than that of the standard  $\text{UO}_2$  tested as part of the same program (see Table 7-1).
- 3) The behavior of mechanical energy generation is almost the same for both of the  $\text{Gd}_2\text{O}_3\text{-UO}_2$  fuel rod and the  $\text{UO}_2$  fuel rod.
- 4) In consideration of the radial power profile in the fuel and power shape expected in an actual reactor, the failure threshold in an actual reactor is estimated to be same or greater than that in the present results in the NSRR test reactor.

As described in DG-1327, the deciding factor in fuel rod performance during the first PCMI phase of a RIA pulse is the cladding with its specific mechanical and corrosion properties. DG-1327 lists a number of fuel types that are currently in use, which includes Gadolinia fuel. As shown in the topical report and in response to other RAIs, Gadolinia fuel is bounding for chromia-doped fuel from thermal and mechanical points of view and therefore, it is anticipated that DG-1327 is applicable to chromia-doped fuel.

#### Response to RAI-7.c

As mentioned above, the niobia-doped fuel has similar larger intragranular gaseous swelling and larger grain size as the chromia-doped fuel, though the intragranular gaseous swelling is larger for the niobia-doped fuel. Therefore, the behavior of niobia-doped fuel in RIA pulse tests is relevant and considered to bound the chromia-doped fuel behavior during RIA-type transients.

The program of niobia-doped fuel RIA pulses in NSRR was reported in References 7-5 and 7-6 and the same conclusions as for the Gadolinia fuel program mentioned in response to RAI-7 b, above, have been reached. Specifically, it was identified that the failure mechanisms are the same and failure thresholds are almost the same (slightly higher for niobia-doped fuel) as for standard  $\text{UO}_2$ . The tests reported in Reference 7-5 were performed with unpressurized fuel rods and thus the PCMI and melting failure modes were studied, while the tests reported in Reference 7-6 were performed with pre-pressurized rods, which confirmed the same failure threshold for the ballooning failure mode. The similarity of the failure threshold for the ballooning failure mode shows that transient fission gas release (FGR) is similar to standard  $\text{UO}_2$  fuel.

The larger grain size of chromia-doped fuel implies, as stated in the topical report, a lower grain boundary area and hence a smaller inventory of fission gas on the grain boundaries. The transient FGR during a RIA pulse is dominated by the mechanical cracking mechanism, whereby micro-cracks created during the temperature transient caused by the RIA pulse intersects HBS pores and also the grain boundary bubbles and releases the gas stored in them.

The chromia-doped fuel having a smaller amount of gas in the grain boundary bubbles will have a lower transient FGR amount during the RIA pulse. This has been verified in the NSRR tests with the OI-10 fuel rod (Reference 7-3), which had a larger grain size and the measured FGR was below the lower bound of standard  $\text{UO}_2$  FGR data in RIA pulses (Figure 7-1).

The applicability of DG-1327 provisions regarding transient FGR are further supported by the post-irradiation annealing tests under atmospheric pressure, called TT below, which have been performed on standard and doped fuels in the NFIR program (Figure 7-2). A summary of the tests and main conclusions is as follows:



In conclusions in all but one case, the fission gas release during transients was lower or the same for chromia-doped fuel in comparison to standard non-doped  $\text{UO}_2$ .

The comparison of the fragment sizes after the 1200 °C tests show that for a given microstructure, the higher the burn-up, the smaller the fragments. In addition to these comparisons, no fine-fragmentation had been detected during the TT tests on the standard  $\text{UO}_2$ , the homogeneous MOX 1, the Large Grain  $\text{UO}_2$  and the Cr doped  $\text{UO}_2$  CR2, between 40 and 48 GWd/tHM, even at 1600 °C.

Therefore, it is concluded that the fission gas release model described in Section 4 of DG-1327 is applicable to chromia-doped fuel.



**Table 7—1 Summary of Gadolinia Fuel RIA Tests in NSRR  
(Reference 7-3)**

Test Series	Fuel Rod Type	Threshold Energy
510	17x17 PWR Type $\text{UO}_2$ fuel rod	252 ~ 264 cal/g. $\text{UO}_2$
511	17x17 PWR Type $\text{Gd}_2\text{O}_3$ - $\text{UO}_2$ fuel rod	265 ~ 275 cal/g. $\text{UO}_2$
512	14x14 PWR Type $\text{UO}_2$ fuel rod	232 ~ 246 cal/g. $\text{UO}_2$

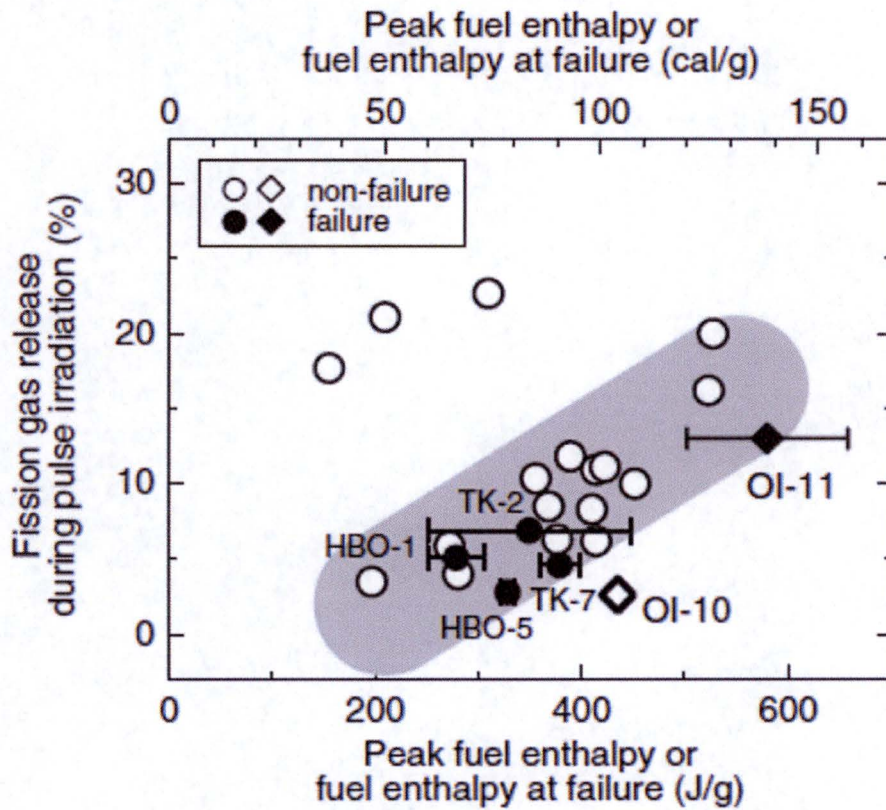


Figure 7—1 Fission Gas Release During RIA Tests in NSRR



**Figure 7—2 Fission Gas Release During Post-Irradiation Annealing  
Tests in NFIR**



**Figure 7—3 NFIR Slow TT on Very High Burnup Fuel**



**Figure 7—4 NFIR Stair-Case TT**

**References for Response 7:**

- 7-1 J.E.Turner et al, "The post-irradiation examination of niobia doped fuel irradiated in the DODEWAARD-BWR," International Topical Meeting on LWR Fuel Performance "Fuel for 90s", Avignon, France, April 21-24, 1991, vol.1, 47.
- 7-2 S. Shiozawa et al, "Study of the Behavior of  $Gd_2O_3$  Fuel Rod Failure under a Reactivity Initiated Accident," JAERI-M 88-084, April 6, 1988.
- 7-3 T. Fuketa, T. Sugiyama and F. Nagase, "Behavior of 60 to 78 MWd/kgU PWR Fuels under Reactivity-Initiated Accident Conditions," Jo. Of Nucl. Sci. and Techn., Vol. 43, No. 9, pp 1080-1088 (2006).
- 7-4 T. Sugiyama et al, "RIA-simulating Experiments on High Burnup PWR Fuel Rods with Advanced Cladding Alloys," Proceedings of the 2004 International Meeting on LWR Fuel Performance, Orlando, Florida, September 19-22, 2004, Paper 1035.
- 7-5 K. Yanagisawa, "Behavior of  $Nb_2O_5$  Doped/Unpressurized  $UO_2$  Fuel under Transient," Jo. Of Nucl. Sci. and Techn., 32(2), pp 111-117 (February 1995).
- 7-6 K. Yanagisawa, "Behavior of  $Nb_2O_5$  Doped/Unpressurized  $UO_2$  Fuel in Reactivity Initiated Accident Conditions," Jo. Of Nucl. Sci. and Techn., 328(5), pp 459-471 (May 1991).
- 7-7 ANP-10333P Revision 0, "AURORA-B: An Evaluation Model for Boiling Water Reactors; Application to Control Rod Drop Accident (CRDA)," AREVA Inc., 2014.

## 8.0 RAI 8

### Question:

Some figures in the LTR contain large and diverse datasets which NRC staff would like to examine in more detail.

- a. Please submit the data used to generate plot 7-8, "Fission Gas Release Measured vs Calculated for Chromia-doped Database". Please include grain size and chromia content for each data point.
- b. Please submit the data used to generate plot 10-1 "Ramp Test Data Showing Increased Fuel Failure Threshold for Chromia-Doped Fuel". Please include grain size and chromia content for each data point.

### Response:

#### Response to RAI-8 a

The following are the tables describing the FGR database, separately for the chromia-doped and standard non-doped fuels, respectively.

**Table 8—1 FGR Database for Chromia-Doped Fuel**

--	--



**Table 8—1 FGR Database for Chromia-doped Fuel (continued)**

**Table 8—2 FGR Dataset of Standard Non-Doped Fuel Associated with the Chromia-Doped Database**

--

Response to RAI-8.b.

The power ramp tables that have been requested are presented below.

First, the standard non-doped liner fuel rods power ramps are presented in Tables 8-3 to 8-5. Next the chromia-doped power ramp data are presented in Tables 8-6 and 8-7 for BWR and PWR fuel types and conditions, respectively.

The grain size and Cr content for the ramped rods are listed in the FGR Table 8-1 of RAI-8 a, being cross-referenced by the reactor in which the steady-state irradiation took place.

**Table 8—3 Standard UO<sub>2</sub> Liner Fuel Rod Power Ramps – Low Burnup**

--

**Table 8—4 Standard UO<sub>2</sub> Liner Fuel Rod Power Ramps – High Burnup**

--

**Table 8—5 Standard UO<sub>2</sub> Liner Fuel Rod Power Ramps – Very High Burnup**

--

**Table 8—6 Chromia-Doped UO<sub>2</sub> Non-Liner Fuel Rod Power Ramps – BWR**

--

**Table 8—7 Chromia-Doped UO<sub>2</sub> Non-Liner Fuel Rod Power Ramps – PWR**

--

**Additional Information:**

The NRC provided an additional comment on the RODEX4 FGR model in an email on March 6, 2018.

**Comment:**

It is difficult to evaluate the quality of the doped FGR data without the context provided by the undoped fuel FGR data. A plot of the chromia-doped FGR data plotted against the predicted values using a 95/95 upper bound (rather than BE) for LHGR and diffusion coefficient would help provide context and demonstrate appropriateness of the model. (This plot exists in Rodex4 RAI responses for undoped fuel transient cases).

**Response:**

The primary information to use to determine the adequacy of the RODEX4 fission gas release (FGR) model for chromia-doped fuel is Figure 7-8 from ANP-10340P. [

]

The BE RODEX4 fuel code is applied within the framework of the approved RODEX4 realistic methodology, which consists of a statistical uncertainty propagation method that calculates the upper bound of the outcome of interest for compliance with licensing criteria. The realistic methodology takes into account the scatter of the differences between calculations and measurements determined during the benchmarking of the BE code and employs the modeling parameters' uncertainties determined to encompass any local bias. The FGR release dataset for chromia doped fuel was re-run with the 95/95 upper bounds for the linear heat generation rate (LHGR) and the diffusion coefficient.

[

]

Additional information is provided in Table 8-1 in the response to RAI 8a, in which it is shown that the FGR database covers the Cr concentration and grains size ranges envisaged for the chromia-doped fuel specification.

In conclusion, the RODEX4 FGR model provides a [

] for both chromia doped fuel and standard non-doped fuel and thus is adequate for the evaluation of internal rod pressure from a safety perspective.



**Figure 8—1 FGR Results for the Chromia-Doped Database with  
LHGR and Diffusion Coefficient Biased to the 95%/95% Upper  
Bounds**

## 9.0 RAI 9

### Question:

The Halden reactor is an instrumented heavy water moderated BWR used extensively to perform safety-focused research into materials and fuel behavior under prolonged irradiation programs. Halden instrumented fuel assembly (IFA) – 716 studied the behavior of large grain  $\text{Cr}_2\text{O}_3$ -doped fuel and large grain  $\text{UO}_2$  fuel. Please include the data generated from Halden-716 to validate the RODEX4 models.

### Response:

The response to this RAI has been supplemented by simulation of IFA-677 test, the precursor to IFA-716 test. The simulation of these two Halden tests with RODEX4 was the subject of a paper presented at the EHPG meeting in Sept. 2017 (Reference 9-1), which is the basis for this response.

### Test Description: Measurement Techniques, Irradiation Rig and Materials

These two recent tests, IFA-677 and IFA-716, were aimed at investigating FGR for fuels with different microstructures that are characterized by different grain sizes. The main objective of this response is to simulate relevant fuel rods from the two tests with RODEX4 in order to confirm its capabilities with respect to FGR for a broad grain size range. To that end the rod gas pressure and center bore temperature, which have been measured online, are compared with code calculations based on input decks prepared from data provided by Halden. A discussion of the experimental uncertainties is presented that is used in the test results interpretation.

The IFA-677 test titled "High Initial Rating Test," was designed to provide FGR data on modern fuel operated with power histories starting at high power and gradually declining, but remaining at relatively high power levels throughout. The six fuel rods in the test rig consisted of four standard  $\text{UO}_2$  and two doped ( $\text{Al}_2\text{O}_3$ - $\text{Cr}_2\text{O}_3$ ) fuel rods,



equipped with online instrumentation for internal gas pressure, fuel center bore temperature and fuel/cladding elongation.

IFA-716 was largely designed as a follow-up to IFA-677, using the same rig and online instrumentation for a combination of standard and doped ( $\text{Cr}_2\text{O}_3$  and  $\text{BeO}$ ) fuel rods, but with power histories at a lower power level than in IFA-677, to cover the impact of larger grain size of doped fuel in the lower temperature range.

The test rig in both tests is the same: a cluster of six experimental fuel rods, with an active fuel length of ~ 400 mm and an initial enrichment of 4.95%, placed inside a loop with natural circulation of the Halden reactor coolant, which nominally has 34 bar pressure and the corresponding saturation temperature of ~ 235 °C.

The experimental fuel rods were fabricated at Kjeller from fuel pellets and cladding received from different fuel suppliers. Hollow pellet columns were prepared by drilling a 1.8 mm diameter central hole, in which thermocouples (T/C) were inserted. Bellows pressure transducers (PF in the Figures 9-1 and 9- 2) have been attached at one end of the rods with a significant corresponding volume in case of the IFA-677 test, in which a bypass line was needed to attach the pressure transducer (Figure 9-1) and a somewhat smaller transducer volume for IFA-716, in which the PF was attached at the bottom without a bypass line (Figure 9-2).

The plenum length and associated volume are relatively larger than for a typical LWR (PWR, specifically) fuel rod and in order to compensate for that, a lower fill gas pressure was used: 13.5 bar for IFA-677 and 10 bar for IFA-716.

For both tests, the starting point was the very detailed power history logged on-line by Halden, with records every minute and even more frequently during power changes. A power history condensation technique was used to filter the small power variations with sufficient resolution such that significant power changes are kept, while small power fluctuations are smoothed out and thus a condensed power history is obtained that is manageable for fuel code analysis. The resulting condensed power history eliminated

all periods of shutdown and zero power. In addition, the processing of the measured data was done so that the power history timeline is matched with the times for the online measurements of internal rod pressure and temperature.

One of the fuel microstructure characteristics that is often subject to ambiguity is grain size. In several cases, the issue is the lack of characterization of the grain size stated in fabrication reports or papers. This is in spite of the existence and widespread application of the ASTM E-112 standard on grain size measurement and reporting, which describes the definition and measurement technique for the MLI (Mean Linear Intercept) as measure of grain size.

In many instances the reported grain size is described as MLI, but in other cases the planar "equivalent diameter" or spatial/3D equivalent diameter are presented. These two other grain size metrics are quite different from MLI, by factors of 1.13 and 1.56, respectively.

Another complication of the grain size metric is related to the possible departure from uniform (mono-modal) grain size distribution of the microstructure. The generally equiaxed, uniform grain distribution characterizes the standard  $\text{UO}_2$  microstructure with small grains (7 to 20  $\mu\text{m}$ , MLI). Larger grain size fuel is often associated with a wider and in many cases bimodal grain-size distribution. In this case, it is desirable to define an effective grain size that is more suitable for fission gas release models.

Both situations are present in the characterization of the fuels used in the two IFA tests (IFA-677 and IFA-716). The definition of grain size is very important for all fuel codes, but more so for RODEX4, which uses internally the 3D value for FGR and gaseous swelling modelling. However, RODEX4 accepts either MLI or 3D grain size definitions as an input, with proper identification.

For the IFA-677 case, a fuel characterization information sheet provided by Halden contained the needed clarification regarding the definition of the grain size, while the published report (Reference 9-2) used the "average grain size" title. In the fuel

characterization information sheet three of the six fuel rods of IFA-677, contained values for grain size as both "linear intercept" and "average grain size", which differed by a factor of ~ 1.5. Therefore, it was inferred that the average grain size stated in the official reports is the 3D grain size.

In the case of IFA-716, the non-doped large grain size fuels have been fabricated by special sintering processes, either in oxidizing conditions in one case, or very active ADU powders with small amounts of grain growth dopants in another case. There is evidence for the former case of a bi-modal grain size distribution. Also, the doped fuels used in two fuel rods in IFA-716 have been fabricated in a laboratory-type furnace with only one H sintering gas entry point. This leads to somewhat oxidizing conditions in the high-temperature zone of the furnace and a wider, bi-modal grain distribution is also considered to be present in the doped fuel rods of IFA-716. Based on these considerations the grain size for large grain fuel rods has been amended to an effective lower grain size that is more representative for FGR models.

The non-doped large grain size fuel used for a couple of rods in IFA-716 were reported to be significantly hyperstoichiometric (see Tables 9-1 and 9-2, typical production range is below 2.001) from the point of view of thermal conduction property and therefore, the inputs for those rods included a thermal conductivity adjustment factor of 0.9 (References 9-3 and 9-4).

These major characteristics of the fuel rods from the two tests, which have been modelled with RODEX4, are summarized in Tables 9-1 and 9-2.

The axial power profile was provided by Halden as average LHGRs over three equal-sized axial segments, top, mid and bottom. Also, the LHGR at the T/C location was included; the LHGR for hollow pellet segments are affected by the lack of heat generation in the central hole and therefore lower than the LHGR of a solid pellet segment at the same position in the core. The length of the hollow pellet columns either top or bottom are almost equal to one third of the total pellet stack length and therefore little difference exists between LHGR at T/C location and corresponding axial segment

average LHGR; this was verified with the data provided by Halden and for ease of input preparation the LHGR at T/C location was used for the corresponding axial segments.

A note is made regarding the power histories provided by Halden, which will be mentioned later when discussing the comparison of code calculations with measurements. First, an uncertainty of  $\sim 5\%$  (one sigma) is assumed to be applicable to power measurement/calculation in the Halden reactor. Indeed, the LHGR in the IFA-677 and IFA-716 test rigs in question is the combined result of local flux measurement (neutron detectors (ND) in Figures 9-1 and 9-2) and calculation with a transport neutronics code that estimates the 3D flux map and calculates LHGRs based on a fuel burnup calculation. Therefore, the LHGR uncertainty is the combination of experimental and calculational uncertainties. In a test reactor, which has a small core, the influence of either driver fuel or other test rigs in adjacent locations is another source of uncertainty.

For the tests in question, two series of 3 NDs at two elevations were placed in order to measure neutron flux and provide data for neutronics code analysis. Unfortunately, the majority of NDs malfunctioned or were not used for IFA-716 and therefore, the uncertainty of LHGR both radially and axially is greater for IFA-716 than for IFA-677.

The uncertainty analysis presented in Reference 9-5 did not consider the uncertainty associated with calculations involved in the procedure and only assigned a value for the Power Conversion Factor (PCF) uncertainty, namely 4% as a best-estimate for one sigma. A more comprehensive uncertainty analysis is presented in Reference 9-6, where uncertainty values are given for all three factors in Equation (1); significant uncertainty is associated with the power calibration by calorimetry, which varies during irradiation from 5% to 7.5% for the test analyzed in [8]. Also, significant uncertainties were noticed for HELIOS core calculations, e.g. HELIOS calculations were offset by 10% from calorimetric calibration factor (KG) value. It was also noted in Reference 9-6 that failure of one ND in cycle 9 contributed to increase power uncertainty after its failure. The power uncertainty ( $\pm$  one sigma) was estimated to be:  $\pm 7\%$  at BOL, increasing to  $\pm 8\%$  by cycle 9 and reaching  $\pm 10\%$  by EOL.

In IFA-716 only two NDs functioned during the test and therefore, the radial profile was only available by calculation, while the axial profile could rely on the two NDs being at two different elevations. However, only two ND being available for axial flux profile determination increased its uncertainty. Therefore, it is considered that the power uprate of ~ 7% that was needed to get agreement with rod pressure readings in the second half of IFA-716 irradiation, is plausible and well within the typical 95/95 uncertainty range of Halden power determination, which was augmented in IFA-716 because of ND failures right at the start of the test.

#### RODEX4 Benchmarking Results

The main results of the RODEX4 calculations for selected, representative rods from the two tests are summarized below and the FGR measurements and calculations presented in Tables 9-1 and 9-2. For all rods, the comparisons between calculations and measurements are made for the rod internal pressure and center bore temperature data. The internal rod pressure plot also shows the evolution of FGR, which is just calculated.

No adjusting factor was applied to IFA-677 power histories, while nominal and x1.07 increased power histories were calculated for IFA-716 after the power uprate at 10,000 h (in some cases, for ease of input preparation and to check the impact on fuel temperature, the power was increased by 7% through the entire irradiation time).

First, the high rating test IFA-677 is illustrated with three rods, as follows:

- rods 677-2 and 677-6 with standard small grain size  $\text{UO}_2$  (11  $\mu$  and 7.8  $\mu$ , MLI) and
- rod 677-1 with  $(\text{Al}_2\text{O}_3\text{-Cr}_2\text{O}_3)$  doped  $\text{UO}_2$  and with the largest grain size (37.3  $\mu$ , MLI) in IFA-677

The evolution of rod internal pressure and temperature for the top and bottom T/C locations for the large grain size rod 677-1 is presented in Figures 9-3 through 9-5,

respectively. Good agreement is obtained for rod internal pressure, both in magnitude as well as in the transients, which are associated with the power history transients.

The temperature plots in Figures 9-4 and 9-5 show good agreement overall for both top and bottom T/C locations; it can be observed that a small under prediction for the first half and a small over prediction for the second half of the irradiation history exists. This characteristic is common to most of the modelled rods and is further discussed below.

The next two figures show the evolution of rod internal pressure for rods; 677-6 in Figure 9-6 and 677-2 in Figure 9-7. Very good agreement is shown for the rod internal pressure for 677-6, while some over prediction occurred for 677-2; however, the temperature agreement is equally good for the two rods and consistent with the first rod, with a somewhat larger under prediction at the beginning of irradiation for 677-6 (temperature plots in Reference 9-1).

The power histories for the three rods modelled in IFA-677 are similar in magnitude and evolution and therefore the calculated FGR is similar for the two small grain size rods 677-2 and 677-6 at ~ 20%. The FGR for the larger grain size rod 677-1 is lower at ~ 16%. However, internal rod pressure is higher for rod 677-1, which can be correlated with the higher power of this rod in the second half of the irradiation lifetime, which leads to larger fuel deformations and consequently lower free volume; nevertheless, a slight under prediction of rod internal pressure is noticed at the end of life for 677-1.

Five rods were modelled for IFA-716 test (only temperature data are reliable for rod 716-2):

- chromia-doped rods 716-1 and 716-6 with grain sizes of 50-70  $\mu$  and 40-55  $\mu$ , MLI, respectively
- non-doped, large grain size  $\text{UO}_2$  rods 716-4 and 716-5 with grain sizes of 40-55  $\mu$  and 40-55  $\mu$ , MLI, respectively
- standard, small grain size rod 716-2 with grain size of 11  $\mu$ , MLI

The evolution of rod internal pressure is illustrated in Figures 9-8 through 9-10. The figures showing the temperature benchmarking (with good agreement for all rods) are presented in Reference 9-1 and two examples are shown in Figures 9-11 and 9-12 for the chromia-doped rods 716-1 and 716-6, respectively.

The two tests IFA-677 and IFA-716 have provided useful data in order to assess the impact of grain size on FGR. The good agreement between measurements and RODEX4 calculations emphasize the need to take into account grain size in FGR models. The fission gas amount that is released from the fuel is the result of the two main stages of thermal FGR, namely, intragranular diffusion and grain boundary bubble development and interlinkage. Only after the grain boundary is saturated with gas bubbles that become interlinked along grain edges, is fission gas vented to the open voidage (Reference 9-7).

A larger grain size affects the two processes in different ways: the intragranular diffusion is delayed because of increased diffusion length and enhanced trapping by intragranular bubbles, but the grain boundary area is decreased and hence fission gas retention in grain boundary bubbles is diminished. Therefore, the magnitude of the effect of larger grain size is not constant and is dependent on power history and burnup during steady-state irradiations: FGR is lower in large grain size fuel, but to an extent that is affected by the lower saturation inventory of the reduced grain boundary area.

This is illustrated in the IFA-677 test, as mentioned above, for a high LHGR power history. Also, IFA-716 shows that saturation on grain boundaries is achieved for both small and large grain size fuels after the initial 10,000 h period of relatively low LHGR, because of the rod pressure rise after the power uprate at 10,000 h. This is possible because the reduced intragranular diffusion to grain boundaries in the large grain size fuel is compensated to a large degree by the smaller grain boundary area, hence lower grain boundary saturation capacity of the large grain size fuel.

**Table 9—1 Salient Features and Measured Data for Modelled Rods of IFA-677**

Rod	677-1	677-2	677-6
Fuel type	(Cr-Al) <sub>2</sub> O <sub>3</sub> doped	Standard	Standard
Grain size (MLI)	37.3	11	7.8
Stoichiometry	2.002	2.004	2.002
Fill gas pressure (bar)	13.5	13.5	13.5
FGR from online pressure (%)	22	19.7	19.1
FGR from PIE (%)	N/A	N/A	19
Calculated FGR (%)	16.2	21.8	20.1



**Table 9—2 Salient Features and Measured Data for Modelled rods of IFA-716**

Rod	716-1	716-2	716-4	716-5	716-6
Fuel type	Cr <sub>2</sub> O <sub>3</sub> doped	Standard	Large grain, non-doped	Large grain, non-doped	Cr <sub>2</sub> O <sub>3</sub> doped
Grain size (MLI)	50 (70)	11	45	45 (55)	50 (59)
Stoichiometry	2.005	2.001	2.005	2.006	2.002
Fill gas pressure (bar)	10	10	10	10	10
FGR from online pressure (%)	5.71	N/A	6.75	6.6	7.84
FGR from PIE (%)	N/A	N/A	N/A	4.32	5.73
Calculated FGR (%)	2.4	3.1	1	4.1	1.8

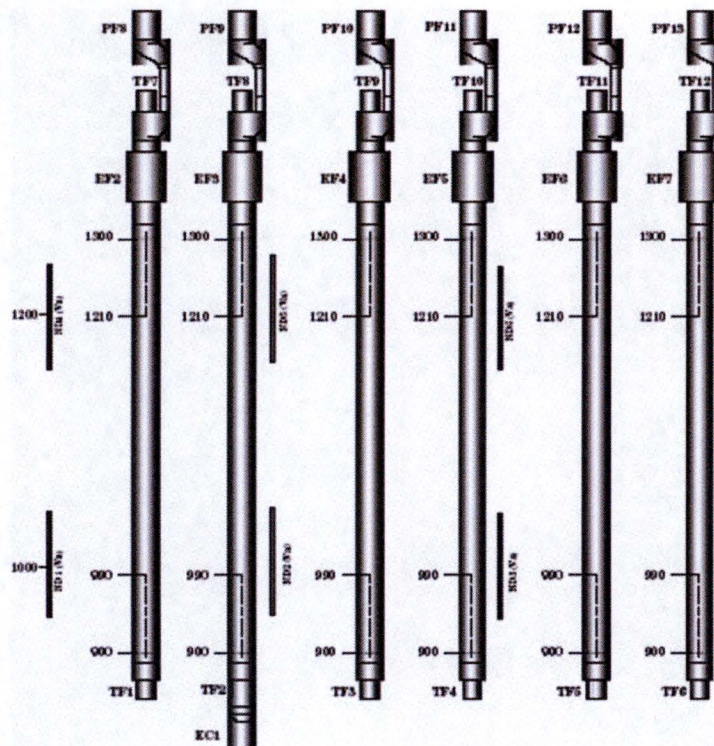


Figure 9—1 Fuel Rods in the IFA-677 Rig (from Reference 9-1)

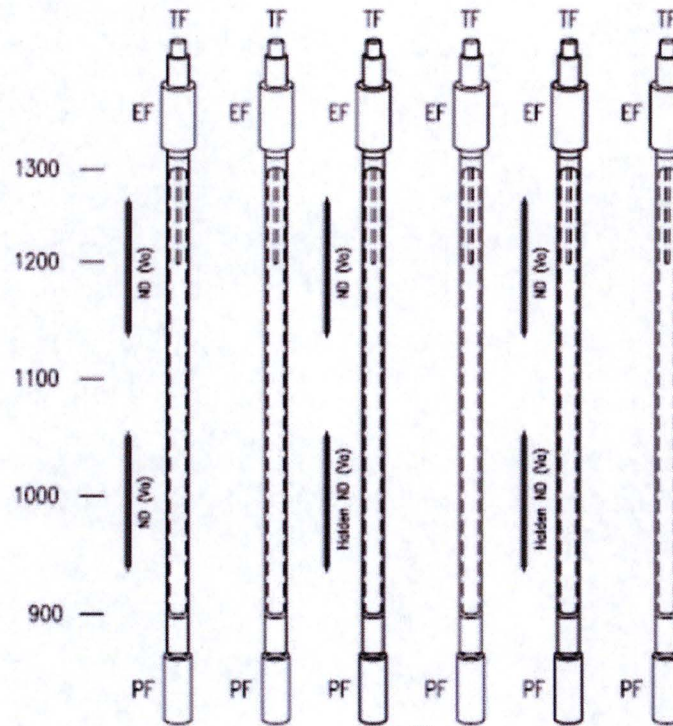


Figure 9—2 Fuel Rods in the IFA-716 Rig



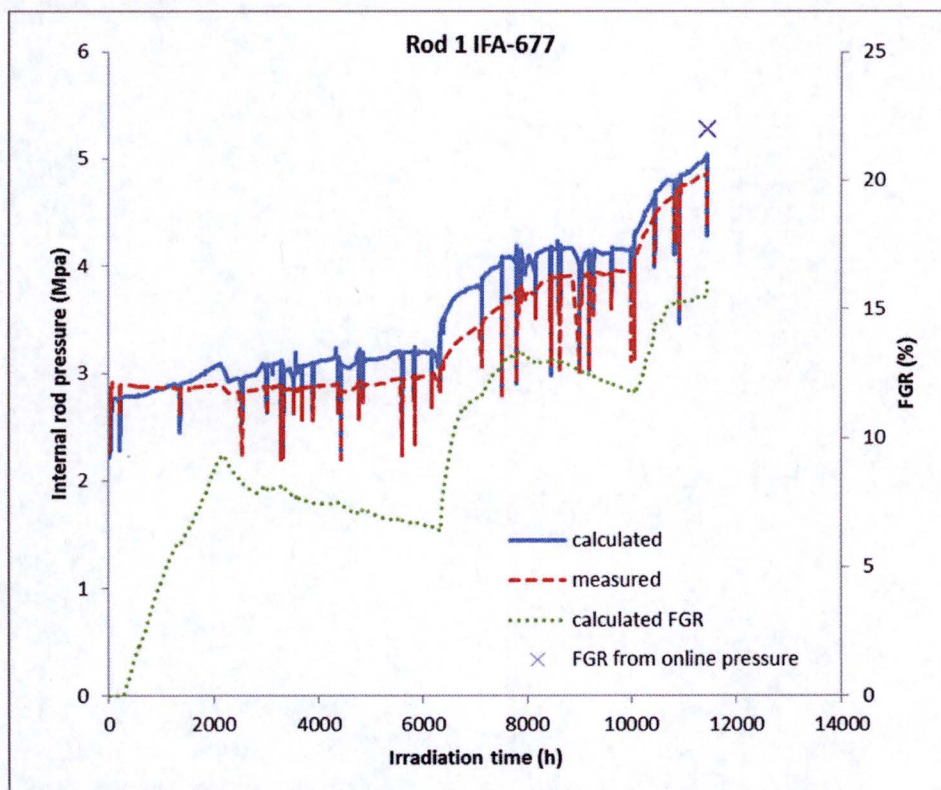


Figure 9—3 Rod Pressure and FGR for Rod 677-1

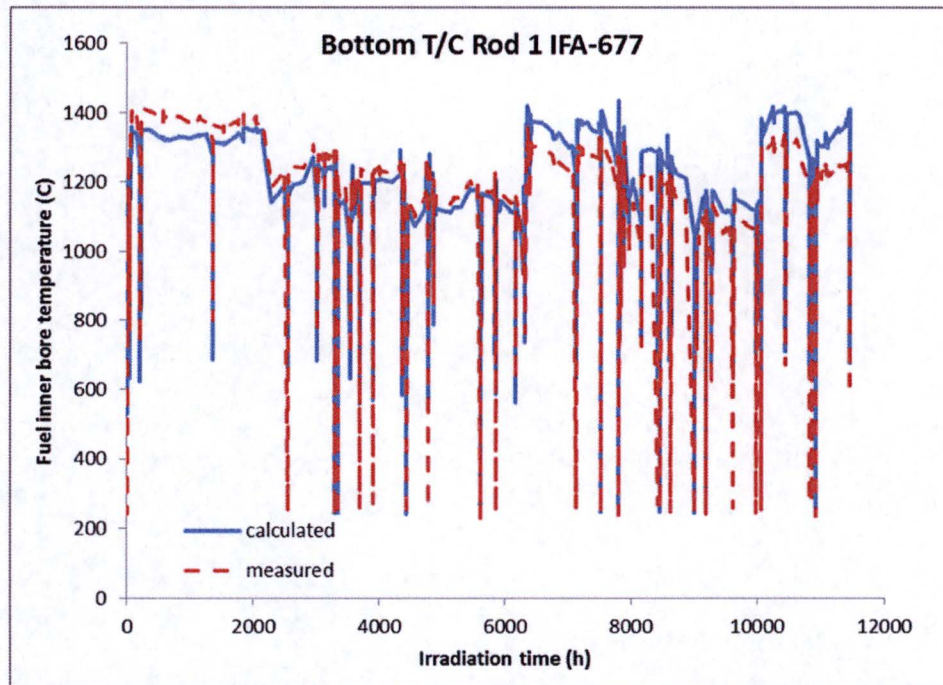


Figure 9—4 Center Temperature at Bottom T/C for Rod 677-1



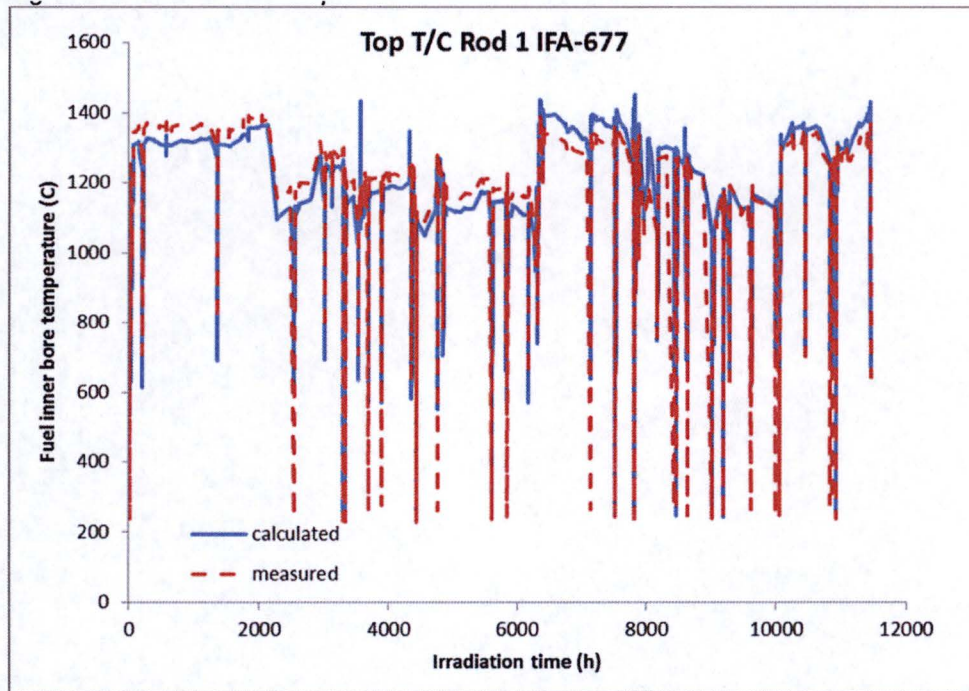


Figure 9—5 Center Temperature at Top T/C for Rod 677-1

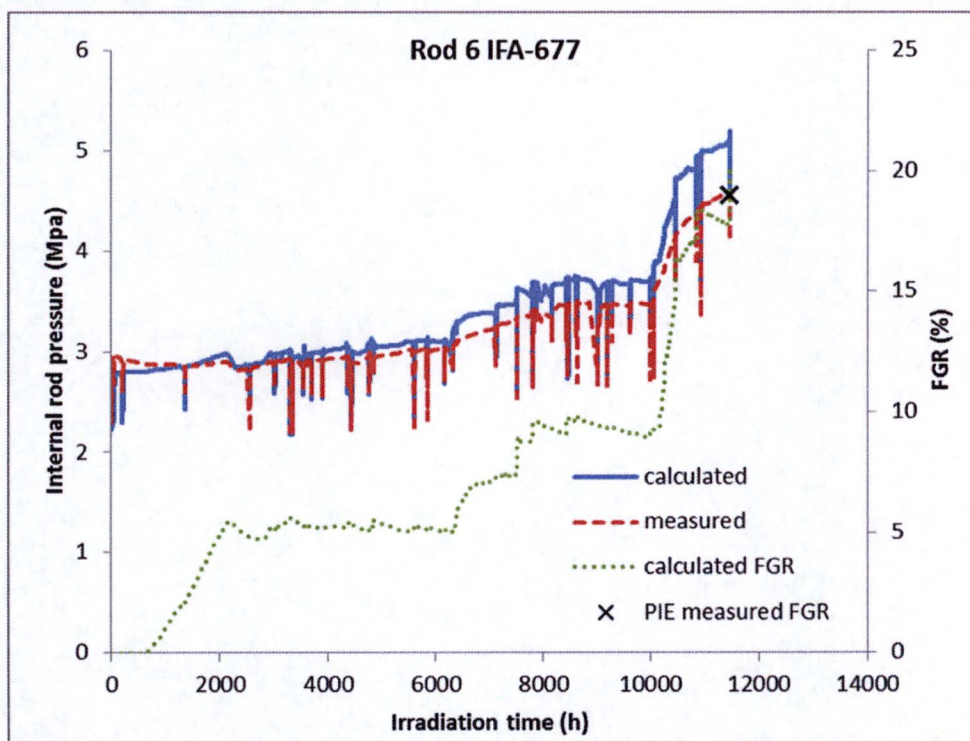


Figure 9—6 Rod Pressure and FGR for Rod 677-6

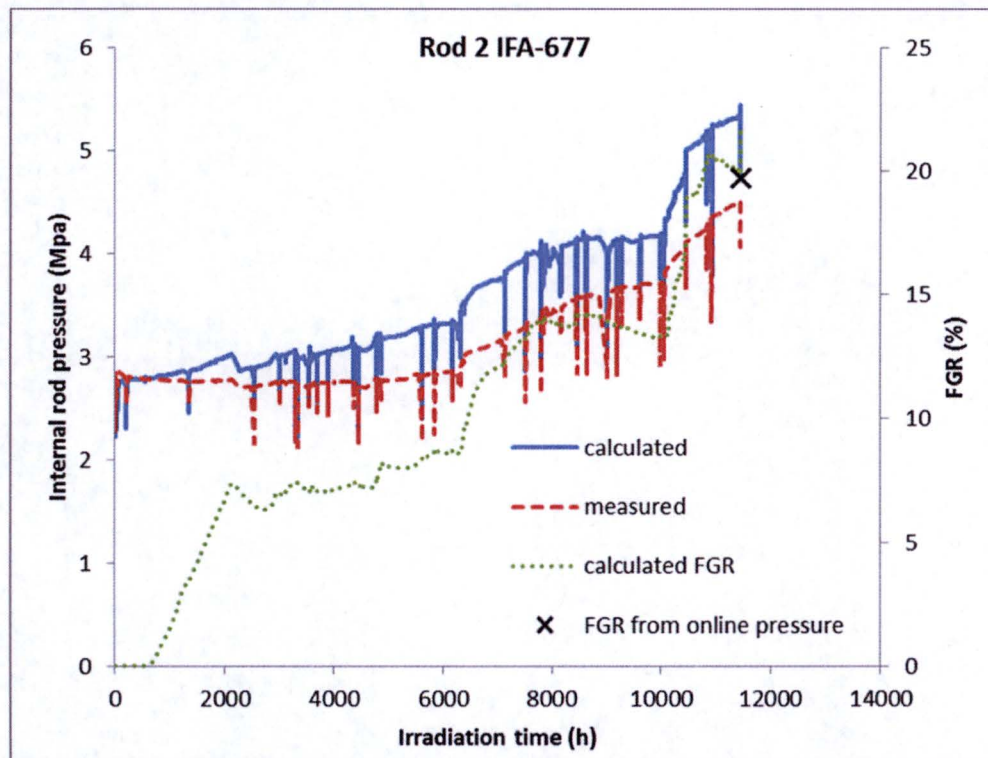


Figure 9—7 Rod Pressure and FGR for Rod 677-2



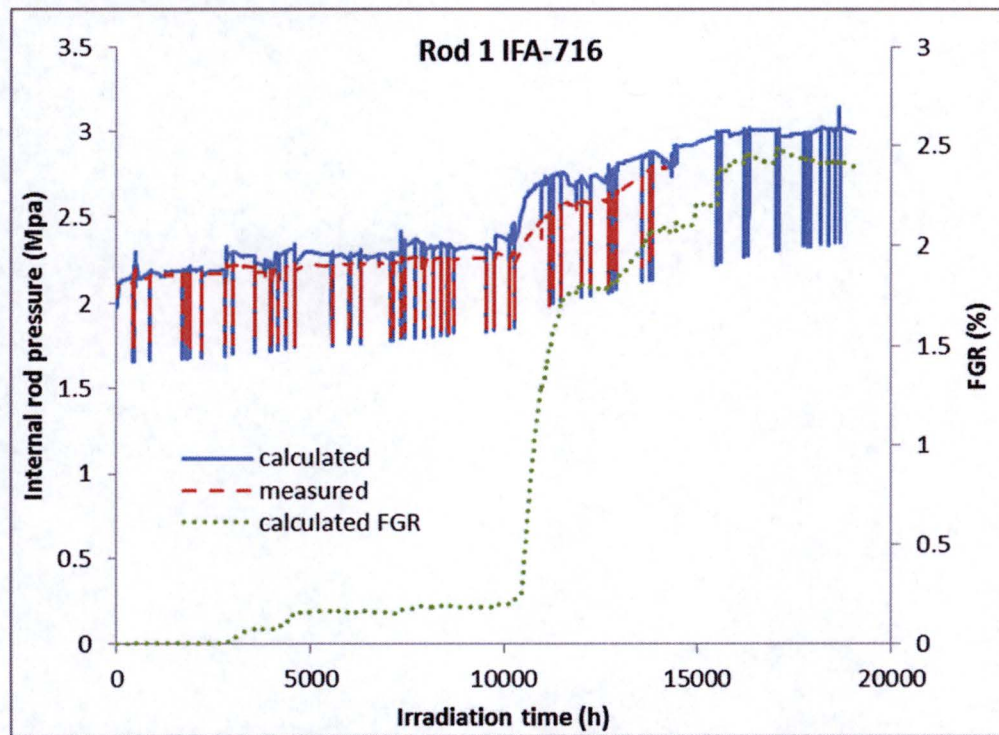


Figure 9—8 Rod Pressure and FGR for Rod 716-1 with 7% Power Uprate After 10 khr

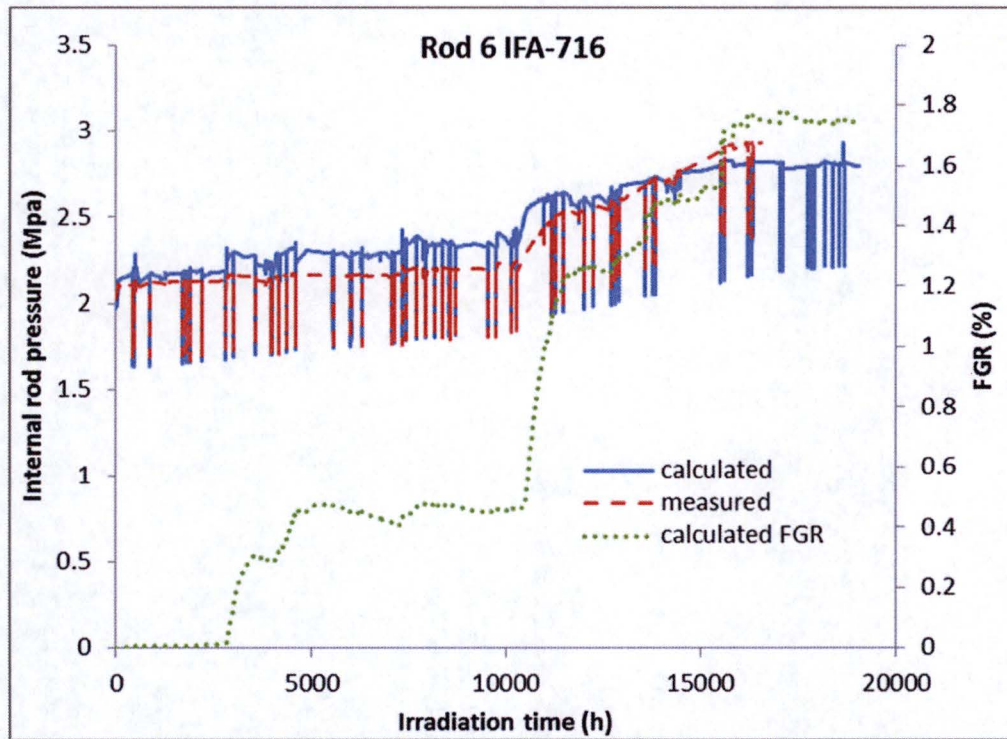


Figure 9—9 Rod Pressure and FGR for Rod 716-6 Without 7% Power Uprate



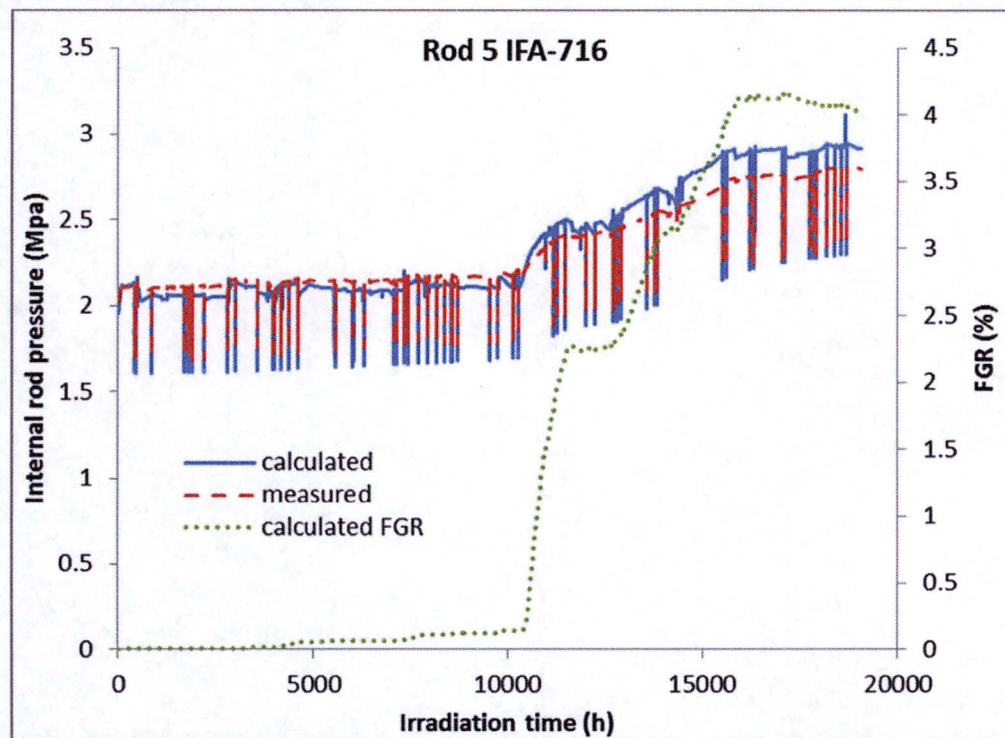
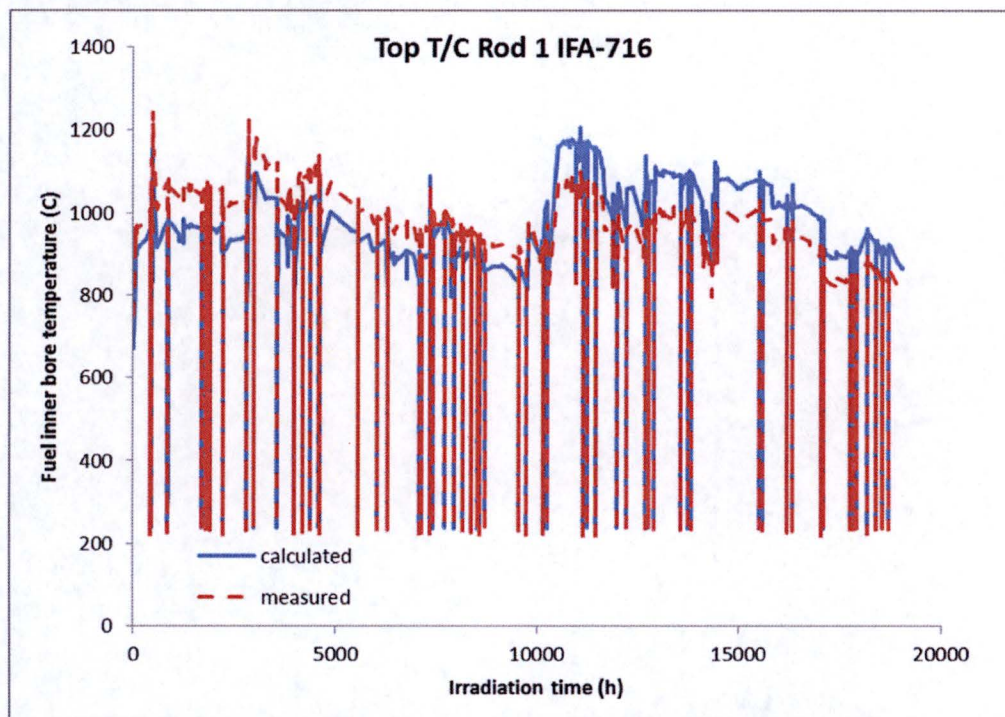
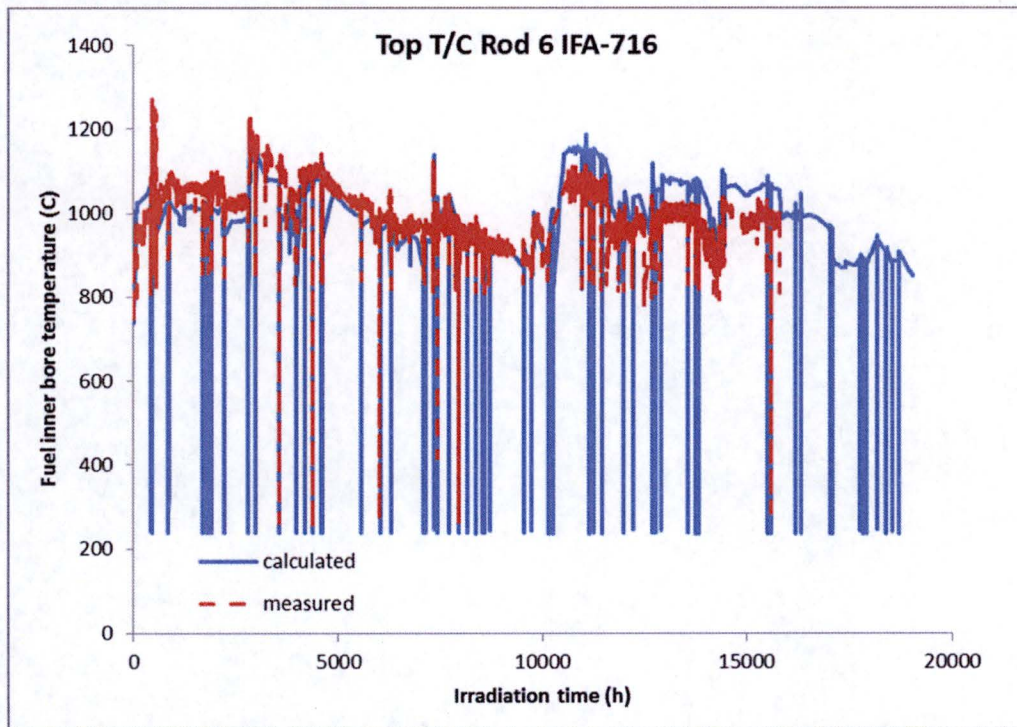


Figure 9—10 Rod Pressure and FGR for Rod 716-5 with 7% Power Uprate



**Figure 9—11 Center Temperature at Top T/C for Rod 716-1 with 7% Power Up-rate After 10 khr**





**Figure 9—12 Center Temperature at Top T/C for Rod 716-6 with 7% Power Uprate**

**References for Response 9:**

- 9-1 I. Arimescu, T. Davis, "Analysis of IFA-677 and IFA-716 tests results by using RODEX4 fuel code," EHPG Meeting, Lillehammer, Sept 25-28, 2017.
- 9-2 R. Josek, "The High Initial Rating Test IFA-677.1: Final Report on In-Pile Results," HWR-872, 2008.
- 9-3 *SCDAP/RELAP5/MOD3.1 Code Manual. Volume IV: MATPRO – A Library of Materials Properties for Light-Water-Reactor Accident Analysis*, NUREG/CR-6150, EGG-2720, Volume IV, November 1993.
- 9-4 P. G. Lucuta et al, "Thermal Conductivity of hyperstoichiometric SIMFUEL," Jo. of Nucl. Mat. 223 (1995) 51-60.
- 9-5 T. Ikonen, "Monte Carlo uncertainty and sensitivity analysis of the power determination in a Halden test rig containing multiple rods," HWR-1141, 2014-12-16.
- 9-6 F. Khattout, "The Gadolinia fuel test IFA-681: Overview of in-pile measurements from beginning of irradiation to unloading," HWR-1038, 2013-03-11.
- 9-7 EMF-2994P, "RODEX4 Theory Manual," AREVA Inc., 2004.

**10.0 RAI 10****Question:**

At an audit, AREVA highlighted their request (as stated in the LTR) to remove the staff's limitation on analytical grain size placed on the approval of RODEX4. Section 2 of the LTR states: qualification of RODEX4 to chromia-doped fuel also justifies the removal of the grain size restriction imposed in the Safety Evaluation for Reference 20. NRC staff need additional information to evaluate the appropriateness of this change with respect to standard  $\text{UO}_2$ .

- a. Please submit supporting evidence for fission gas release, as well as any other properties which include grain size in RODEX4.
- b. The LTR details the addition of a new intragranular swelling model for chromia-doped  $\text{UO}_2$ .
  - i. Will this model also be applied to standard  $\text{UO}_2$ ?
  - ii. If so, will it be applied to all standard  $\text{UO}_2$ , or will it only apply above a certain grain size threshold?
  - iii. Please show that existing swelling experimental data is correctly predicted using the configuration that is being requested for approval.

**Response:**Response to RAI-10 a

The grain size limitation imposed in the safety evaluation for RODEX4 was in relation to FGR modeling; RODEX4 fully accounts for actual grain sizes, while the audit code, FRAPCON, used by the NRC, employs a fixed default grain size value. A few cases with larger grain size were present in the database used for RODEX4 benchmarking but

were not considered sufficient to support a larger grain size limitation and thus the upper bound of grain size range of the FGR database was used to impose the limitation on grain size for RODEX4.

The FGR prediction for large grain size fuel was illustrated in response to RAI-4 (Reference 10-1). In Figures 4.8 and 4.9 of Reference 10-1 6 cases are shown in the [ ] microns mean linear intercept (MLI) range and other 3 cases at [ ] microns MLI. These larger grain-size fuels were obtained by sintering for a longer than the standard sintering time.

The rather small dataset of large grain size fuel cases with FGR measurements in the RODEX4 topical report are supplemented by the significantly larger database of [ ] chromia-doped fuel cases (see the response to RAI-8) with grain sizes in the [ ] microns MLI range. Also, in the chromia-doped database, there are [ ] cases with non-doped standard  $\text{UO}_2$  in the [ ] microns MLI (Figure 10-1 below). In addition there is one case with an intermediate grain size of 37 microns MLI present in the IFA-677 test that is described in response to RAI-9.

This combined large-grain size fuel FGR dataset consisting of the initial RODEX4 topical report cases, the data from IFA-677 and IFA-716 (see RAI-9 response) and the much larger chromia-doped database is considered sufficient. This supports removing the grain size limitation on RODEX4. This is further justified by the fact that no change was made to RODEX4 FGR model for benchmarking the chromia-doped database. The grain size is an input to RODEX4.



Response to RAI-10 bi.

The intergranular swelling model (IGSW) can be applied to standard  $\text{UO}_2$  fuel. The acceptability of this is demonstrated by the parametric study described in response to sub-question "iii", below.

ii.

As shown in response to sub-question "iii" below, the impact of activating the IGSW model for standard  $\text{UO}_2$  with grain size in the typical low grain size range of up to [ ] microns MLI, is very small and practically negligible. The IGSW model is only used for the large grain size range above [ ] microns MLI.

The value of [ ] microns MLI is the upper bound on the grain size that can be achieved by the standard sintering process for standard non-doped  $\text{UO}_2$ , while doped fuel grain size is controlled in the greater than [ ] microns MLI range. It is unlikely that any fuel produced by AREVA will have a grain size in the intermediate range and therefore the application range is fully covered by the database.

iii.

The RODEX4 database for standard  $\text{UO}_2$  was reanalyzed with a RODEX4 version in which the IGSW model was activated for all fuel types. This procedure was adopted in order to support the use of the IGSW model for standard non-doped fuel for grain sizes larger than [ ] microns MLI, the threshold for activating IGSW model as proposed in response to item "ii".

There is no impact on the temperature benchmarking. The anticipated small impact was with respect to FGR and hoop strain. The hoop strain is directly affected by IGSW, and is mostly impacted during power ramps. FGR is not directly impacted by IGSW,

since it provides an input to the IGSW model the amount of gas atoms inside the grain that have not diffused to grain boundaries. A small feedback loop involving IGSW is present in the case of strong PCMI, by IGSW enhancing the pellet-to-cladding contact pressure, which can delay and diminish in some cases FGR.

Figure 10-2 compares the FGR for the RODEX4 database with the IGSW model turned off (as approved in the RODEX4 topical report) and turned-on, respectively. It can be observed that the vast majority of cases are not, or are very little affected, while a handful of cases show a somewhat large impact, with the more conservative result being for the initial RODEX4 version, i.e. IGSW model turned off.

Figure 10-3 shows the same comparison between the IGSW turned-off and turned-on RODEX4 versions for cladding strain increment during power ramps, while Figure 10-4 displays the comparison between the two RODEX4 versions for cladding diameter change after steady-state irradiation. The negative and small positive values in Figure 1-4 represent the steady-state data, which are the result of creep down and creep out at high burnup, after pellet-to-cladding contact that leads to strain reversal, respectively. The positive strain values in Figure 10-3 represent the strain increment accumulated during power ramps. While the negative cladding deformation due to creepdown is practically unaffected by the IGSW model, the positive steady-state strains after steady-state irradiations and the positive strain increment during power ramps are slightly increased when the IGSW model is activated. This is as expected because an additional pellet swelling is contributed by the IGSW model and the initial RODEX4 model was calibrated with the grain boundary swelling model only.

As anticipated, the effect of IGSW is small for standard  $\text{UO}_2$  and its inclusion for standard  $\text{UO}_2$  could be achieved by re-calibrating the code on the strain increment database, which however is not envisaged. Moreover, as can be observed in Figures 10-3 and 10-4 the inclusion of the IGSW model biases the strain increment prediction slightly in the conservative direction. The best-estimate character and the uncertainties determined for the RODEX4 would not be affected by turning on IGSW for standard

non-doped fuel for grain sizes above [ ] microns MLI, while there will be a potential small conservative bias for standard  $\text{UO}_2$  with grain size between [ ] microns, before entering the large grain size of the chromia-doped database for which RODEX4 was calibrated with the IGSW activated.



**Figure 10—1 Grain Sizes for the Fuels Used in the FGR Chromia-Doped Database**



**Figure 10—2 IGSW RODEX4 vs. Standard RODEX4: Fission Gas Release**



**Figure 10—3 IGSW RODEX4 vs. Standard RODEX4: Strain Increment  
During Power Ramps**



**Figure 10—4 IGSW RODEX4 vs. Standard RODEX4: Clad Diameter Change After Steady-State Irradiation**

**References for Response 10:**

- 10-1 BAW-10247Q1P, "Response to Request for Additional Information – BAW-10247(P)," AREVA Inc., 2007

**11.0 RAI 11****Question:**

At an audit, AREVA clarified that approval for gadolinia doped fuel with chromia dopant is being requested as well. The LTR includes some discussion of Gad+Cr properties, but many properties of this fuel are not discussed. For the properties listed below, please discuss if AREVA expects there to be a difference between Gad and Gad+Cr fuel pellets, the justification for this, and if a change will be made to licensing calculations.

- a. Microstructure – This plays a prominent part in many of the explanations in the LTR; how does the addition of gadolinia dopant impact the microstructure of chromia doped fuel?
- b. Grain size and growth – this section relies heavily on the microstructure of the fuel as a justification for the behavior.
- c. Tensile fracture strength
- d. Creep and plastic deformation
- e. Fuel pellet cracking
- f. In-reactor densification
- g. High Burnup Structure formation
- h. Washout behavior
- i. Performance under LOCA conditions
- j. Performance during a RIA
- k. PCI benefits



**Response:**

Doping Gadolinia fuel with chromia does not appreciably change the Gadolinia fuel microstructure or properties. Therefore, with regards to items a and b, it can be stated that chromia-doped Gadolinia fuel is equivalent to non-doped Gadolinia fuel.

The grain size for doped Gadolinia fuel is [ ] the range of doped  $\text{UO}_2$  and in most cases [ ]

The thermal properties, namely thermal conductivity and melting point, have been shown in ANP-10340P not to be affected by chromia doping Gadolinia fuel. This is in large part explained by the fact that the chromia content being one to two orders of magnitude lower than the Gadolinia content and therefore is negligible with respect to additive effects on thermal properties.

The in-reactor densification (item f) is assessed based on the resintering test performed during fabrication. Based on the manufacturing data, chromia-doped Gadolinia fuel has the same [ ] resintering and hence [ ] densification as non-doped Gadolinia fuel.

With regards to fuel mechanical behavior (items c to e), doped Gadolinia fuel (3 % wppm) has been studied regarding creep behavior. To test the mechanical behavior under high temperature, creep tests were performed by AREVA. Pellets with intermediate density were exposed to a pressure of 30, 45, and 60 MPa (see Figure 11- 1). All experiments were performed at 1500 °C (calibration via linear pyrometer) in an Ar-95% H<sub>2</sub> atmosphere.

The data points lie well on one line in a logarithmic scale. The measured creep rates are between the regions of experiences for Cr-doped fuel and standard fuel since the additional Gadolinia (3%) content reduces the plasticity of the fuel.

The experiment at 60 MPa was additionally repeated with one pellet of low density, and one pellet of high density. The results (Figure 11-1) are well within the normal deviation between measurements and prove that the variation of density has no significant influence on the mechanical behavior at high temperatures.

Based on the negligible effect of a much smaller amount of chromia than the gadolinia content in chromia-doped Gadolinia fuel, on thermal and mechanical properties, the negligible impact can be extended to items g, i and j.

The wash-out behavior of Cr-doped  $\text{UO}_2/\text{Gd}_2\text{O}_3$  fuel was performed in a refreshing autoclave under BWR conditions:

Steam / 290 °C / 70 bar / 6 days

Steam / 360 °C / 70 bar / 6 days

Medium: de-ionized water + 70 ppm  $\text{H}_2\text{O}_2$

Similar wash-out trials were made with Cr-doped  $\text{UO}_2$  fuel in 2006. In case of the 290° C temperature condition a [ ] of the Cr-doping compared to undoped  $\text{UO}_2/\text{Gd}_2\text{O}_3$  was present (Figure 10-2). Both kinds of  $\text{UO}_2/\text{Gd}_2\text{O}_3$  fuels show nearly the same visual aspects.

At temperatures higher than 360 °C a clear [ ]

]

With respect to PCI behavior it can be stated based on industry-wide operational experience and a sizable dataset of power ramps in test reactors that Gad fuel is more PCI resistant than standard  $\text{UO}_2$ . Recent support for this was provided by studies

performed in the frame of the Studsvik Cladding Improvement Program (SCIP) international research program.

Some relevant information related to Gad fuel performance during power ramps was included in Reference 11-1, showing that incipient cracks on the inner cladding surface of Gd-doped fuel that have been blunted off by the oxide grown during the power ramp (see Figure 11-5). It appears that the same mechanism of oxygen release during the power ramp with the associated passivating oxidation of the clad inner surface is operational in both Gd-doped and chromia-doped fuel types (the latter addressed in response to RAI-5).

In conclusion, the non-doped Gadolinia fuel characteristics can be used for doped Gadolinia fuel licensing analyses.



**Figure 11—1 Creep Behavior of Chromia-Doped Gadolinia Fuel**



**Figure 11—2 Washout Studies on Gd-Doped Fuel in High Pressure  
Steam for 5 Days**



**Figure 11—3 Washout Studies on Gd-Doped Fuel in High Pressure  
Steam (BWR Conditions) for 6 Days**



**Figure 11—4 Visual Aspect After 6 Days High Pressure Steam Wash-Out Studies**

## Inner oxide comparison

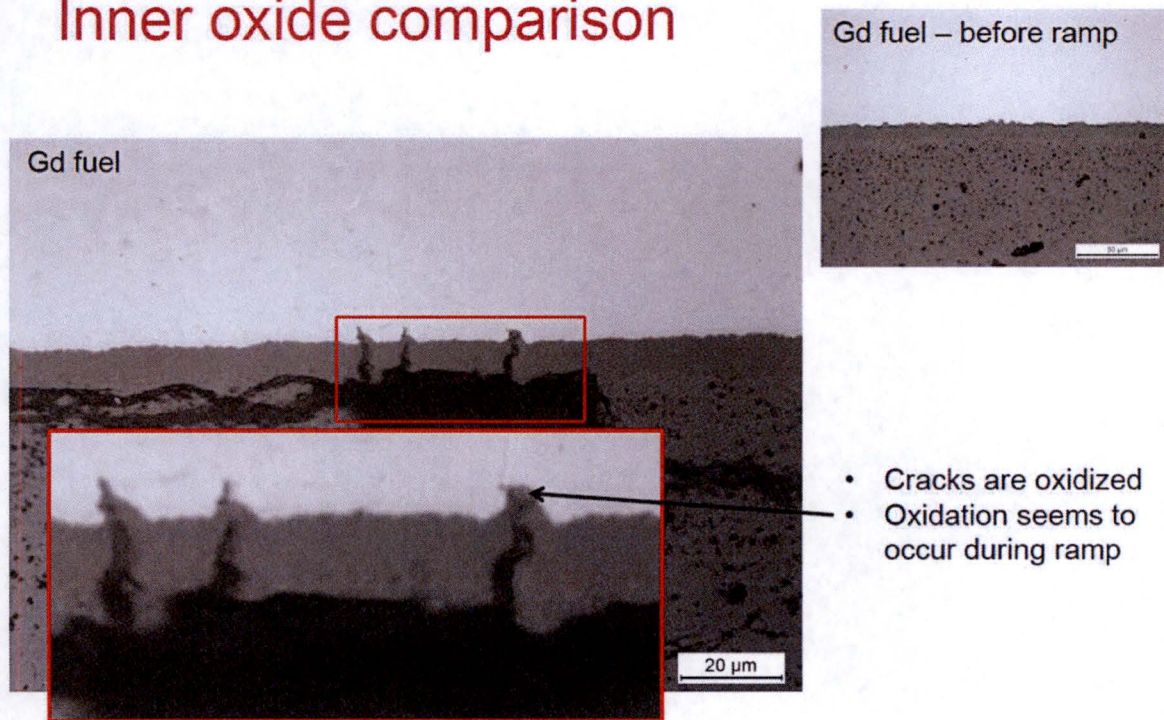


**Figure 11—5 Incipient Cracks Arrested by Oxidation for Ramped Gd-Doped Fuel, (Slide 12 from SCIP Meeting, Nov 2013 Presentation “SCIP 2 Workshop: Oxygen Supply to Cladding”)**

### References for Response 11:

- 11-1 D. Jadernas et al, “PCI Mitigation Using Fuel Additives,” Proceedings of 2015 Topfuel, pp 349-358, Sept. 2015, Zurich.



## 12.0 RAI 12

### Question:

Section 5.3.1 discusses the performance of  $\text{Cr}_2\text{O}_3$ -doped fuel under LOCA conditions. The LTR states: Fuel examinations up to high burnup levels show that the cracking pattern for chromia-doped fuel, as well as the pellet-clad interface bonding are very comparable to that for  $\text{UO}_2$ . Please provide supporting evidence from the fuel examinations.

### Response:

Hot-cell PIE of fuel rods with standard non-doped and chromia-doped fuel after steady-state irradiation or following power ramps has been performed. Cracking patterns during steady-state irradiation are illustrated in Figure 12-1, while cracking caused by power ramps are illustrated in Figure 12-2.

The pellet-cladding bonding is similar in chromia-doped fuel and standard non-doped fuel rods. The bonding is established after hard pellet-to-cladding mechanical contact is established at high burnup and consists of a mixed fuel and cladding oxide layer that replaces the previous pellet-to-cladding gap. These features have been observed on chromia-doped fuel examined in the hot-cells, as illustrated in Figure 12-3.

Post-irradiation annealing studies (temperature transients relevant for LOCA scenarios) have been performed in NFIR on high burnup disks made from different fuel types and pre-irradiated in IFA-649. This topic is still under research and no conclusive observations have been made. As an example, Figure 12-4 shows overall similar fragment size distributions for small and large grain standard  $\text{UO}_2$  fuels, with somewhat larger fragments for the large grain size fuel.

However, it can be stated that while a link between transient FGR and cracking/fragmentation of the HBS zone has been detected, the role of the other pellet microstructural regions, such as pre-rim and gas bubble rich annuli are also significant

with respect to transient FGR. This has been highlighted in Reference 12-1, which concluded that the rim zone with its large gas pores does not have a particular influence on FGR during LOCA conditions.

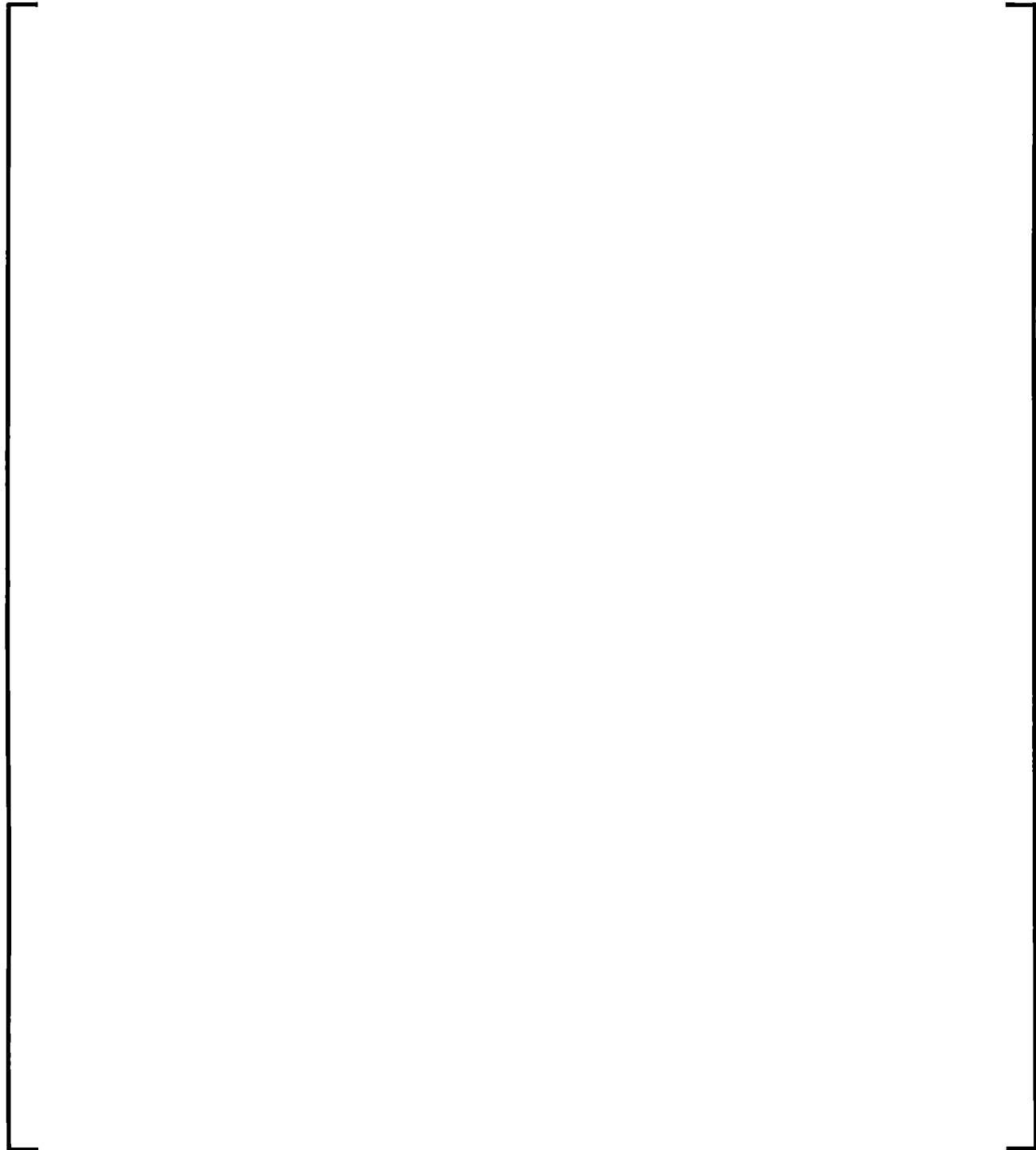


**Figure 12—1 Cracking Patterns During Steady-State Irradiation for  
Doped and Non-Doped Fuels**

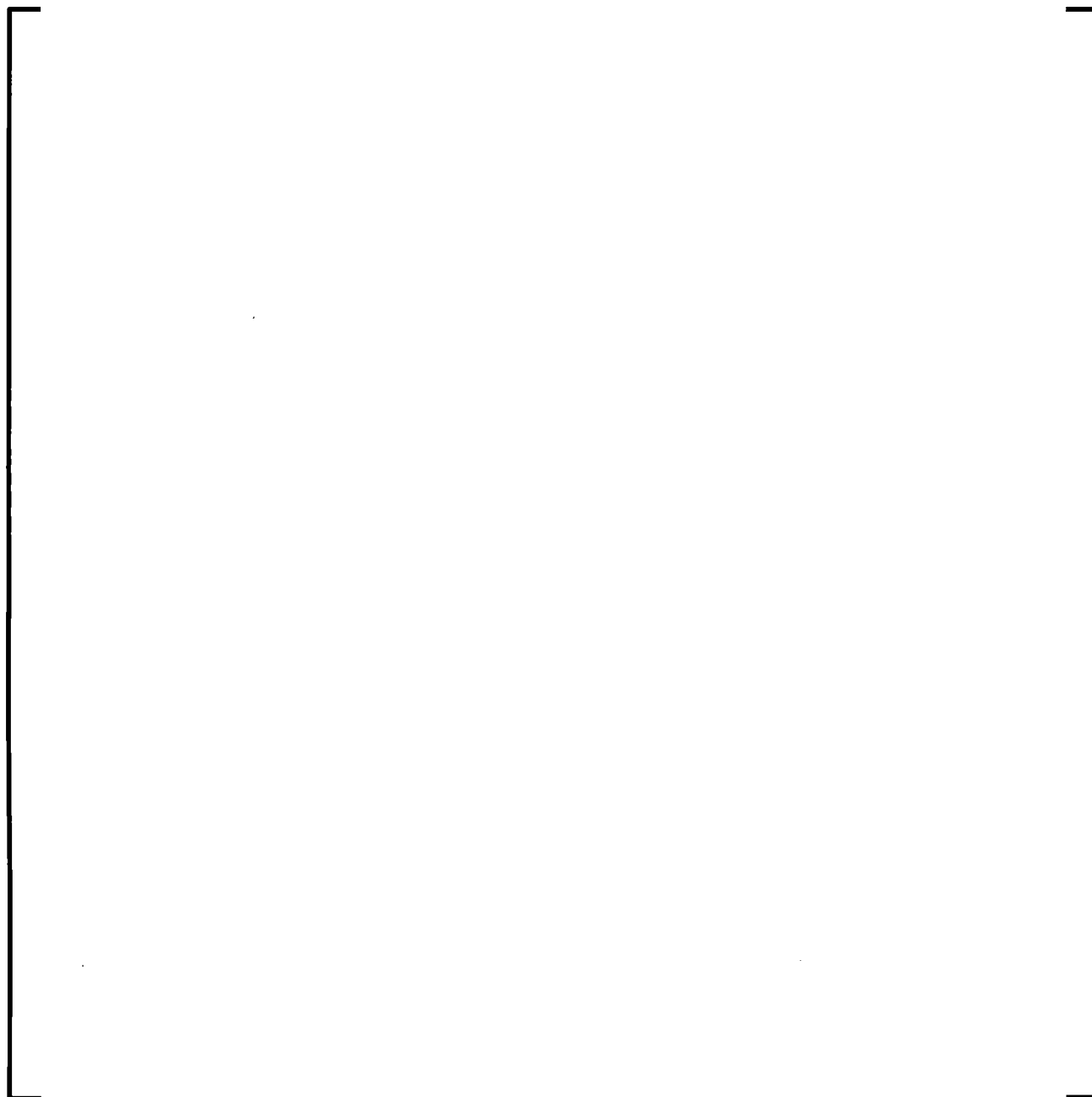


**Figure 12—2 Cracking Patterns Following Power Ramps for Doped  
and Non-Doped Fuels**



**Figure 12—3 Evolution of Pellet-Cladding Bonding of Chromia-Doped Fuel**



**Figure 12—4 Fragment Size Histogram After NFIR Post-Irradiation  
Annealing Test for Standard Small and Large Grain Fuels**

**References for Response 12:**

- 12-1 H. Sasajima et al, "Identification of Radial Position of Fission Gas Release in High-Burnup Fuel Pellets under RIA Conditions," Jo. of Nucl. Sci. and Techn. 47:2, pp 202-210, 05 Jan 2012.

### 13.0 RAI 13

**Question:**

NUREG-1465 describes a more realistic estimate of the radiological species released to containment in the event of a severe reactor accident involving substantial meltdown of the core. That document describes the specific nuclide types, quantities, chemical form, phase and timing of release into containment. Please provide justification for the applicability of NUREG-1465 to  $\text{Cr}_2\text{O}_3$ -doped fuel.

**Response:**

The methodology and assumptions in NUREG-1465 are bounding for chromia-doped fuel and therefore NUREG-1465 is applicable to chromia-doped fuel.

This conclusion is based on:

- The inventories for AST analyses are not impacted by chromia-doping as represented by Gadolinium doping that is on the list of fuel types in NUREG-1465.
- The number of failed rods due to fuel melting is part of the plant specific analysis.

The nature and amount of the stable or radioactive species released from the fuel during either steady-state or transients are not impacted by chromia doping. There is a negligible impact on neutron flux-spectrum and no impact on the yield fractions from the fissile isotopes. Therefore, the method described in NUREG-1465 to derive the source term is applicable to chromia-doped fuel.

**14.0 RAI 14****Question:**

Section 4.12 of the LTR discusses the effect of chromia dopant on the formation of the High Burnup Fuel Pellet Rim Structure (HBS). The following questions refer to this section.

- a. During the discussion on HBS, the burnups levels which experience HBS formation are compared for doped and standard  $\text{UO}_2$ . The TR states: [

] The data presented is illogical and does not support the conclusions. Please explain if this statement is in error.

- b. Please provide evidence from the hot-cell post irradiation examination studies supporting the statements for chromia-doped fuel regarding HBS.

**Response:**

Data summarized in the quoted text of Section 4.12 of ANP-10340P are from a hot-cell PIE study by CEA that compared doped fuel from the early chromia-doped variants (CONCERTO program) and standard  $\text{UO}_2$  fuel with regards to HBS formation and evolution and concluded that no fundamental difference exist between the two fuel types, although the doped fuel has larger grain size.

These HBS data are from the of examination of ceramographies in the hot-cell on two doped fuel rods and several standard fuel rods with varying fuel designs and irradiation conditions. HBS incubation and development are dependent on a number of fuel characteristics and on irradiation conditions (Reference 14-1). The local temperature



and hydrostatic stress, both of which are power history dependent, play a significant role in HBS initiation and development. Therefore, a variability range is to be expected for both burnup threshold and thickness of the HBS rim zone for different fuels operated under different irradiation conditions (LHGR level and burnup).

The comparison described in Section 4.12 of ANP-10340P is semi-quantitative and the dataset only supports a qualitative conclusion that doped fuel behavior, with respect to HBS formation and development, is not significantly different from standard fuel.

Specifically, the data for standard fuel show two different fuel rods with not very different burnups but HBS rim thickness differing by [ ] and the thicker HBS layer being observed for the lower burnup case. This apparent contradiction is due to the variability and uncertainty associated with irradiation conditions. This variability is also the main reason for the difference between the HBS outer layer thicknesses of the doped and standard fuel samples at ~62 MWd/kgU.

Supporting evidence for this variability in HBS formation and development is presented in Figure 14-1, which illustrates the relatively large differences between different hot-cell studies of different PWR fuels. This figure shows a range greater than the differences mentioned above for the doped and non-doped fuel HBS data presented in the topical report.

Another contributing factor to the different HBS characteristics of the CONCERTO fuel is that its chromia concentration is [ ] Chromia solubilization in  $\text{UO}_2$  is associated with the creation of chromium clusters, which might influence the formation of planar defects that are considered as a preliminary step in the formation of HBS (Reference 14-2). The CONCERTO chromia-doped fuel that was fabricated initially had chromia content about [ ] above the solubility limit for the sintering conditions used for that fuel. Therefore, more Cr precipitates were present in that fuel and could have resulted in an earlier onset of HBS.

In addition to the data presented in Section 4.12 of ANP-10340P, a more recent CEA hot-cell PIE was reviewed and the findings related to HBS are presented below. The chromia-doped fuel that was examined in this recent hot-cell PIE had the nominal chromia content of 1600 wppm/ $\text{UO}_2$ . Comparison to standard non-doped fuel rods that had similar, but not identical, power histories supports the following observations.

The chromia-doped fuel rods have been examined after 3 cycles (burnup 50-52 MWd/kgU) and after 5 cycles (burnup ~ 80 MWd/kgU). The HBS rim layer was [ ] The pre-rim microstructure, characterized as heterogeneous spots of partially transformed HBS is present after 3 cycles, at [ ] and is almost consumed after 5 cycles, at [ ] by the fully transformed HBS layer towards the periphery and by the mid-radius gas bubble rich zone towards the center. The HBS evolution in the case of these chromia-doped rods with the nominal chromia content is slower than in the case of the CONCERTO rods, which showed [ ]

After considering the information acquired in the additional hot-cell PIE presented above, which is more relevant because of the Cr concentration being at the nominal value, it is concluded that chromia-doped fuel has similar HBS evolution to standard non-doped  $\text{UO}_2$ .

#### Response to RAI-14 b.

Many of the fuel disks irradiated in IFA-649 to high burnup at relatively low temperatures have been examined and subject to post-irradiation annealing tests in NFIR. The Cr-doped disks contributed by AREVA have the characteristically large grain size of Cr-doped fuel. The results obtained in the NFIR studies, which are relevant to HBS formation in chromia-doped fuel, are summarized.

Some of the irradiated disks in IFA-649 have been examined at JRC/ITU and some at CEA. The results obtained by the two laboratories are consistent and complementary.

The results of QIA (Quantitative Image Analysis) performed at JRC/ITU are presented as total porosity, HBS fraction and mean ECD of the HBS pores. These are plotted as function of burn-up in Figures 14-2 to 14-4.

The porosity and volume percentage of the high burn-up structure in standard and large grain  $\text{UO}_2$  is plotted versus burn-up in Figures 14-2 and 14-3, respectively. It is clearly seen that the formation and development of the high burn-up structure, as manifested by the large pores (Figure 14-2) and restructured microstructure (Figure 14-3), is delayed in large grain non-doped  $\text{UO}_2$  (green triangle symbols).

However, with the possible exception of gadolinium, the addition of dopants [ ] the development of the high burn-up structure. It can be seen from Figures 14-2 and 14-3 that at high burn-up ( $\sim 100 \text{ MWd/kgHM}$ ) both the large porosity and the volume fraction of high burn-up structure in the  $\text{UO}_2$  discs doped with chromium, kaolinite and niobium are similar to those measured in standard non-doped and small grain size  $\text{UO}_2$  irradiated under similar conditions. It appears the gadolinium promotes the nucleation of the high burn-up structure in  $\text{UO}_2$ , but then slows down its development with increased burn-up.

Figure 14-4 shows that the size of the large pores that develop in the HBS zone is similar for all fuel types and therefore, the findings of the lower porosity and HBS volume fraction for non-doped large grain size  $\text{UO}_2$  is indicative of a retardation of HBS formation in the latter fuel type.

However, Figure 14-5 shows that the HBS large pores in the large grain non-doped  $\text{UO}_2$  are pressurized to higher pressures than other fuel types, which is most likely an effect of the lower creep rate of large grain non-doped  $\text{UO}_2$  and indicates an increased propensity for fuel fragmentation during temperature transients of the HBS region of large grain non-doped  $\text{UO}_2$  fuel.

As mentioned above, similar conclusions regarding HBS formation and development for doped and non-doped fuels have been reached from the CEA hot-cell examinations, which are summarized below and illustrated in Figures 14-6 through 14-9.

The examination of a large grain  $\text{UO}_2$  at [ ] confirmed the high HBS formation resistance of this fuel. HBS formed along all the grain boundaries and in patches situated in the central part of the grains. The average HBS formation fraction, in the central part of the disc is around [ ] much lower than for the standard  $\text{UO}_2$  fuel for which HBS conversion was complete. At the disc periphery, where the burn-up is higher and where the fabrication conditions led to smaller grains, the HBS formation fraction is higher, reaching almost [ ] at the periphery while it is around [ ] at 250  $\mu\text{m}$  from the rim of the disc. [ ] of the measured xenon was found in bubbles. In spite of the differences in the HBS formation fraction, the situation of the gas in the HBS bubbles is similar to that of previously examined HBS.

Figures 14-6 and 14-7 are similar to Figures 14-2 and 14-3, both regarding the trend of delayed HBS formation in large grain non-doped  $\text{UO}_2$  as well as regarding quantitative differences between different fuel types.

According to Reference 14-1, which is confirmed by the CR2 variant results at high burn-up, it seems that [ ]

However, in spite of the lower chromium content of the CR1 discs, when compared to CR2 ones, the HBS had also formed all over the examined disc, [ ] A lower bubble density was found, with less small bubbles than in the CR2 disc, but the amount of gas stored in the bubbles and the remaining Xe level outside the bubbles were the same as for the CR2 disc.

A conclusion highlighted in Reference 14-3 is that a large grain size delays the HBS transformation. The explanation proposed is that the HBS transformation is initiated at grain boundaries essentially because vacancies are provided from grain boundaries;

therefore a reduction of the grain boundaries surface delays the HBS process. In this case large grains were obtained using oxidative/longer sintering or Al-Si additive liquid sintering techniques. These conclusions are consistent with observations from a hot-cell PIE of a BR3 fuel rod in TUI (Reference 14-4) with an average pellet burn-up of 68 GWd/MtU and an initial grains size of 17  $\mu\text{m}$  obtained by longer sintering time. The grain subdivision was greatly delayed despite a local burn-up in the pellet rim ranging from 80 to 100 GWd/MtU.

It is concluded that large grain in non-doped fuel does not change HBS incubation burnup but delays its full development. Chromia-doped fuel showed [

] This is assumed to be mainly due to Cr precipitates impact on bubble nucleation.



**Figure 14—1 HBS Layer Width vs Pellet Average Burnup from  
Various Investigations**

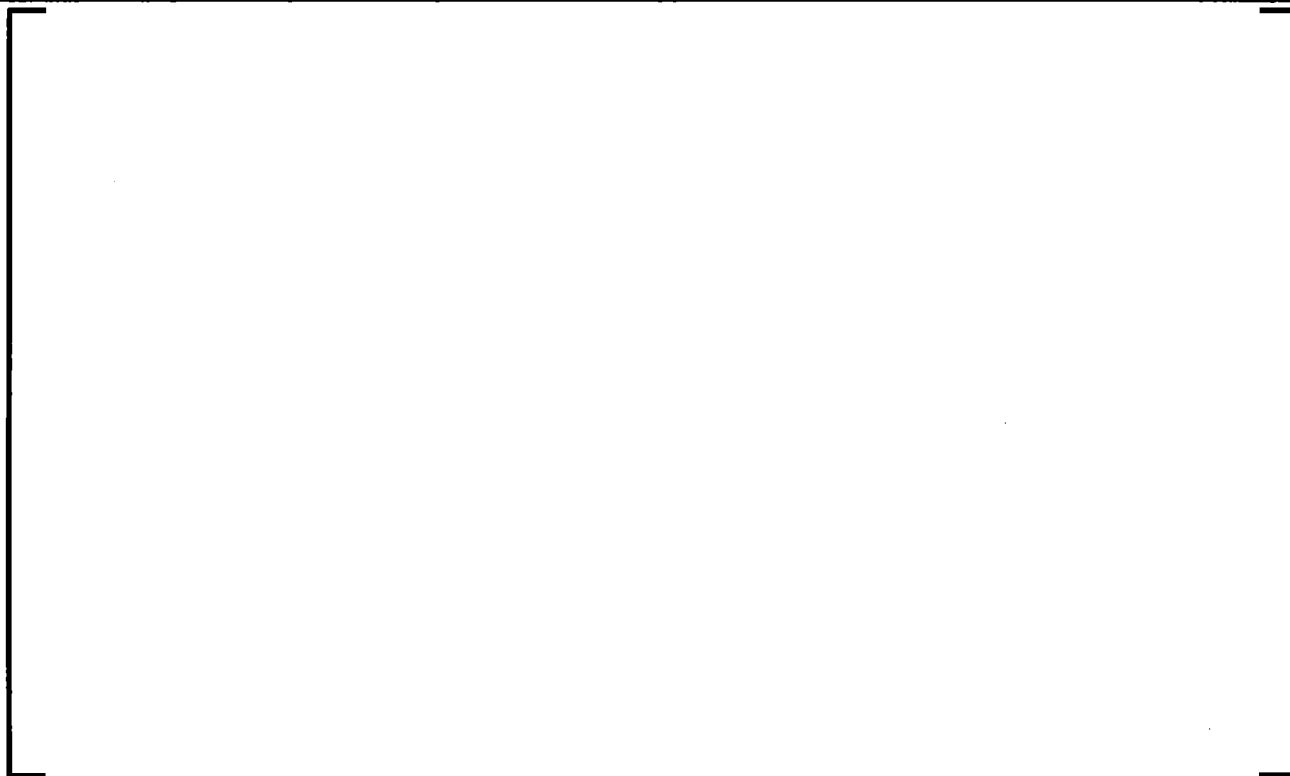


**Figure 14—2 Total Porosity of Irradiated Disks as a Function of  
Burnup from JRC/ITU Studies**



**Figure 14—3 HBS Area Fraction of Irradiated Disks as a Function of  
Burnup from JRC/ITU Studies**





**Figure 14—4 Mean ECD of the HBS Pores as a Function of Burn up  
from JRC/ITU Studies**



**Figure 14—5 JRC/ITU Calculated Pressure in the HBS Pores as a Function of Burn up**



**Figure 14—6 HBS Porosity in CEA Studies**



**Figure 14—7 HBS Volume Fraction from CEA Studies**



**Figure 14—8 Ratio of Xe in Bubbles / Total Xe from SIMS Studies at  
CEA**

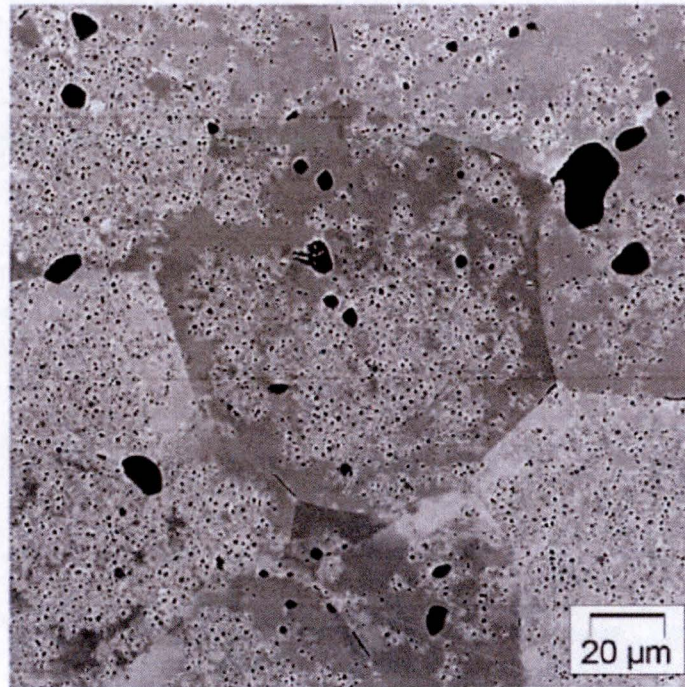


**Figure 14—9 HBS Nucleation Both on Grain Boundaries and Inside the Grain for Chromia-Doped Fuel**

**References for Response 14:**

- 14-1 Baron, M. Kinoshita, P. Thevenin and R. Largenton, "Discussion about HBS Transformation in High Burn-Up Fuels," Nuclear Engineering and Technology, VOL. 41 NO. 2, March 2009.
- 14-2 J. Noirot , L. Desgranges, J. Lamontagne, "Detailed characterisations of high burn-up structures in oxide fuels," Journal of Nuclear Materials 372, (2008), 318–339.
- 14-3 K.Une, M.Hirai, K.Nogita, et al, "Rim Structure Formation and High Burn-up Fuel Behaviour of large-grained UO<sub>2</sub> Fuels", *Journal of Nucl. Mat.* 278, (2000), n°1 pp54-63.
- 14-4 J.Spino, D.Baron, M.Coquerelle, A.D.Stalios, "High Burnup Rim Structure: Evidence that Xenon Depletion, Pore Formation, and Grain Subdivision start at Different Local Burn-ups", *Journal of Nucl. Mat.* 256, (1998), 189-196.

## **15.0 REFERENCES**

- 15-1 ANP-10340P, Revision 0, "Incorporation of Chromia-Doped Fuel Properties in AREVA Approved Methods," AREVA Inc., April 2016.
- 15-2 Letter, Jonathan G. Rowley (NRC) to Gary Peters (AREVA) "Request for Additional Information Regarding AREVA Inc. Topical Report ANP-10340P, Revision 0, 'Incorporation of Chromia-doped Fuel Properties in AREVA Approved Methods'," (CAC NO. MF7707), August 4, 2017.



**16.0 MARKUP PAGES**

<b>New Page Number</b>	<b>Original Page Number</b>	<b>RAI Number</b>
13	13	2
14	14	2
16	16	2
49	49	2
92	92	2

on various microstructure types to identify how much  $\text{Cr}_2\text{O}_3$  is needed to achieve the enhanced viscoplastic behavior for chromia-doped fuel.

The  $\text{Cr}_2\text{O}_3$ -doped  $\text{UO}_2$  fuel grain morphology characteristics are specified to achieve the greatest improvement in enhanced fuel viscoplasticity. To that end, the optimum  $\text{Cr}_2\text{O}_3$  concentration of [ ] was identified, which leads to an average grain size of [ ] as shown in Figure 4-1, and significantly improves the fuel viscoplastic properties.

For the chosen chromia concentration, [ ]

].

#### 4.2 Theoretical Density

[ ]

]

The theoretical density of the oxide at 20 °C is equal to the average mass of four molecules composing the elementary cell that is divided by the volume of the elementary cell:

$$\rho_{th} = \frac{4M_{ox}}{N_{av}a_{ox}^3} \quad (4-1)$$

where:

$N_{av}$  Avogadro's number

$a_{ox}$  oxide lattice parameter

$M_{ox}$  oxide molecular mass

The average molecular weight of the doped oxide is by definition:

$$M_{ox\ doped} = (1 - E_{m\ Cr_2O_3})M_{UO_2} + E_{m\ Cr_2O_3}M_{Cr_2O_3} \quad (4-2)$$

Finally, the mole fraction of chromia in the oxide, which is needed in Equation 4-2, is given by the following:

$$E_{m\ Cr_2O_3} = \frac{\frac{E_{w\ Cr_2O_3}}{M_{Cr_2O_3}}}{\frac{E_{w\ Cr_2O_3}}{M_{Cr_2O_3}} + \frac{(1-E_{w\ Cr_2O_3})}{M_{UO_2}}} \quad (4-3)$$

where:

$E_{w\ Cr_2O_3}$  weight fraction of  $Cr_2O_3$  in the oxide

$M_{Cr_2O_3}$  molecular mass of  $Cr_2O_3$

$M_{UO_2}$  molecular mass of  $UO_2$

Therefore, the density of the chromia-doped  $UO_2$  follows from Equation 4-1 by dividing the formulas for doped and standard fuels:

$$\rho_{th\ doped} = \frac{M_{ox\ doped}}{M_{ox}} \rho_{th\ non-doped} \quad (4-4)$$

In formulating Equation 4-4, the experimental finding that the lattice parameter suffers only a minor, negligible decrease was used (Reference 3). Therefore, the parameter  $a_{ox\ doped}$  is assumed equal to  $a_{ox}$ .



The specific heat of unirradiated  $\text{UO}_2$  and  $\text{Cr}_2\text{O}_3$ -doped  $\text{UO}_2$  fuel pellets was measured by differential scanning calorimetry at the Materials Research Unit of JRC-ITU using a cover gas of high-purity argon and a heating rate of 25 K/min (Reference 15). The relative uncertainty on the specific heat determined by this technique is estimated to be 7% (Reference 15). The JRC-ITU measured values for the specific heat of standard and chromia-doped  $\text{UO}_2$  fuel types is displayed in Figure 4-2, in which the high-temperature measurements from previous studies at JRC-ITU (Reference 7) are also shown.

A negligible effect of the chromia additive on the specific heat of  $\text{UO}_2$  is observed in Figure 4-2 for the low to medium (about 1500 K) temperature range. The slightly higher specific heat of chromia-doped fuel is in agreement with the law of mixtures and it is appropriate to ignore the negligible increase in specific heat due to chromia additive. The negligible effect of the chromia additive at high temperatures, where data are not available, is justified based on theoretical arguments, which apply over the full temperature domain. The same negligible effect of the chromia additive was also determined for chromia-doped gadolinia fuel.

It is shown in Reference 8 that in the low to medium temperature range the specific heat is well represented by the Debye and Einstein models, which describe the contribution of harmonic and anharmonic lattice vibrations; while at high temperatures (above 1500 K) the rapid increase in specific heat is attributed to point defect formation, especially Frenkel defects (pairs of uranium cation vacancies and interstitials). The chromium additive occupies **mostly interstitial** a small fraction of substitutional positions and has little impact on the uranium cation sub-lattice (although it can affect the oxygen sub-lattice) and thus it does not affect the formation of Frenkel defects at high temperatures. Consequently, the chromium additive has a negligible impact on the Chromia-doped  $\text{UO}_2$  specific heat in the high temperature range.

It is concluded that the addition of a small quantity of chromia dopant has a negligible effect on the specific heat of the urania matrix, [ ]. Therefore, chromia-doped fuel will be described with the same specific heat formulation as standard  $\text{UO}_2$ . Since specific heat and enthalpy are fully correlated variables (the

RIA is a fast rise of fuel power and temperature. The power excursion may lead to failure of the nuclear fuel rods and release of radioactive material in the primary reactor coolant.

Pulse irradiation tests show that fuel rod susceptibility to failure increases with increasing fuel burnup. It is also clear that the burnup dependent state of the rod and, in particular, the degree of waterside corrosion and related hydride induced embrittlement is very important for the survivability of fuel rods. Regarding fuel pellets, the factors of particular importance to the behavior include: heat-up rates, melting, fragmentation, fission gas induced transient swelling and transient fission gas release.

Under the initial phase of a RIA, the fuel pellet is heated almost adiabatically, i.e. without heat transfer taking place either inside the fuel pellets or across the pellet-clad gap. Due to the surface-peaked temperature distribution in combination with the burnup-induced depression of fuel melting temperature at the pellet periphery, peak temperature under rapid RIAs will first occur at a radial position of about 0.2 to 0.5 mm beneath the pellet surface. To extend the discussion on fuel temperature and the potential risk for fuel melting with a change from  $\text{UO}_2$  to chromia-doped fuel it is necessary to consider that:

[

]

All these elements indicate that the radial average fuel enthalpy threshold for incipient melting of chromia-doped fuel is not significantly different from the  $\text{UO}_2$  fuel enthalpy threshold.



transient when most of the initial stored energy has dissipated. The clad surface heat transfer rate and PCT are essentially determined by decay heat, minimizing the PCT impact of initial stored energy due to chromia-doping.

The large break case shows a larger increase in PCT because the PCT occurs earlier such that a portion of the initial stored energy still remains and contributes in a small way to the clad surface heat transfer rate, resulting in a slightly increased PCT when chromia-doping is used. For these LOCA test cases, the effect of chromia-doping on PCT is similar to the effect that occurs when gadolinium doping is used, also resulting in reduced fuel thermal conductivity and increased initial stored energy. Table 9-4 summarizes the LOCA evaluation results.

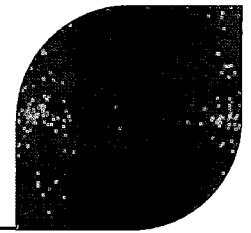
This CRDA test case shows the results of a BWR control rod drop accident. The increase in initial stored energy associated with chromia-doping resulted in an insignificant increase in both the peak channel enthalpy rise and the average enthalpy rise for all modeled channels. Table 9-4 summarizes the CRDA evaluation results.

### **9.3      *Impact on Nuclear Design Requirements***

There is no impact on reactor physics calculations because chromium and oxygen cross sections are included in the nuclear data library of the CASMO-4 lattice code. Additions of  $\text{Cr}_2\text{O}_3$  to the fuel will require no changes to existing neutronics codes or methodologies.

The absorption cross section of the chromium additive (3.1 barn) is very small in comparison to that of the fuel. Moreover, the chromium atoms occupy ~~mostly~~ **interstitial** a small fraction of substitutional positions in the  $\text{UO}_2$  lattice, which is therefore practically not disturbed, resulting in the reactivity coefficients of the chromia-doped fuel being unchanged in comparison to standard fuel.

The requirements of both GDC 11 and GDC 26 regarding the reactivity coefficients of the fuel and the capability of the reactivity control system to maintain the reactor subcritical under cold conditions in situations that include equipment malfunctions, will be satisfied by the specific reload analyses that will be performed for chromia-doped



---

# **Incorporation of Chromia-Doped Fuel Properties in AREVA Approved Methods**

ANP-10340NP  
Revision 0

## **Topical Report**

April 2016

AREVA Inc.

---

© 2016 AREVA Inc.

### Nature of Changes

Item	Revision Number	Section(s) or Page(s)	Description and Justification
1.	0	All	This is the initial release.



## Contents

	<u>Page</u>
1.0 INTRODUCTION .....	1
2.0 SUMMARY .....	2
3.0 APPLICABLE REGULATORY GUIDANCE .....	4
4.0 MATERIAL PROPERTIES.....	12
4.1 Microstructure .....	12
4.2 Theoretical Density .....	13
4.3 Thermal Expansion .....	15
4.4 Specific Heat and Enthalpy.....	15
4.5 Thermal Conductivity .....	17
4.5.1 Laser flash diffusivity technique .....	17
4.5.2 Chromia-doped thermal diffusivity database .....	18
4.6 Grain Size and Growth.....	20
4.7 Elastic Moduli.....	21
4.8 Tensile Fracture Strength .....	21
4.9 Creep and Plastic Deformation .....	22
4.10 Fuel Pellet Cracking.....	24
4.11 In-reactor Densification .....	25
4.12 Effect of Additive on the High Burn-up Fuel Pellet Rim Structure .....	25
5.0 BEHAVIORAL ASSESSMENT .....	43
5.1 Washout Characteristics .....	43
5.2 Fuel Melting .....	45
5.3 Behavior During Accidental Conditions.....	47
5.3.1 Loss of coolant accidents .....	47
5.3.2 Reactivity initiated accidents .....	48
6.0 QUALIFICATION DATA .....	57
6.1 Steady-state Qualification Dataset.....	57
6.2 Ramp Database Qualification Dataset.....	58
7.0 QUALIFICATION OF RODEX4 FOR CHROMIA-DOPED FUEL .....	62
7.1 RODEX4 Thermal Conductivity Model for Chromia-doped Fuel.....	62

7.1.1	Adaptation of RODEX4 thermal conductivity model to unirradiated chromia-doped fuel.....	64
7.1.2	Validation of RODEX4 thermal conductivity model to irradiated chromia-doped fuel .....	67
7.2	RODEX4 Fission Gas Release Model for Chromia-doped Fuel.....	68
7.3	RODEX4 Intragranular Gaseous Swelling Model for Chromia-doped Fuel .....	69
8.0	QUALIFICATION OF AURORA-B TO CHROMIA-DOPED FUEL .....	84
9.0	LICENSING CRITERIA ASSESSMENT .....	85
9.1	Steady-state and AOO Analyses (Thermal-Mechanical Evaluation).....	85
9.2	Safety Analyses .....	90
9.3	Impact on Nuclear Design Requirements .....	92
9.4	Licensing Criteria Conclusion .....	93
10.0	OPERATING EXPERIENCE .....	99
10.1	Steady State Irradiation .....	99
10.2	Ramp Testing and Demonstrated PCI Benefit of Chromia-doped Fuel.....	99
11.0	REFERENCES.....	104

### List of Tables

Table 3-1	Standard Review Plan Section 4.2 Criteria .....	6
Table 4-1	Thermal Conductivity Test Database Composition, 2015 .....	27
Table 4-2	Thermal Conductivity Test Database, 2015 – Material Characteristics .....	28
Table 4-3	Grain Sizes of Chromia-Doped Database .....	29
Table 5-1	Fuel Sample Characteristics for Thermogravimetry Testing.....	51
Table 5-2	Melting Temperature Measurements of Doped and Non-Doped samples at JRC-ITU .....	52
Table 5-3	Melting Temperature Measurements of Doped and Non-Doped Gadolinia Fuel Samples at JRC-ITU .....	53
Table 6-1	Chromia-Doped Fuel Irradiation Database.....	61
Table 9-1	Chromia-Doped Thermal-Mechanical Analysis Sample Case Results.....	94
Table 9-2	Fast AOO Sample Case Comparing Chromia-Doped UO <sub>2</sub> Fuel and Non-Doped UO <sub>2</sub> Fuel Analyses.....	96
Table 9-3	Fast AOO Sample Case Comparing Chromia-Doped GAD Fuel and Non-Doped GAD Fuel Analyses.....	97
Table 9-4	Impact of Chromia-Doping on BWR Sample Test Cases .....	98
Table 10-1	Operating Experience with Chromia-doped Fuel.....	102

### List of Figures

Figure 4-1	Illustration of Grain Morphology in Standard and Chromia-Doped Fuels .....	30
Figure 4-2	Specific Heat Measurement Data at JRC-ITU of Doped and Non-Doped Fuels .....	31
Figure 4-3	Experimental Laser-flash Technique to Measure Thermal Diffusivity at Low to Medium Temperatures .....	32
Figure 4-4	Schematic Diagram of Laser Flash Thermal Diffusivity Apparatus for High Temperature used at JRC-ITU .....	33
Figure 4-5	Thermal Conductivity Measurements at AREVA in 2015 .....	34
Figure 4-6	Thermal Conductivity Measurements at JRC-ITU in 2015 .....	35
Figure 4-7	Thermal Conductivity Measurements at AREVA in 2006 .....	36
Figure 4-8	Thermal Conductivity Measurements at JRC-ITU in 2006 .....	37
Figure 4-9	Diffusivity Measurements at JRC-ITU on AREVA Doped and Non-Doped Fuels .....	38
Figure 4-10	Yield Strength of Doped and Non-Doped Fuels at 1500 °C .....	39
Figure 4-11	Creep Strain of Doped and Non-Doped Fuels at 1500 °C .....	40
Figure 4-12	Comparison of Creep Data for Doped and Non-Doped Fuels .....	41
Figure 4-13	Post-Irradiation Ceramography Comparing Doped and Non-Doped Fuels .....	42
Figure 5-1	Fuel Ceramography Showing Reduced Oxidation of Doped Fuel in Comparison to Non-Doped Fuel .....	54
Figure 5-2	Grain Structure Showing Reduced Oxidation Penetration of Doped Fuel .....	55
Figure 5-3	Melting Temperature Experimental Setup at JRC-ITU .....	56
Figure 7-1	MATPRO and Fink Specific Heat Correlations .....	74
Figure 7-2	Re-evaluation of JRC-ITU 1999 Standard UO <sub>2</sub> Diffusivity Data with Consistent Specific Heat Correlation .....	75
Figure 7-3	Diffusivity Measured Data vs Predicted RODEX4 Values for Non-Doped Standard UO <sub>2</sub> .....	76
Figure 7-4	Thermal Resistivity for Different Chromia Concentrations .....	77
Figure 7-5	Chromia-Doped RODEX4 Model .....	78
Figure 7-6	Calculated vs Measured Temperatures in the REMORA2 Test .....	79

Figure 7-7	Calculated and Measured Temperatures vs Linear Power in the REMORA2 Test .....	80
Figure 7-8	Fission Gas Release Measured vs Calculated for Chromia-Doped Database .....	81
Figure 7-9	Illustration of Intragranular Porosity Developing in Chromia-Doped Fuel.....	82
Figure 7-10	Strain and Strain Increment Measured vs Calculated for Chromia-Doped Database .....	83
Figure 10-1	Ramp Test Data Showing Increased Fuel Failure Threshold for Chromia-Doped Fuel .....	103

*This document contains a total of 118 pages.*

## Nomenclature

Acronym	Definition
AOO	Anticipated Operational Occurrence
BWR	Boiling Water Reactor
CEA	Commissariat a l'Energie Atomique
CPR	Critical Power Ratio
CRDA	Control Rod Drop Accident
CRWE	Control Rod Withdrawal Error
CWSR	Cold-Worked Stress-Relieved
FDL	Fuel Design Limit
FGR	Fission Gas Release
HBS	High Burnup Structure
JRC-ITU	Joint Research Centre – Institute for Transuranium Elements
LFA	Lead Fuel Assembly
LHGR	Linear Heat Generation Rate
LOCA	Loss of Coolant Accident
LWR	Light Water Reactor
MLI	Mean Linear Intercept
PCI	Pellet-Cladding Interaction
PCMI	Pellet-Cladding Mechanical Interaction
PCT	Peak Cladding Temperature
PIE	Post-Irradiation Examination
PWR	Pressurized Water Reactor
RIA	Reactivity Initiated Accident
RTL	Ramp Terminal Level
RXA	Recrystallized Annealed
TD	Theoretical Density

## ABSTRACT

AREVA has developed chromia-doped fuel by adding a small quantity of chromia ( $\text{Cr}_2\text{O}_3$ ) to standard fuel. This doped fuel is similar to standard fuel, but the chromia dopant greatly enhances grain growth during sintering; and therefore, chromia-doped fuel is characterized by larger grain size than standard fuel. This topical report examines the effect of the use of chromia-doped fuel and its implementation in AREVA methodology.

A discussion is presented of the applicable regulatory guidance related to fuel material. This guidance is found primarily in NUREG-0800 Sections 4.2 through 4.4. The effects the incorporation of chromia-doped fuel has on the methods which support the applicable NUREG-0800 criteria are provided.

The material properties and behavioral aspects of the chromia-doped fuel in comparison to standard fuel are described. Chromia-doped fuel is similar to standard fuel and the few properties that differ are identified. The available chromia-doped fuel database of both separate-effects and integral tests that can be used for fuel model qualification is presented. While the qualification database, material, and behavioral sections of this report are valid for both BWR and PWR applications, the model adaptation to chromia-doped fuel is code specific.

A description of how AREVA's BWR codes have been modified and validated to support the use of chromia-doped fuel is provided. Code adjustments were made to accommodate changes in the thermal conductivity and gaseous swelling models. No other changes to any of the current BWR methodologies were necessary.

The adaptation and qualification of RODEX4 and S-RELAP5 to chromia-doped fuel is presented. Sample cases of design analyses are provided that cover the entire range for fuel licensing under RODEX4-based BWR methodologies for thermal-mechanical analyses, thermal limits and safety analyses.

Finally, the report summarizes AREVA's experience with chromia-doped fuel for both steady state irradiation and ramp testing, and demonstrates the chromia-doped fuel benefit with respect to reduced fuel failure.



## 1.0 INTRODUCTION

AREVA has developed chromia-doped fuel by adding a small quantity of chromia ( $\text{Cr}_2\text{O}_3$ ) to standard fuel. This doped fuel is similar to standard fuel, but the chromia dopant greatly enhances grain growth during sintering; and therefore, chromia-doped fuel is characterized by larger grain size than standard fuel. This results in a reduction of fission gas release and also a diminished potential for fuel washout from a failed fuel rod. At the same time, chromia-doped fuel has improved behavior during power transients, which is translated into higher pellet-cladding interaction (PCI) failure thresholds in comparison with standard fuel.

The benefits of chromia-doped fuel are relevant to both BWR and PWR fuel rods and in each type of reactor conditions. While the qualification database, material, and behavioral sections of this report are valid for both BWR and PWR applications, the model adaptation to chromia-doped fuel is code specific.

BWR fuel methods are addressed by describing the qualification of the RODEX4 fuel code for chromia-doped fuel, together with the related upstream and downstream codes and methods. BWR fuel rod growth is the one performance characteristic affected by chromia-doped fuel that is not addressed within this report. Fuel rod growth will be addressed in a separate topical report for NRC approval prior to licensing of BWR chromia-doped fuel.

## 2.0 SUMMARY

This report provides a description of the changes to AREVA's RODEX4 fuel code and its validation in order to support the use of chromia-doped BWR fuel. In addition the upstream neutronics codes and methods and the downstream thermal-hydraulic codes and methods have been analyzed for any needed adaptation to chromia-doped fuel. No adaptation was identified for the neutronics codes and methods, while an update of the thermal conductivity model for the S-RELAP5 code was identified for the downstream thermal-hydraulic codes and methods.

The report provides the material properties of chromia-doped fuel in Section 4.0 with the associated qualification dataset, which provides the basis for properties that are different from those of standard fuel. For the material properties that are not affected by the chromia dopant, experimental and/or theoretical justification is provided to support the continued use of the material property for chromia-doped fuel.

Section 5.0 describes the chromia-doped fuel characteristics that are related to in-reactor behavior during normal operation, accident conditions, and following fuel failure.

The validation and verification (i.e. qualification) database that is required in order to qualify a fuel code for chromia-doped applications is described in Section 6.0. This data is presented in Section 7.0. Measurements taken on fuel rods during and after irradiation testing are used in combination with separate-effects testing to provide data to characterize material properties.

Sections 7.0 through 9.0 describe how the general properties of chromia-doped fuel are modeled in the AREVA RODEX4-based BWR methodology to generate sample licensing evaluations in support of typical core designs. The adaptation and qualification of RODEX4 to chromia-doped fuel are described in Section 7.0. The qualification of RODEX4 to chromia-doped fuel also justifies the removal of the grain size restriction imposed in the Safety Evaluation for Reference 20. Section 8.0 provides information regarding qualification of the AURORA-B S-RELAP5 models for chromia-doped fuel. Finally, for illustration purposes, Section 9.0 presents sample cases of

design analyses that cover the full range of calculations for fuel licensing under RODEX4-based BWR methodologies to demonstrate compliance with the licensing criteria which are discussed in Section 3.0.

The operating experience with chromia-doped fuel in power reactors is contained in Section 10.0. This section also describes the comprehensive power ramp program that is the basis for the quantification of the PCI performance improvement with chromia-doped fuel.

### 3.0 APPLICABLE REGULATORY GUIDANCE

Regulatory guidance for the review of fuel system designs and adherence to applicable General Design Criteria is provided in NUREG-0800, "Standard Review Plan for the Review of Safety Analysis Reports for Nuclear Power Plants", Section 4.2, "Fuel System Design" (Reference 1).

The SRP Section 4.3 is not discussed in this report because there are no changes required for the application of the neutronics codes and methods to chromia-doped fuel. Chromium neutron cross-sections are present in the lattice codes, and the neutronics methods accurately model this element as described in Section 9.3 of this report.

The SRP Section 4.4, which refers to the thermal and hydraulic design, is also not impacted by the chromia-doped fuel because the small change to fuel composition has no effect on any of the processes and phenomena related to thermal and hydraulic design of the core. However, the results of the analyses required by SRP Section 4.2 (which are also cross-referenced in SRP Section 4.4) are slightly modified by the specific properties of chromia-doped fuel. Therefore, the corresponding design basis topics are included in the following discussion of compliance with the applicable regulatory guidance.

In accordance with the Standard Review Plan Section 4.2, the objectives of the fuel system safety review are to provide assurance that:

- The fuel system is not damaged as a result of normal operation and anticipated operational occurrences (AOOs).
- Fuel system damage is never so severe as to prevent control rod insertion when it is required.
- The number of fuel rod failures is not underestimated for postulated accidents, and
- Fuel coolability is always maintained.

As there is no change to cladding materials or fuel assembly design and structural materials, only the Standard Review Plan fuel design criteria from Section 4.2 that are germane to implementation of chromia-doped fuel are described in Table 3-1. The only exception is the fuel rod growth model which is not addressed in this report. It is more appropriate to address fuel rod growth in the fuel mechanical topical report to be consistent with the suite of current AREVA BWR methods.

SRP Chapter 15 acceptance criteria for AOOs and accidents are addressed in Section 9.2, where representative events are analyzed and the effect of employing chromia-doped fuel on margins to acceptance criteria limits are evaluated. Table 3-1 addresses the SRP Chapter 15 acceptance criteria for the Section 4.2 design criteria that apply.

Data is provided in this topical report to allow removal of the grain size restriction imposed in the Safety Evaluation for Reference 20. The removal of this restriction is needed due to the larger grain size of chromia-doped fuel.

Table 3-1 Standard Review Plan Section 4.2 Criteria

1. Design Bases	Item	Topic	Assessment	Location in this Report
<b>A. Fuel System Damage</b>	i	Stress, strain, or loading limits (fuel rod cladding)	[ ]	See row B.vi of this table for information on cladding strain.
	ii	Fatigue (fuel rod cladding)	[ ]	Section 9.1 provides analysis results.
	iii	Fretting wear (fuel rod cladding)	[ ]	Since neither the method nor calculated results are affected by the use of chromia-doped fuel, this topic is not included in the report.
	iv	Oxidation, hydriding, crud (fuel rod cladding)	[ ]	Since neither the method nor calculated results are affected by the use of chromia-doped fuel, this topic is not included in the report.
	v	Dimensional changes (fuel rod growth)	[ ]	The chromia-doped fuel rod growth correlation will be addressed in a separate topical report.
	vi	Rod internal gas pressure	[ ]	Section 4.6 provides the grain size characterization. Section 7.2 discusses benchmarking the FGR model.

1. Design Bases	Item	Topic	Assessment	Location in this Report
	vii	Assembly liftoff	[  ]	Since neither the method nor calculated results are affected by the use of chromia-doped fuel, this topic is not included in the report.
	viii	Control rod reactivity and insertability	[  ]	Since neither the method nor calculated results for control rod insertability are affected by the use of chromia-doped fuel, this topic is not included in the report. Neutronics methods are discussed in Section 9.3.
B. Fuel Rod Failure	i	Hydriding (fuel rod cladding)	[  ]	Since neither the method nor calculated results are affected by the use of chromia-doped fuel, this topic is not included in the report.
	ii	Cladding collapse	[  ]	Section 4 provides the material properties and Section 9.1 provides analysis results.
	iii	Overheating of cladding	[  ]	Section 4 provides the material properties and Section 9.2 illustrates the impact of chromia-doped fuel on PCT.

1. Design Bases	Item	Topic	Assessment	Location in this Report
	iv	Overheating of fuel pellets	[	Section 4 provides the material properties. Section 9.1 illustrates the impact of the setting of power-dependent LHGR reduction factors for the peak pellet power versus peak pellet exposure-dependent FDL as needed to ensure the AOO licensing criteria are met. Section 9.2 presents the CPR analyses.
	v	Excessive fuel enthalpy	[	Section 5.3.2 discusses chromia-doped fuel behavior during RIA and Section 9.2 illustrates the impact of chromia-doped fuel on deposited enthalpy calculations.
	vi	Pellet/cladding interaction	[	Sections 4 and 7.3 provide the material properties that affect PCMI. Section 9.1 presents the results of the cladding strain analysis. Section 10.2 discusses the ramp test database.



1. Design Bases	Item	Topic	Assessment	Location in this Report
	vii	Bursting	[	Section 9.2 illustrates the impact of Chromia-doped fuel on criteria dealing with swelling and rupture.
	viii	Mechanical fracturing	[	Since neither the method nor calculated results are affected by the use of chromia-doped fuel, this topic is not included in the report.

1. Design Bases	Item	Topic	Assessment	Location in this Report
C. Fuel Cool-ability	i	Cladding embrittlement	[	Section 9.2 illustrates the impact of chromia-doped fuel on criteria dealing with ballooning and rupture.
	ii	Violent expulsion of fuel	[	Since neither the method nor calculated results are affected by the use of chromia-doped fuel, this topic is not included in the report.
	iii	Generalized cladding melting	[	Since neither the method nor calculated results are affected by the use of chromia-doped fuel, this topic is not included in the report.

1. Design Bases	Item	Topic	Assessment	Location in this Report
	iv	Fuel rod ballooning	[	Section 9.2 illustrates the impact of chromia-doped fuel on criteria dealing with ballooning and rupture.
	v	Structural deformation (fuel rod cladding)	[	Since neither the method nor calculated results are affected by the use of chromia-doped fuel, this topic is not included in the report.

## 4.0 MATERIAL PROPERTIES

Chromia-doped fuel is fabricated by adding a small amount of chromia ( $\text{Cr}_2\text{O}_3$ ) [

]. The following sub-sections describe the impact of chromia dopant on the material properties of the chromia-doped fuel in comparison to standard fuel.

Throughout the report, the  $\text{UO}_2$  fuel is called standard fuel, reference fuel, or non-doped in cases where the contrast to chromia-doped fuel is emphasized.

The chromia-doped fuel manufactured by AREVA is characterized by an additive concentration [ ]. Section 6.0 describes the qualification database which spans the chromia concentration manufacturing uncertainties.

### 4.1 *Microstructure*

Chromia,  $\text{Cr}_2\text{O}_3$ , is known as an effective dopant to produce fuel with a microstructure characterized by an enhanced grain size, [

]. However,  $\text{Cr}_2\text{O}_3$  was also found to accelerate fission gas diffusion coefficients when added in quantities of approximately 5000 wppm (Reference 2), which led to dopant segregation on grain boundaries during irradiation. The chromia concentration was established below this concentration level in order to control the dopant distribution within the fuel matrix, while still achieving the goal of having a large grain microstructure.

The fundamental mechanisms governing  $\text{UO}_2$  doping with  $\text{Cr}_2\text{O}_3$  were clarified during the initial development stages in the 1990's. For example, the sintering conditions which favor chromia dissolution in the  $\text{UO}_2$  matrix and the solubility limit of chromium in  $\text{UO}_2$  were studied. Also, extensive mechanical characterization tests were carried out

on various microstructure types to identify how much  $\text{Cr}_2\text{O}_3$  is needed to achieve the enhanced viscoplastic behavior for chromia-doped fuel.

The  $\text{Cr}_2\text{O}_3$ -doped  $\text{UO}_2$  fuel grain morphology characteristics are specified to achieve the greatest improvement in enhanced fuel viscoplasticity. To that end, the optimum  $\text{Cr}_2\text{O}_3$  concentration of [ ] was identified, which leads to an average grain size of [ ] as shown in Figure 4-1, and significantly improves the fuel viscoplastic properties.

For the chosen chromia concentration, [ ]

].

#### 4.2 Theoretical Density

[ ]

]

The theoretical density of the oxide at 20 °C is equal to the average mass of four molecules composing the elementary cell that is divided by the volume of the elementary cell:

$$\rho_{th} = \frac{4M_{ox}}{N_{av}a_{ox}^3} \quad (4-1)$$

where:

$N_{av}$  Avogadro's number

$a_{ox}$  oxide lattice parameter

$M_{ox}$  oxide molecular mass

The average molecular weight of the doped oxide is by definition:

$$M_{ox\ doped} = (1 - E_{m\ Cr_2O_3})M_{UO_2} + E_{m\ Cr_2O_3}M_{Cr_2O_3} \quad (4-2)$$

Finally, the mole fraction of chromia in the oxide, which is needed in Equation 4-2, is given by the following:

$$E_{m\ Cr_2O_3} = \frac{\frac{E_{w\ Cr_2O_3}}{M_{Cr_2O_3}}}{\frac{E_{w\ Cr_2O_3}}{M_{Cr_2O_3}} + \frac{(1 - E_{w\ Cr_2O_3})}{M_{UO_2}}} \quad (4-3)$$

where:

$E_{w\ Cr_2O_3}$  weight fraction of  $Cr_2O_3$  in the oxide

$M_{Cr_2O_3}$  molecular mass of  $Cr_2O_3$

$M_{UO_2}$  molecular mass of  $UO_2$

Therefore, the density of the chromia-doped  $UO_2$  follows from Equation 4-1 by dividing the formulas for doped and standard fuels:

$$\rho_{th\ doped} = \frac{M_{ox\ doped}}{M_{ox}} \rho_{th\ non-doped} \quad (4-4)$$

In formulating Equation 4-4, the experimental finding that the lattice parameter suffers only a minor, negligible decrease was used (Reference 3). Therefore, the parameter  $a_{ox\ doped}$  is assumed equal to  $a_{ox}$ .

The theoretical density of  $\text{UO}_2$  doped with chromia [

], compared to  $10.96 \text{ g/cm}^3$  for standard  $\text{UO}_2$ . A similar small correction is applied to chromia-doped gadolinia fuel.

#### **4.3 Thermal Expansion**

Thermal expansion of the fuel pellet must be defined in order to calculate heat transfer characteristics of the fuel, which are largely dependent on the gap between the fuel and the cladding. Thermal expansion and pellet swelling due to accumulation of fission gases must be taken into consideration when designing the fuel rod so that adequate clearance is achieved between the cold pellet and cladding during rod loading, and that the pellet-to-cladding gap can be accurately predicted during subsequent irradiation cycles.

When compositional changes to  $\text{UO}_2$  may be considered as a solid solution component, these changes have been shown to have a minor influence on the linear coefficient of thermal expansion. This has been demonstrated in the evolution of thermal expansion for mixed oxide (U, Pu) fuel up to 30 wt%  $\text{PuO}_2$  addition, and for gadolinia (U, Gd) fuel up to 12 wt%  $\text{Gd}_2\text{O}_3$  addition. Also, the thermal expansion of irradiated fuel does not significantly differ from unirradiated fuel despite the creation of fission products within the  $\text{UO}_2$  matrix as shown in Reference 4.

Therefore, a  $\text{Cr}_2\text{O}_3$ -doping level that is in the range of impurity content has a negligible effect and the thermal expansion of this fuel will be the same as for standard  $\text{UO}_2$ .

#### **4.4 Specific Heat and Enthalpy**

Specific Heat ( $C_p$ ), or specific heat capacity, is an important materials property which is required in order to predict thermal behavior of the  $\text{UO}_2$  fuel pellet during the transients considered in reactor safety calculations. Also specific heat is required to compute thermal conductivity from thermal diffusivity, as will be further explained in Section 4.5. The enthalpy and specific heat are coupled, fully correlated variables, with specific heat being the partial derivative of enthalpy with respect to temperature.

The specific heat of unirradiated  $\text{UO}_2$  and  $\text{Cr}_2\text{O}_3$ -doped  $\text{UO}_2$  fuel pellets was measured by differential scanning calorimetry at the Materials Research Unit of JRC-ITU using a cover gas of high-purity argon and a heating rate of 25 K/min (Reference 15). The relative uncertainty on the specific heat determined by this technique is estimated to be 7% (Reference 15). The JRC-ITU measured values for the specific heat of standard and chromia-doped  $\text{UO}_2$  fuel types is displayed in Figure 4-2, in which the high-temperature measurements from previous studies at JRC-ITU (Reference 7) are also shown.

A negligible effect of the chromia additive on the specific heat of  $\text{UO}_2$  is observed in Figure 4-2 for the low to medium (about 1500 K) temperature range. The slightly higher specific heat of chromia-doped fuel is in agreement with the law of mixtures and it is appropriate to ignore the negligible increase in specific heat due to chromia additive. The negligible effect of the chromia additive at high temperatures, where data are not available, is justified based on theoretical arguments, which apply over the full temperature domain. The same negligible effect of the chromia additive was also determined for chromia-doped gadolinia fuel.

It is shown in Reference 8 that in the low to medium temperature range the specific heat is well represented by the Debye and Einstein models, which describe the contribution of harmonic and anharmonic lattice vibrations; while at high temperatures (above 1500 K) the rapid increase in specific heat is attributed to point defect formation, especially Frenkel defects (pairs of uranium cation vacancies and interstitials). The chromium additive occupies a small fraction of substitutional positions and has little impact on the uranium cation sub-lattice (although it can affect the oxygen sub-lattice) and thus it does not affect the formation of Frenkel defects at high temperatures. Consequently, the chromium additive has a negligible impact on the Chromia-doped  $\text{UO}_2$  specific heat in the high temperature range.

It is concluded that the addition of a small quantity of chromia dopant has a negligible effect on the specific heat of the urania matrix, [ ]. Therefore, chromia-doped fuel will be described with the same specific heat formulation as standard  $\text{UO}_2$ . Since specific heat and enthalpy are fully correlated variables (the



specific heat is the derivative with respect to temperature of the enthalpy), it can also be concluded that the same enthalpy formulation can be used for chromia-doped fuel as standard  $\text{UO}_2$ .

#### **4.5 Thermal Conductivity**

Additives in either substitutional or interstitial solute form cause a decrease in the lattice thermal conductivity because of the additional scattering impact on phonons (quantum particles of the lattice vibration) when the additive has a different atomic mass than the host atoms. Therefore, it was anticipated that chromia doping (atomic mass 52 for chromium compared to 238 for uranium) will decrease the  $\text{UO}_2$  thermal conductivity, as was also experienced with other doped fuel types, such as gadolinia fuel.

In order to quantify the chromia doping impact on  $\text{UO}_2$  thermal conductivity, diffusivity measurements were performed on chromia-doped  $\text{UO}_2$  and gadolinia fuels, as well as standard  $\text{UO}_2$ , using the laser flash technique.

##### **4.5.1 Laser flash diffusivity technique**

To perform laser flash diffusivity measurements, a thin disc specimen is subjected to a radiant energy pulse with high-intensity and short duration. The energy of the pulse is absorbed on the front surface of the specimen, and the resulting rear face temperature rise as a function of time is recorded (Figure 4-3). The thermal diffusivity value is then calculated as a function of the specimen thickness and the time required for the rear face temperature rise to reach certain percentages of its maximum value (References 5 and 6).

The samples are heated to the desired temperature in a tube furnace, or heated with simultaneous high power pulses as in the JRC-ITU very high temperature technique (Reference 7 and Figure 4-4). Measurements are typically performed at several temperature levels, with long enough hold times at each temperature in order to achieve stable conditions before performing the measurement. The maximum achievable temperature level is limited by the furnace, being approximately 1650°C for the measurements reported herein. The temperature is measured directly on the sample by

a certified W (tungsten) thermocouple. Most experiments were conducted under inert gas atmosphere (argon).

The thermal conductivity is not directly measured by this laser flash technique, which is a dynamic type thermal property measurement of thermal diffusivity. Instead the thermal conductivity is calculated as a function of diffusivity, density, and specific heat as shown in Equation 4-5.

$$k(T) = \alpha(T) \cdot \rho(T) \cdot c_p(T) \quad (4-5)$$

where:

$k(T)$	-	thermal conductivity	[W/mK]
$\alpha(T)$	-	diffusivity	[m <sup>2</sup> /s]
$\rho(T)$	-	density	[kg/m <sup>3</sup> ]
$c_p(T)$	-	specific heat	[J/kg]
$T$	-	temperature	[K]

In most cases reported in the literature, specific formulations have been used for the density and specific heat. Moreover, for some JRC-ITU data, the actual measured specific heat values have been used. In order to eliminate this additional source of scatter, all the diffusivity data employed in this report have been processed with the specific heat formulation recommended by the MATPRO compendium of nuclear materials properties (Section 2.2 of Reference 8).

#### 4.5.2 Chromia-doped thermal diffusivity database

Two in-house laser flash diffusivity measurement campaigns were conducted in 2006 and 2015. In addition, in both cases a sub-set of samples used for the in-house measurements were sent to JRC-ITU for complementary measurements.

[

]

Figure 4-5, Figure 4-6, Figure 4-7, and Figure 4-8 display the results (all conductivity values normalized to 95% TD) of the two measurement campaigns both in-house and at JRC-ITU. The following general observations can be drawn from the two measurement campaigns:

[

]

[

]

#### 4.6 *Grain Size and Growth*

The enlarged grain microstructure is one of the two major features of the chromia-doped fuel that are different from the standard  $\text{UO}_2$  fuel, the other one being the thermal conductivity. There have been a number of chromia-doped lots fabricated in small scale batches for the different lead fuel assembly (LFA) programs and one large-scale study, with the reported grain sizes listed in the first column of Table 4-3.

Grain growth occurs by grain boundary migration so that the larger grains are enlarged at the expense of the smaller adjacent grains. Therefore, it is expected that very little grain growth occurs in the chromia-doped fuel during irradiation since considerable grain growth already occurred during sintering. This leads to a stable grain structure.

[

]

#### **4.7      *Elastic Moduli***

The possible variation of elastic properties is not fundamentally affecting the fuel behavior under normal operating conditions or AOO and accidental conditions.

According to the data published in the literature, the Young's modulus of standard  $\text{UO}_2$  can vary with characteristics such as grain size, stoichiometry or fuel porosity, however, the effect of these parameters is very limited compared to that of temperature (Reference 9). Moreover, the intrinsic impact of additives, including gadolinium or plutonium, up to high amounts (10-20 wt%) remains low with respect to Young's modulus and negligible for Poisson's ratio (Reference 9).

Considering that the chromia addition in  $\text{UO}_2$  is low [                      ], no effect is anticipated on the  $\text{UO}_2$  fuel Young's modulus and Poisson's ratio. Therefore, the same models that are currently used for standard fuel remain applicable to chromia-doped fuel.

#### **4.8      *Tensile Fracture Strength***

During normal steady-state or variable power conditions, the fuel pellet develops cracks because the thermal stresses, which are created by the quasi-parabolic temperature distribution across the fuel pellet, reach values above the fracture strength of the fuel.

Consequently, the fuel fracture strength is important. As a general trend,  $\text{UO}_2$  tensile strength decreases when the deformation rate increases, and this trend is more pronounced at high temperature. At room temperature,  $\text{UO}_2$  tensile strength decreases with increases in fuel pellet porosity, pore size and grain size.

The transition temperature between brittle and ductile behavior increases with increased grain size and the fuel tensile strength is reduced by approximately 40% (Reference 10). Finally, the effect of additives on fuel fracture strength is the result of microstructural modifications induced in the fuel matrix.

Comparative studies between  $\text{UO}_2$  and  $\text{Cr}_2\text{O}_3$ -doped unirradiated fuels were performed by AREVA [

]

This behavior for the chromia-doped fuel is fully consistent with results published in the literature (Reference 11) and accounts for the Chromia-doped fuel matrix with larger grain size. The plasticity temperature is lowered and therefore the bridging annulus is closer to pellet outer radius, meaning a narrower cracked outer rim with more numerous and smaller radial cracks, which is beneficial for PCI performance.

#### **4.9 Creep and Plastic Deformation**

For standard  $\text{UO}_2$  fuel (unirradiated samples), significant steady-state thermal creep occurs for temperatures exceeding approximately 1100 °C. Two creep mechanisms are active depending on the magnitude of the applied stress in comparison to a transition stress ( $\sigma_t$ ) (dependent on the matrix grain size) as follows:

- $\sigma < \sigma_t$ : pellet deformation according to diffusion creep mechanisms and inversely proportional to the matrix grain size
- $\sigma > \sigma_t$ : pellet deformation according to dislocation creep mechanisms and independent of the matrix grain size

The effect of additives on fuel steady-state creep behavior is difficult to identify because it is compounded with other fuel matrix characteristics affected by the additive: grain size, stoichiometry, equilibrium defect concentration, formation of secondary phases -- all things which might change diffusion coefficients, and/or grain boundary properties.

To assess the viscoplastic properties of the chromia-doped  $\text{UO}_2$  fuel pellets, extensive uniaxial mechanical compression tests were performed. These tests were performed under controlled atmosphere to prevent oxidation and stoichiometry changes of samples during the measurements. The main findings for the  $\text{Cr}_2\text{O}_3$ -doped fuel are summarized below.

[

]

Contrary to standard fuel with a smaller grain size, the viscoplastic deformation of the doped fuel [

].

#### **4.10 Fuel Pellet Cracking**

An adequate description of the crack patterns (number of cracks and orientation) which develop in fuel pellets during base load operation (including power ramps) is needed in order to calculate fuel pellet deformation and hence the pellet-clad mechanical interaction.

As the fuel rod power increases, pellets crack due to thermal stresses induced by the radial temperature gradient. At beginning of life, the minimum power required to initiate this radial cracking is approximately [ ]. However, while certain crack patterns are always noted after irradiation, there are no direct observations of the crack patterns at power. Inferences must be made on the basis of the parameters that are known to be important: the irradiation conditions, the fuel rod dimensions, and the cladding properties.

As discussed in Section 4.8, chromia doping affects the pellet tensile fracture strength and therefore also affects the fuel cracking pattern in operation. However, from the comparison given in Figure 4-13, it appears that  $\text{Cr}_2\text{O}_3$ -doped fuel cracking is fundamentally the same as for  $\text{UO}_2$ . In both cases, the main cracking component is radial, due to the tensile tangential stress in the outer pellet annulus. The circumferential crack is assumed to be formed, as generally accepted, during cooling at the final shut down.

It was observed from hot-cell PIE of chromia-doped fuel pellets following steady-state irradiations that a similar number of radial and axial cracks are present for both PWR and BWR fuel rods. After power ramp testing, it was observed that in comparison to standard fuel, [ ]



#### **4.11 *In-reactor Densification***

In-reactor densification is a phenomenon induced by irradiation and is thermally activated. Densification results from the elimination of fine porosity. First, the small-sized porosities (less than 1  $\mu\text{m}$ ) disappear, and then the medium-sized pores (about 1 to 3  $\mu\text{m}$ ) are progressively eliminated. The densification phase results in an increase of the fuel density by a decrease in the volume. The kinetics and the magnitude of the densification depend mainly on the fuel porosity distribution, which is a function of the powder used and of the pellet production process.

For such oxide fuels, experimental results have shown that the density variation observed under irradiation was close to that observed after a 24-hour out-of-reactor thermal stability test at 1700 °C, even if the mechanisms involved are different. Therefore, the resintering data are used to quantify the in-reactor densification of any fuel types.

[

]

#### **4.12 *Effect of Additive on the High Burn-up Fuel Pellet Rim Structure***

A local burnup of about 60 MWd/kgU at the pellet periphery is usually considered necessary for initiation of the high burnup structure (HBS) in  $\text{UO}_2$  fuel under low temperature conditions of less than 500 °C (Reference 12). [

]

This behavior is consistent with previous studies such as those reported in Reference 13. Grain recrystallization can develop when nucleus grains, i.e. sub-divided grains, are present. It is hypothesized that nucleus grains with high-angle grain boundaries are formed by inhomogeneous accumulations of dislocations.

In particular, grain boundaries are special areas for inhomogeneous dislocation accumulations because they inhibit the motion of dislocations. A smaller grain size will have a larger grain boundary surface area per volume, which will result in a higher density of dislocations. Such a fuel matrix will be prone to recrystallization, in contrast to a large grain matrix. [

]

The main conclusions from AREVA hot-cell PIE studies regarding HBS of chromia-doped fuel are as follows:

[

]

Overall, there is no significant difference in burnup thresholds and porosity of the HBS compared to standard fuel. The following trends were observed:

[

]

**Table 4-1 Thermal Conductivity Test Database Composition, 2015**

**[**

**]**

**Table 4-2 Thermal Conductivity Test Database, 2015 – Material  
Characteristics**

[

]

**Table 4-3 Grain Sizes of Chromia-Doped Database**

**[**

**]**

[

]

**Figure 4-1 Illustration of Grain Morphology in Standard and Chromia-Doped Fuels**

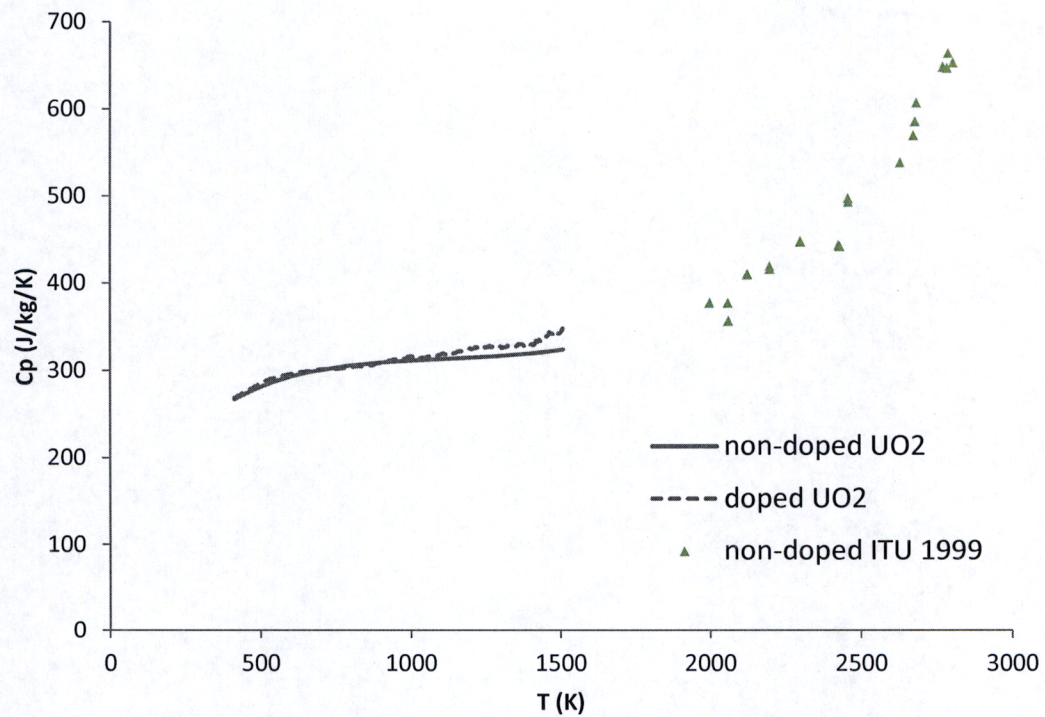


Figure 4-2 Specific Heat Measurement Data at JRC-ITU of Doped and Non-Doped Fuels



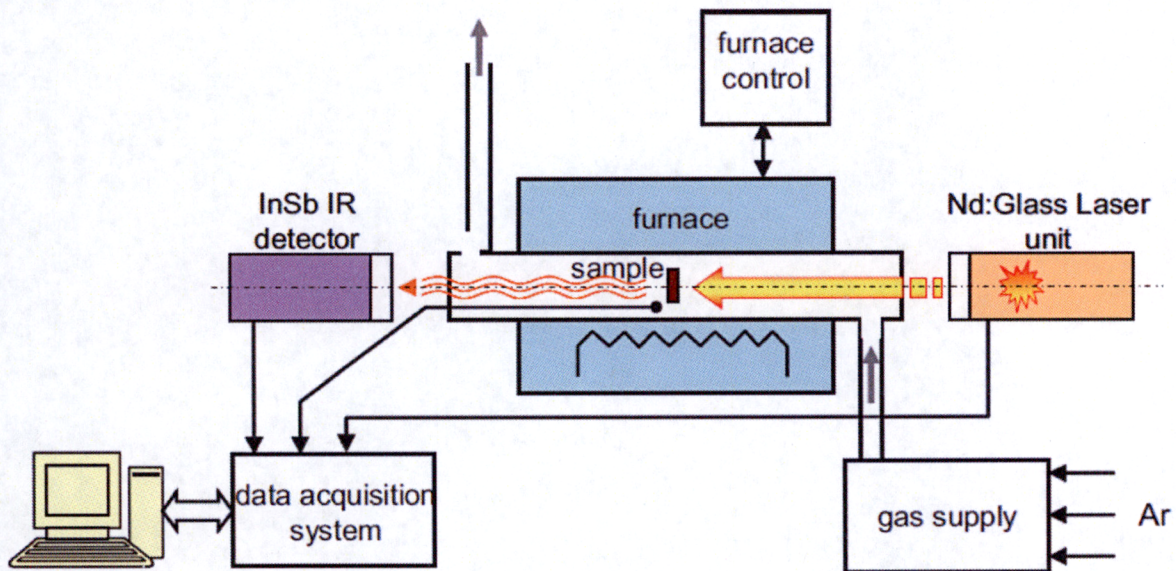
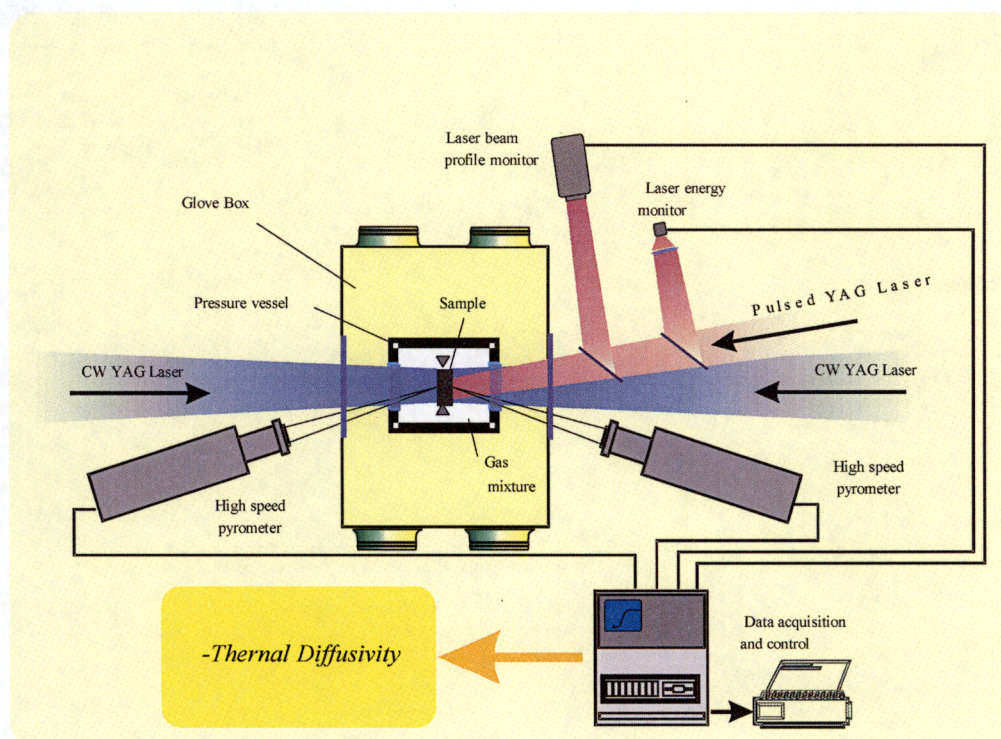


Figure 4-3 Experimental Laser-flash Technique to Measure Thermal Diffusivity at Low to Medium Temperatures





**Figure 4-4 Schematic Diagram of Laser Flash Thermal Diffusivity Apparatus for High Temperature used at JRC-ITU**

[

]

**Figure 4-5 Thermal Conductivity Measurements at AREVA in 2015**

[

]

**Figure 4-6 Thermal Conductivity Measurements at JRC-ITU in 2015**

[

]

**Figure 4-7 Thermal Conductivity Measurements at AREVA in 2006**

[

]

**Figure 4-8 Thermal Conductivity Measurements at JRC-ITU in 2006**

[

]

**Figure 4-9 Diffusivity Measurements at JRC-ITU on AREVA Doped  
and Non-Doped Fuels**

[

]

**Figure 4-10 Yield Strength of Doped and Non-Doped Fuels at 1500 °C**

[

]

**Figure 4-11 Creep Strain of Doped and Non-Doped Fuels at 1500°C**



[

]

**Figure 4-12 Comparison of Creep Data for Doped and Non-Doped  
Fuels**

[

]

**Figure 4-13 Post-Irradiation Ceramography Comparing Doped and  
Non-Doped Fuels**

## 5.0 BEHAVIORAL ASSESSMENT

The chromia-doped fuel behavior described in this section refers to special cases of either fuel failure or accident situations; and fuel melting is therefore included here as it is a key parameter for AOO and accidental conditions.

The behavior during accident conditions is analyzed with safety codes and methods. The adaptation of the codes and methods for application to chromia-doped fuel is described in Section 8.0 with sample problems provided in Section 9.0.

### 5.1 *Washout Characteristics*

Failed fuel degradation after the occurrence of primary defects (fuel rod leaks) can significantly affect reactor operations. As occasionally observed during some BWR fuel failures, axial split-type secondary failure of cladding results in a large release of fission products into the reactor coolant and may also lead to fuel washout due to direct contact of the fuel pellets with the coolant. Even though there are no licensing methodologies or criteria associated with washout, out-of-pile lab testing was performed to assess the washout behavior of chromia-doped pellets for comparison to standard  $\text{UO}_2$  fuel.

First, the reaction of fuel pellets with oxygen has been investigated by thermogravimetry at 380 °C (Reference 33). For a better understanding of the mechanisms involved, various types of  $\text{Cr}_2\text{O}_3$ -doped pellets having different density and grain size characteristics were tested (Table 5-1). The absolute mass changes that were measured during the tests showed that samples A and B, corresponding to the optimum grain size chromia-doped fuel, has up to 50% improved resistance against oxidation; while the chromia-doped sample C with a smaller grain size shows roughly a similar behavior to standard  $\text{UO}_2$ .

In Figure 5-1, ceramographic examinations show the difference in the oxidation occurring in the different fuel pellet samples. For standard  $\text{UO}_2$ , an intergranular corrosive attack is revealed with an outer surface oxidation which is quickly followed by intergranular oxidation and cracking and later spalling of oxidized grains. Similar features also appear in the case of the chromia-doped sample C.

On the contrary, in the case of the optimum grain size chromia-doped fuel samples A and B, the oxidation of the outer surface is not accompanied by generalized oxidation along grain boundaries. The outer oxidized layers are a barrier for oxygen diffusion and therefore the oxidation rate diminishes in time with very few intergranular cracks being formed. Thus, the larger grain size characteristic of chromia-doped fuel is the key parameter for reducing fuel oxidation.

In a second study, fuel corrosion behavior was investigated in autoclave leaching tests performed under representative BWR conditions (360 °C – 70 bars – 70 ppm H<sub>2</sub>O<sub>2</sub> in feed water), which showed [

]. Examinations

of chromia-doped samples from this second study showed:

[

]

The oxidation and washout behavior of unirradiated standard and Cr<sub>2</sub>O<sub>3</sub>-doped UO<sub>2</sub> fuel pellets have been analyzed in the two studies described above by thermogravimetry and by autoclave leaching tests at BWR conditions, respectively. The testing program demonstrates that chromia doping enhances the corrosion resistance of the fuel pellets. Such a feature is desired to prevent fuel pellet disintegration in case of failed fuel rods and the resulting contamination of the LWR primary coolant.

The main driver of the corrosion resistance improvement is [

].

It is worth noting that this trend observed in unirradiated fuel samples remains valid for irradiated fuel. This is supported by the conclusions drawn from the studies reported in Reference 14. More particularly these studies highlighted that the grain boundary penetration corrosion depths of irradiated pellets are approximately equivalent to values for unirradiated pellets. Consequently, it was stated that fuel irradiation, i.e. accumulation of fission products and irradiation damage, had no significant effect on the fuel corrosion.

## **5.2 Fuel Melting**

One of the variables that influence the melting point of  $\text{UO}_2$  is the total quantity of elemental impurities dispersed within the crystal structure. As impurities or trace dopants increase in  $\text{UO}_2$ , the melting point decreases.

The impact of chromia dopant on the melting temperature was determined by measurements performed at JRC-ITU (Reference 15) on standard and doped uranium dioxide, as well as chromia-doped (U-Gd)  $\text{O}_2$  samples.

The melting temperature was determined by laser heating and fast multi-channel pyrometry, an experimental method developed at JRC-ITU (References 16 and 17). The technique is illustrated in Figure 5-3. During the laser heating, a mixed oxide disk is held in a sealed autoclave under a controlled atmosphere (slightly pressurized air or argon at 0.35 MPa). In experiments carried out in pressurized argon, the absolute pressure of oxygen was checked to be smaller than 10 Pa. The controlled atmosphere together with the relative short duration of the experiments permitted only minimal sample decomposition, particularly linked to oxidation or oxygen losses, depending on

the initial composition. This approach aims to maintain the sample integrity and its composition as close as possible to its initial nominal value throughout the melting and freezing process.

Thermograms were measured with sub-millisecond resolution pyrometry on samples laser heated beyond melting. Pulses of different duration (100 ms to 1000 ms) and maximal power (315 W to 585 W) were repeated on a 5 mm diameter spot on a single sample surface, as well as on different samples of the same composition in order to obtain statistically significant datasets for each composition. Such pulses lead to maximum temperatures between 3500 K and 4000 K, which are considerably higher than the known melting temperature of uranium dioxide. This allows a sufficient amount of material to melt during the test in order to obtain a consistent thermal analysis during the cooling stage of the experiment.

Excessive thermal shocks were minimized by starting each series of laser pulses from a pre-set temperature of about 1500 K, at which each sample was held for 30 seconds before starting a series of high-power laser pulses. The pre-heating treatment also ensured better homogenization of the sample surface.

Each series consisted of four heating-cooling pulses on the same sample spot without cooling the material below an intermediate temperature of approximately 1500 K. The peak intensity and duration of the high power pulses were changed from one heating-cooling cycle to the other, in order to check the repeatability under slightly different experimental conditions and the effect of non-congruent vaporization or segregation phenomena. The sample cooled naturally when the laser beam was switched off during the thermal cycle. Thermal arrests corresponding to exothermic phase transitions (solidification) were then observed on the thermograms recorded by the fast pyrometers. The results are listed in Table 5-2 and Table 5-3 for chromia-doped  $\text{UO}_2$  and chromia-doped gadolinia fuels, respectively.

The test data was processed to determine the melting point of chromia-doped fuel on the following basis:

[ ]

Applying this methodology to the data presented in Table 5-2, the fuel melting temperature of chromia-doped  $\text{UO}_2$  is [ ] in comparison to standard  $\text{UO}_2$  fuel.

With respect to gadolinia fuel, [ ] This conclusion is validated by the measurements performed at JRC-ITU (Table 5-3) which show that [ ]

1.

### 5.3 *Behavior During Accidental Conditions*

The following two sections justify the conclusion that the anticipated behavior of chromia-doped fuel during the LOCA and RIA design basis accidents is [ ]

1.

#### 5.3.1 **Loss of coolant accidents**

During normal operation, oxide fuel pellets develop many radial and transverse cracks because of the thermal stresses generated by the quasi-parabolic radial temperature distribution across the fuel pellet. Therefore, the pellet can be viewed as a conglomerate of several millimeter-sized cracked fragments that are only loosely joined. During a temperature transient associated with a LOCA scenario, the cladding can deform outward due to loss of primary system pressurization (the term ballooning is

used for this process). It is possible that some of the fragments may move out of place and fill the additional open void created by the ballooning.

At high burnup however, several new phenomena are encountered which may counteract this behavior during a LOCA event. With the onset of pellet-to-cladding contact, bonding develops between the fuel pellet and the cladding. The higher the burnup, the thicker and larger the circumferential and axial surface coverage of the bond layer becomes. The development of this bond layer inhibits the ability of the pellet and cladding to move independently, and thereby affects load transfer from the pellet to the cladding and the subsequent cladding stress state. Another high burnup effect is the increasing amount of fission gas atoms in the fuel which may result in gaseous bubble swelling of the fuel when it reaches high temperatures. A third high burnup effect that might have an impact on LOCA behavior is related to the high burnup structure (HBS) at the pellet rim, with its associated large pores.

The LOCA testing programs at Studsvik and Halden have identified a tendency towards fine fuel fragmentation (called pulverization) and dispersal for simulated LOCA tests on high burnup fuels. It was identified that the susceptibility to pulverization is highly correlated to the formation of HBS at the rim of the pellet (Reference 18).

With respect to all these phenomena, chromia-doped fuel behaves [

]

### **5.3.2 Reactivity initiated accidents**

A Reactivity-Initiated Accident (RIA) is a nuclear reactor accident that involves an unwanted increase in fission rate and reactor power. The immediate consequence of a



RIA is a fast rise of fuel power and temperature. The power excursion may lead to failure of the nuclear fuel rods and release of radioactive material in the primary reactor coolant.

Pulse irradiation tests show that fuel rod susceptibility to failure increases with increasing fuel burnup. It is also clear that the burnup dependent state of the rod and, in particular, the degree of waterside corrosion and related hydride induced embrittlement is very important for the survivability of fuel rods. Regarding fuel pellets, the factors of particular importance to the behavior include: heat-up rates, melting, fragmentation, fission gas induced transient swelling and transient fission gas release.

Under the initial phase of a RIA, the fuel pellet is heated almost adiabatically, i.e. without heat transfer taking place either inside the fuel pellets or across the pellet-clad gap. Due to the surface-peaked temperature distribution in combination with the burnup-induced depression of fuel melting temperature at the pellet periphery, peak temperature under rapid RIAs will first occur at a radial position of about 0.2 to 0.5 mm beneath the pellet surface. To extend the discussion on fuel temperature and the potential risk for fuel melting with a change from  $\text{UO}_2$  to chromia-doped fuel it is necessary to consider that:

[

]

All these elements indicate that the radial average fuel enthalpy threshold for incipient melting of chromia-doped fuel is not significantly different from the  $\text{UO}_2$  fuel enthalpy threshold.

In ceramography examinations of high burnup fuel which has undergone a simulated RIA in pulse reactors, it is usually found that the outermost part of the pellet is fragmented. Typically a large number of radial cracks are seen at the pellet surface, and these cracks extend a few millimeters towards the fuel center, i.e. well beyond the re-structured rim zone.

These cracks are attributed to the large tensile radial and hoop stresses created during the early heat-up phase. The cracked fragments are large in size for low to medium burnup fuel, but for high burnup fuel, much finer fragments (less than 50  $\mu\text{m}$ ) have been observed in post-test examinations. These small-size fragments are found predominantly in the external part of the  $\text{UO}_2$  fuel pellets and are potentially available for fuel dispersal after fuel rod fracture during a severe RIA transient. The fine fragments are most likely a result of grain boundary decohesion, caused by over-pressurization of gas filled pores and intergranular bubbles under rapid rise in temperature (Reference 19).

[

]

**Table 5-1 Fuel Sample Characteristics for Thermogravimetry Testing**

Pellet type	Pellet density (% TD)	Pellet grain size ( $\mu\text{m}$ )	
		Linear intercept value	3D calculation value
Standard $\text{UO}_2$	97.0	8	12
$\text{Cr}_2\text{O}_3$ -doped – A	97.1	57	89
$\text{Cr}_2\text{O}_3$ -doped – B	98.2	55	86
$\text{Cr}_2\text{O}_3$ -doped – C	96.8	28	44

**Table 5-2 Melting Temperature Measurements of Doped and Non-Doped samples at JRC-ITU**

[

]

**Table 5-3 Melting Temperature Measurements of Doped and Non-Doped Gadolinia Fuel Samples at JRC-ITU**

[

]

[

]

**Figure 5-1 Fuel Ceramography Showing Reduced Oxidation of  
Doped Fuel in Comparison to Non-Doped Fuel**

[

]

**Figure 5-2 Grain Structure Showing Reduced Oxidation Penetration  
of Doped Fuel**

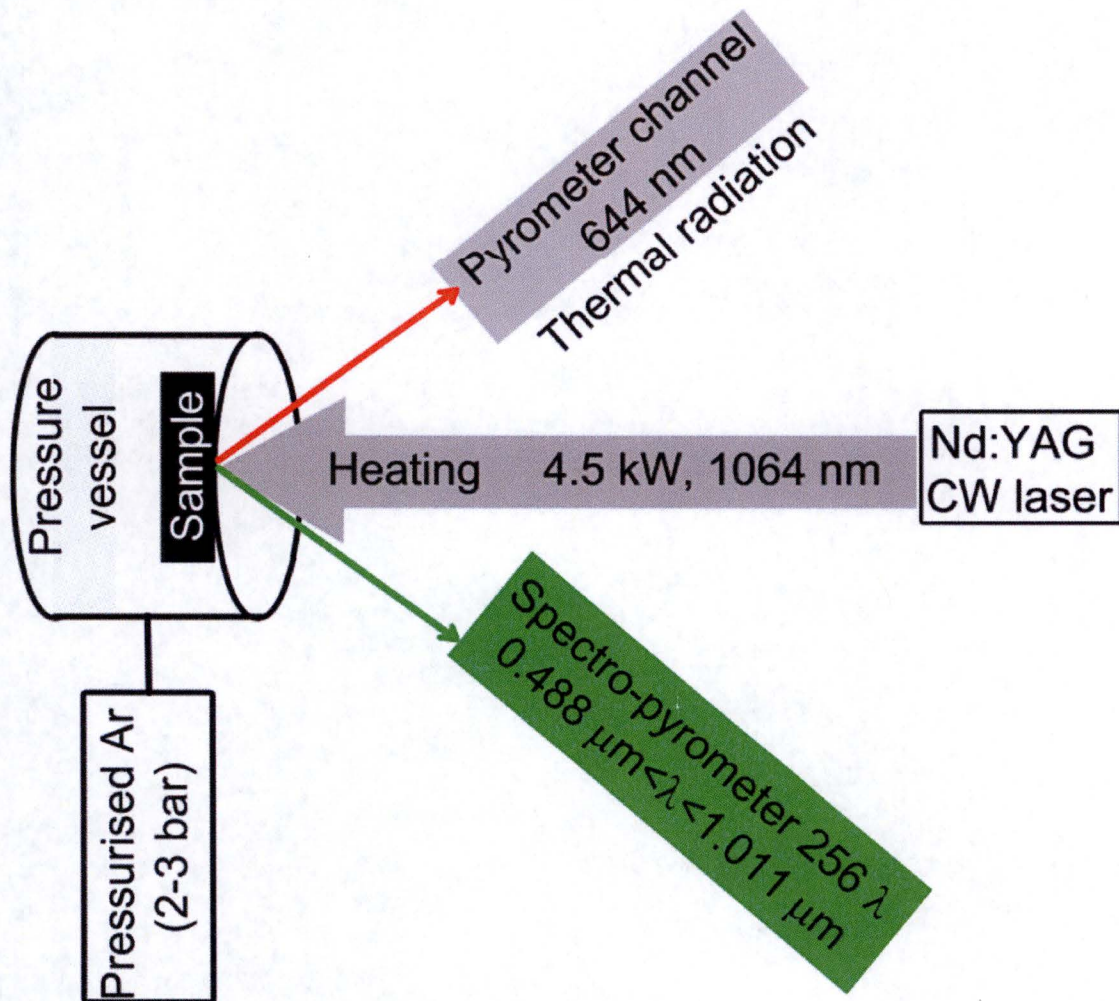


Figure 5-3 Melting Temperature Experimental Setup at JRC-ITU



## 6.0 QUALIFICATION DATA

The program to develop and study chromia-doped fuel pellets was initiated almost twenty years ago in French PWRs with actual plant irradiations starting in 2001. The irradiation program continued with operation in base load and load-follow transient conditions up to 75 MWd/kgU.

A large set of irradiation data in both power reactors and research reactors in steady-state and power ramp operational modes and in conditions specific to both BWR and PWR reactors was acquired in the last fifteen years. This comprehensive database covers the application range in terms of burnup and power, and is used to qualify the fuel codes for application to chromia-doped fuel. [

]

### 6.1 *Steady-state Qualification Dataset*

The chromia-doped fuel was irradiated in both BWR and PWR fuel rods, covering a range of designs and cladding materials. The range of the burnup achieved during steady-state irradiations is summarized in Table 6-1.

The cladding materials for the chromia-doped steady-state database are as follows:

[

]

The following fuel rod designs were used for the chromia-doped steady-state database:

[

]

Following irradiation, the following PIE measurements were acquired:

[

]

The fuel rods were either full-length or a string of rodlets that underwent power ramps in research reactors after the base irradiation. In some irradiation campaigns, rods with standard fuel were also irradiated in the same fuel assembly as the rods with chromia-doped fuel.

[

]

Temperature measurements were collected to support separate effects testing for high burnup fuel (~60 MWd/kgU). A segment cut from a rod base-irradiated in a commercial reactor was refabricated and instrumented with a central thermocouple and further irradiated in a test reactor with on-line temperature measurement during the steady state phase and two intermediate steps to higher power levels.

[

]

## **6.2 Ramp Database Qualification Dataset**

The cladding materials for the chromia-doped power ramp database are as follows:

[

]

The following fuel rod designs were used for the chromia-doped steady-state database:

[

]

Following irradiation, in which the burnup range is summarized in Table 6-1, the following PIE measurements were acquired:

[

]

The power ramp parameters, conditioning power level, power increment and hold time at the ramp terminal power level which were achieved in both the BWR and PWR power ramps programs cover the operational domain. This ramp test data has been used to determine the PCI benefit of the chromia-doped fuel as described in Section 10.2.

[

]

[

]

---

\* ATRIUM is a trademark of AREVA Inc.

**Table 6-1 Chromia-Doped Fuel Irradiation Database**

**[**

**]**

## **7.0 QUALIFICATION OF RODEX4 FOR CHROMIA-DOPED FUEL**

The RODEX4 fuel code was approved for BWR fuel rod design and licensing analyses in conjunction with its associated realistic methodology (Reference 20). The unique properties of chromia-doped fuel, which have been described in Section 4, necessitate minor adaptation of select code models so that RODEX4 can be applied to chromia-doped fuel for BWR analyses using the same realistic methodology.

The verification and validation of RODEX4 for qualification to chromia-doped fuel used the qualification database presented in Section 6 and consists of the following:

[

]

The qualification of RODEX4 to chromia-doped fuel also justifies the removal of the grain size restriction imposed in the Safety Evaluation for Reference 20. The qualification database includes larger grain sizes as indicated in Table 4-3.

The following describes the model adaptations or additions that were required, as well as the benchmarking of the qualification database. [

]

### **7.1 *RODEX4 Thermal Conductivity Model for Chromia-doped Fuel***

The JRC-ITU 1999 data (Reference 7) are generally considered the most qualified laser flash diffusivity data and therefore are used to validate the RODEX4 thermal conductivity model. As stated in Section 4.5, the 1999 JRC-ITU thermal conductivity

values were calculated by using either JRC-ITU measured specific heat or a known correlation for the specific heat. Therefore the calculation versus measurement comparison of thermal conductivity is significantly affected by which specific heat correlation was used to derive thermal conductivity from the measured thermal diffusivity.

The specific heat model in RODEX4 was taken from the MATPRO library of material properties prepared by INL (Reference 8), which is widely used in the nuclear industry. Another common source for specific heat is the material properties compendium sponsored by IAEA (Reference 21) largely based on the work led by J.K. Fink at ANL (Reference 22). The two specific heat correlations are quite comparable, with about 1% relative difference in the low to medium temperature range and larger differences of up to 4% relative in the high temperature range, as can be observed in Figure 7-1.

The JRC-ITU 1999 thermal conductivity values reported in Reference 7 used the Fink specific heat formulation for the low temperature range and their own measurements for the high temperature range. RODEX4 (i.e. MATPRO) over-predicts those data, especially in the high temperature range where the measurements present a large scatter band. The directly measured quantity is thermal diffusivity, while the thermal conductivity is calculated using a specific heat correlation that is independently obtained from separate measurements. To have an equivalent comparison of thermal conductivity, it is necessary to recalculate thermal conductivity from the thermal diffusivity data in Reference 7 using a common specific heat correlation.

The effect of using the specific heat correlation and density relations from RODEX4 (taken from MATPRO) to convert the JRC-ITU 1999 thermal diffusivity data into thermal conductivity is illustrated in Figure 7-2. This figure shows that the re-evaluation of thermal conductivity leads to a better agreement with the RODEX4 model. Therefore, it is concluded that the JRC-ITU 1999 laser flash measurements are in reasonable agreement with the RODEX4 model when a consistent specific heat correlation is used.

It is noticeable that the high temperature scatter band for thermal conductivity is greatly reduced when using the MATPRO specific heat formulation, which results from

elimination of the large uncertainty range of the JRC-ITU specific heat measurements in this high temperature range.

The results of the previous analysis have been further confirmed by including the JRC-ITU measurements of standard  $\text{UO}_2$  from the two campaigns conducted by AREVA on chromia-doped fuel (see Section 4.5). In order to remove inconsistencies related to the specific heat formulation used, the thermal diffusivity was calculated with the RODEX4 model and compared to measured thermal diffusivity values, corrected to 95% theoretical density. The results demonstrate a best-estimate prediction over the whole temperature range (Figure 7-3). It is observed that AREVA data from the two chromia-doped campaigns fill most of the gap in the temperature domain that was not covered by the JRC-ITU 1999 data and demonstrate consistency among the three datasets and with the nominal RODEX4 model.

The adaptation of the RODEX4 thermal conductivity model and its subsequent validation is discussed below.

#### **7.1.1 Adaptation of RODEX4 thermal conductivity model to unirradiated chromia-doped fuel**

The processing of the chromia-doped measurements described in Section 4.5 started with the linear fit of the inverse conductivity (thermal resistivity) after normalizing the raw data to 95% theoretical density according to the porosity term in RODEX4. A linear fit is expected for the low temperature range where the phononic term (Equation 7-2) dominates. The anticipated effect of chromia additions was confirmed by this linear plot of the inverse of conductivity, as displayed in Figure 7-4. The thermal resistivity increases (and thermal conductivity decreases) as the chromia content increases.

The dopant effect on thermal conductivity is the result of scattering phonon interactions (lattice vibrations) with impurities in the lattice either in substitutional or interstitial form. The impurities increase the thermal resistance of the lattice to phonon transport and therefore decrease the phonon conduction. The intrinsic thermal resistivity of the lattice is caused by phonon-phonon scattering interactions which increase in strength with temperature. [ ]



[

]

[

]

For completeness, the final adjusted model parameters of the chromia-doped thermal conductivity are listed below in Equations 7-1 to 7-9 and displayed in Figure 7-5:

[

]

[

1

#### **7.1.2 Validation of RODEX4 thermal conductivity model to irradiated chromia-doped fuel**

The previous thermal conductivity model adaptation to chromia-doped fuel was based on unirradiated fuel studies and accounts for the generic impact of the chromia dopant. It was anticipated that the burnup degradation impact on thermal conductivity, as described by Equation 7-5 for standard fuel, is valid for chromia-doped fuel as it was previously shown to be valid in the case of gadolinia fuel.

This was confirmed by the benchmarking of the REMORA2 test in which the pellet centerline temperature was measured online by a central thermocouple that was inserted in the drilled section of the refabricated rodlet. The rodlet was irradiated in the SILOE test reactor after the father rod achieved a rod average burnup of ~ 62 MWd/kgU in a power reactor.

Figure 7-6 below compares calculated and measured temperatures of the REMORA2 tests and demonstrates good agreement over the whole range of test powers. This is further illustrated in Figure 7-7, which shows the same trend vs power for both calculated and measured temperatures. A slight over prediction at the high power end is well within the power uncertainty range.

## **7.2      *RODEX4 Fission Gas Release Model for Chromia-doped Fuel***

Chromia-doped fuel is similar to standard fuel with an enlarged grain microstructure and the same phenomenological FGR model is applicable to both fuel types. In addition, the more oxidizing sintering conditions and the presence of the aliovalent chromia-dopant lead to a special electrochemical state of the chromia-doped fuel that is prone to enhancing diffusion processes which promote enhanced creep and grain growth during sintering. Hence a certain augmentation of the gas atom diffusion was speculated as possible for chromia-doped fuel. [

]

Therefore, the FGR model was not changed for chromia-doped fuel. It is remarked that the larger grain microstructure has two main consequences with opposite effects on FGR. On one hand, the gas atom diffusion to grain boundaries is delayed and diminished, but on the other hand, the grain boundary area and hence the grain boundary gas atom saturation (retention) capacity is decreased. While the first effect leads to FGR reduction, the latter causes a FGR increase. The net result is therefore time and power history dependent. The benchmarking of the chromia-doped FGR database was assessed in conjunction with the standard rods that were irradiated in the same fuel assemblies with the chromia-doped fuel rods, and for which FGR measurement was available.

The larger grain size of the chromia-doped fuel delays the transport of gas atoms to the grain boundary and therefore delays and reduces the final fission gas release to open voidage. Therefore, an exact and proper definition and characterization of the grain size of chromia-doped fuel is crucial for an adequate calculation of FGR. The existing

database consists of chromia-doped fuel manufactured in a small trial and production size setting, with variations and differences in powder mixing and sintering conditions.

[

]

The calculation versus measurement comparison is displayed Figure 7-8. [

]

### **7.3      *RODEX4 Intragranular Gaseous Swelling Model for Chromia-doped Fuel***

The PIE data on chromia-doped fuel rods show larger cladding deformation following both steady-state and power ramp irradiations, which indicates an increased chromia-doped fuel pellet deformation in comparison to standard fuel. Ceramography data show that larger intragranular bubbles exist in the case of chromia-doped fuel, which corroborates with the observed larger cladding deformation. These larger bubbles are interpreted to be a consequence of enhanced intragranular gaseous swelling, which in turn contributes to larger pellet deformation and hence larger cladding deformation, especially during power ramps. Standard  $\text{UO}_2$  exhibits very low intragranular gaseous swelling so this has not been modeled previously in RODEX4. The difference in intragranular gaseous swelling can be observed in hot-cell PIE images (Figure 7-9) indicating a low gas precipitation on grain boundaries and a significant gas precipitation into intragranular bubble form.

The larger intragranular gaseous swelling of the chromia-doped fuel is due to the combination of the two main characteristics of this fuel type: larger grain size and enhanced creep and plasticity. The latter implies greater propensity of the bubbles inside the grain to grow to larger size. The larger grain size means a greater chance for gas atoms being trapped by bubbles as they diffuse towards grain boundaries.

Consequently, an intragranular gaseous swelling model was developed for chromia-doped fuel in RODEX4. [

The hot-cell PIE performed by CEA for AREVA was used to determine the expected range for the model parameters defined above, the most important features revealed by PIE (see Figure 7-9) in relation to intragranular swelling being as follows:

[

]

Then, the number of gas atoms in an intragranular bubble,  $n$ , can be calculated as:

$$n = \frac{f_{ig} C_{gig}}{C_{igb}} \quad (7-12)$$

Replacing  $n$  in Equation (7-11) by the right-hand side of Equation (7-12), a third-order equation for the bubble radius,  $r_b$ , is obtained, as follows:

$$r_b^3 + \frac{2\gamma}{\sigma_h} r_b^2 - \frac{f_{ig} C_{gig}}{C_{igb}} \frac{3kT}{4\pi\sigma_h} = 0 \quad (7-13)$$

A similar third-order equation was obtained for the intergranular bubble radius and the same solver is used to derive the solution of Equation 7-13.

Once the average intragranular bubble radius that is in mechanical equilibrium with the current thermal-mechanical state of the fuel matrix is calculated from the equation above, the intragranular gaseous swelling,  $V_{igs}$ , can be calculated as the volume of all intragranular bubbles, resulting in:

$$V_{igs} = C_{igb} \frac{4\pi r_b^3}{3} \quad (7-14)$$

[

]

The intragranular gaseous swelling is negligible for standard  $UO_2$  but becomes significant for chromia-doped fuel and is manifested in larger diametral strain increment during power ramps and reduced creepdown during steady-state irradiation. The existing database of the above two parameters for chromia-doped fuel irradiated in both BWR and PWR reactors and a variety of cladding materials allows the calibration of the intragranular gaseous swelling described above. The model parameters  $f_{ig}$  and  $C_{gig}$  were parametrically varied to arrive at a best-estimate prediction of both creepdown and transient delta strain.

The creepdown data are represented by negative diameter changes, while the deformation increments during power ramps are represented by positive diameter changes. The outward creep can be either positive or negative depending on exposure (i.e. only at high exposures can the clad diameter deformation reversal reach positive numbers).



The results displayed in Figure 7-10 show that all three cladding deformation stages are equally well predicted, demonstrating consistent cladding modeling with the previous database. This provides the basis for qualifying the new intragranular gaseous swelling model for chromia-doped fuel, which drives the diameter change during power ramps and outward creep.

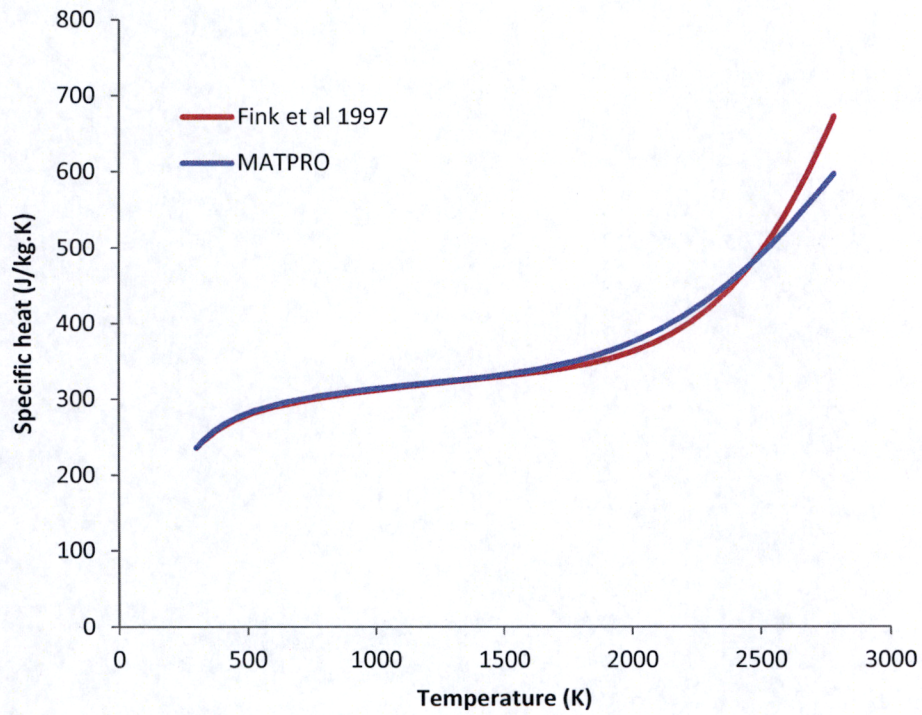


Figure 7-1 MATPRO and Fink Specific Heat Correlations

[

]

**Figure 7-2 Re-evaluation of JRC-ITU 1999 Standard  $\text{UO}_2$  Diffusivity  
Data with Consistent Specific Heat Correlation**

[

]

**Figure 7-3 Diffusivity Measured Data vs Predicted RODEX4 Values  
for Non-Doped Standard  $\text{UO}_2$**

[

]

**Figure 7-4 Thermal Resistivity for Different Chromia Concentrations**

[

]

**Figure 7-5 Chromia-Doped RODEX4 Model**

[

]

**Figure 7-6 Calculated vs Measured Temperatures in the REMORA2  
Test**

[

]

**Figure 7-7 Calculated and Measured Temperatures vs Linear Power  
in the REMORA2 Test**



[

]

**Figure 7-8 Fission Gas Release Measured vs Calculated for  
Chromia-Doped Database**

[

]

**Figure 7-9 Illustration of Intragranular Porosity Developing in  
Chromia-Doped Fuel**

[

]

**Figure 7-10 Strain and Strain Increment Measured vs Calculated for  
Chromia-Doped Database**

## **8.0 QUALIFICATION OF AURORA-B TO CHROMIA-DOPED FUEL**

AURORA-B, a comprehensive evaluation model including the use of both RODEX4 and S-RELAP5 codes, was developed by AREVA for predicting the dynamic response of BWR fuel during transient, postulated accident, and beyond design-basis accident scenarios. RODEX4 provides the realistic evaluation of local thermal-mechanical behavior of fuel rods during such events and S-RELAP5 provides the transient thermal-hydraulic response. The RODEX4 thermal conductivity models for chromia-doped  $\text{UO}_2$  and  $\text{UO}_2\text{-Gd}_2\text{O}_3$  are incorporated directly into S-RELAP5 and evaluated for steady state agreement with RODEX4. As summarized in Section 7.1, the thermal conductivity model is evaluated as a function of local temperature, fuel porosity, local burnup, gadolinium fraction and plutonium fraction.

The AURORA-B evaluation model is documented in three separate topical reports: anticipated operational occurrences (AOO) (Reference 25), loss-of-coolant accidents (LOCA) (Reference 26), and control rod drop accidents (CRDA) (Reference 27).

Section 9.2 summarizes the AURORA-B sample problems which demonstrate the three AURORA-B methodologies.

## 9.0 LICENSING CRITERIA ASSESSMENT

Sections 7.0 and 8.0 described the adaptation and qualification of the RODEX4 and S-RELAP5 codes for application to chromia-doped fuel. Both codes have an input parameter to identify the fuel type which will turn on the chromia-doped models when selected.

There is no fundamental change needed for the thermal-mechanical realistic methodology for RODEX4 (Reference 20), or for the three AURORA-B BWR methodologies associated with S-RELAP5 (References 25, 26, and 27). There is also no change to any of the design or licensing criteria.

The following sub-sections illustrate examples of design analyses performed with the chromia-doped fuel option activated in the RODEX4 and S-RELAP5 codes. The results of those analyses are compared to standard fuel analyses to evaluate the impacts of the dopant. There is no generic design analysis to present as the methodologies are applied for each reload and cycle of operation in the power reactor.

### 9.1 *Steady-state and AOO Analyses (Thermal-Mechanical Evaluation)*

The example thermal-mechanical analysis presented in this report is a repeat of a recent ATRIUM™ 10XM reload calculation performed with the RODEX4 fuel code, but in which the chromia-doped model options were activated by specifying the corresponding input parameters in the RODEX4 input file. In addition, since manufacturing statistics from full batch supply of chromia-doped fuel are not available at this time, the following fuel parameters that are needed to represent the chromia-doped fuel specific behavior were included in the modified input files based on the pre-industrialization manufacturing runs:

[

]

The uncertainty ranges of the gas atom diffusion coefficient and thermal conductivity are the same as for standard UO<sub>2</sub>. The consistent prediction (same scatter band) of the

chromia-doped and standard  $\text{UO}_2$  FGR allows use of the same uncertainty for both fuel types. With regards to the thermal conductivity, the bounding character of the model adaptation for chromia-doped fuel compensates for the reduced dataset.

Besides the model adaptations and changes necessary to represent chromia-doped fuel behavior, the lower melting temperature of chromia-doped fuel is taken into account. As described in Section 5.2 a bounding correction for the chromia-doped fuel was developed as follows:

[ ]

The sample case selected for illustration herein is from the cycle-specific analyses for reactor A23 Cycle 22. The fuel loading for this cycle is comprised entirely of ATRIUM™ 10XM fuel assemblies; thus, there are three batches of fuel assemblies, the first of which were loaded in Cycle 20 and the other two in subsequent 21<sup>st</sup> and 22<sup>nd</sup> cycles. As such, the fuel assemblies in this core approximately span the full range of possible exposure for such fuel.

The results of the sample case are presented in Table 9-1 as the difference between the results for the chromia-doped fuel and the results for standard fuel. A discussion of the difference between the results for the chromia-doped fuel and the results for standard fuel is presented in the following.

[

[

]

Therefore, the main conclusions of the comparison of the results for the two fuel types show that chromia-doped fuel thermal-mechanical calculations will typically have the following characteristics:

[

]

[

]

The second part of the thermal-mechanical licensing analysis is the calculation of fast AOO setback factors. This involves the setting of power-dependent LHGR reduction factors (LHGRFACp) for the peak pellet power versus peak pellet exposure-dependent Fuel Design Limit (FDL) as needed to ensure the AOO licensing criteria are met. The criteria addressed in this section are presented in Section 3.1.2 of the RODEX4 methodology (Reference 20):



- The clad tangential uniform transient strain, elastic plus inelastic, shall not exceed 1%.
- Pellet temperatures during anticipated transients shall be maintained below melting.

For AOOs evaluated with the RODEX4 thermal transient solution, the most limiting rod at the FDL or setback fraction of the FDL must not exceed the transient design criteria with 95% probability and 95% confidence.

The fast AOO sample analysis is based on the same ATRIUM™ 10XM fuel case as used in the steady-state sample analysis. Like in the steady-state analysis, the reload calculations were repeated with the chromia-doped option activated in RODEX4. The analysis included comparisons of results between standard  $\text{UO}_2$  and chromia-doped  $\text{UO}_2$  fuel rods and also between standard gadolinia and chromia-doped gadolinia fuel rods. It is recalled that chromia doping has no impact on the thermal conductivity of gadolinia fuel (Section 4.5), and also that the resintering of the chromia-doped and standard gadolinia fuels are similar. The comparison of the chromia-doped and standard gadolinia results is most relevant because the gadolinia fuel is limiting for fast AOO analysis.

The results of the fast AOO setback sample cases are presented in Table 9-2 for  $\text{UO}_2$  fuel and in Table 9-3 for gadolinia fuel. The results illustrate the following impact of chromia-doped fuel rods on the fast AOO setback analysis:

[

]

[

]

## 9.2 Safety Analyses

This section will summarize sample problems performed for three distinct domains: AOO, LOCA, and CRDA. The AOO transient analyses performed with AURORA-B evaluation model is distinct from the AOO transient analysis performed with the stand-alone RODEX4 code (Section 9.1) and is primarily intended to evaluate thermal-hydraulic effects rather than fuel rod mechanical response. Unlike the steady-state and AOO evaluations described in Section 9.1, the AURORA-B methodologies have not yet been licensed. Representative sample problems similar to those presented in the AURORA-B topical reports (References 25, 26, and 27) were performed to illustrate the impacts of chromia-doped fuel on safety analyses.

Two principal effects associated with chromia-doping of fuel pellets result in small impacts to BWR transients and accidents:

- Chromia-doping increases fuel gaseous swelling thereby reducing gap width, which results in increasing gap conductance, increasing overall fuel rod heat transfer to the coolant and decreasing steady state fuel temperature and initial fuel stored energy.
- Chromia-doping decreases fuel thermal conductivity, especially in the low temperature range, thereby reducing the transfer of heat from the interior of the fuel pellet to the pellet surface, which results in reducing overall fuel rod heat transfer to the coolant and increasing steady state fuel temperature and initial fuel stored energy.

These are competing effects in terms of heat transfer to the coolant and initial stored energy which contributes to the magnitude of impacts on transients and accidents. The discussion in Section 7.1 describes both bounding and best-estimate thermal-conductivity correlations in RODEX4.

The application of the best-estimate (upper-bound) correlation is utilized in the AOO methodology to ensure conservatism by increasing the heat transfer to the fluid which would bring the fuel rod closer to boiling transition. Use of the lower bounding curve is conservative in the LOCA and CRDA domains as it increases the steady state fuel temperature and initial fuel stored energy.

Included in the evaluation of chromia-doped fuel were two transients at the end of cycle; a feedwater controller failure (FWCF) and a turbine trip no bypass (TTNB) to evaluate the impacts of  $\Delta\text{CPR}$ , as well as an anticipated transient without scram (ATWS) event to evaluate the impact on peak pressure. The evaluation of LOCA impacts included both small and large break comparisons. The final sample problem includes an evaluation of chromia-doped fuel for a CRDA.

In the transient test cases,  $\Delta\text{CPR}$  is reduced by chromia-doping, indicating that the fuel thermal conductivity effect is more influential than pellet swelling in these test cases. Heat is transferred more slowly to the coolant during the transient, resulting in less thinning of the coolant film at the clad surface. The reduced gap width due to chromia-doping plays an insignificant role at the end of cycle because the gap is nearly closed at the start of the transient, and the temperature drop across the gap is only a small fraction of the total fuel centerline-to-clad-surface temperature drop. The effect of chromia-doping on maximum system pressure is seen to be negligible for all three transient test cases. Table 9-4 summarizes the transient evaluation results.

In contrast to the AOO evaluation, the BWR LOCA test cases indicate that the impact of chromia-doping on LOCA PCT is primarily due to its effect on initial stored energy, which is more influential on large breaks than small breaks. The use of chromia-doping decreases fuel pellet thermal conductivity, leading to increased initial stored energy. The small break case shows no significant change in PCT since it occurs later in the

transient when most of the initial stored energy has dissipated. The clad surface heat transfer rate and PCT are essentially determined by decay heat, minimizing the PCT impact of initial stored energy due to chromia-doping.

The large break case shows a larger increase in PCT because the PCT occurs earlier such that a portion of the initial stored energy still remains and contributes in a small way to the clad surface heat transfer rate, resulting in a slightly increased PCT when chromia-doping is used. For these LOCA test cases, the effect of chromia-doping on PCT is similar to the effect that occurs when gadolinium doping is used, also resulting in reduced fuel thermal conductivity and increased initial stored energy. Table 9-4 summarizes the LOCA evaluation results.

This CRDA test case shows the results of a BWR control rod drop accident. The increase in initial stored energy associated with chromia-doping resulted in an insignificant increase in both the peak channel enthalpy rise and the average enthalpy rise for all modeled channels. Table 9-4 summarizes the CRDA evaluation results.

### **9.3      *Impact on Nuclear Design Requirements***

There is no impact on reactor physics calculations because chromium and oxygen cross sections are included in the nuclear data library of the CASMO-4 lattice code. Additions of  $\text{Cr}_2\text{O}_3$  to the fuel will require no changes to existing neutronics codes or methodologies.

The absorption cross section of the chromium additive (3.1 barn) is very small in comparison to that of the fuel. Moreover, the chromium atoms occupy a small fraction of substitutional positions in the  $\text{UO}_2$  lattice, which is therefore practically not disturbed, resulting in the reactivity coefficients of the chromia-doped fuel being unchanged in comparison to standard fuel.

The requirements of both GDC 11 and GDC 26 regarding the reactivity coefficients of the fuel and the capability of the reactivity control system to maintain the reactor subcritical under cold conditions in situations that include equipment malfunctions, will be satisfied by the specific reload analyses that will be performed for chromia-doped

fuel. These calculations will account for the very small decrease in fuel density for the chromia-doped fuel, which has a small impact on control rod worth in cold conditions.

#### **9.4      *Licensing Criteria Conclusion***

The general conclusions of the sample cases presented above are:

- Some reduction of margin for a few criteria, but margins remain adequate:
  - strain increment, centerline temperature
- Some criteria show margin improvement:
  - internal rod pressure,  $\Delta\text{CPR}$

Overall, representative sample cases have been selected and analyzed; the results of the analyses are as expected given the performance of chromia-doped fuel.

**Table 9-1 Chromia-Doped Thermal-Mechanical Analysis Sample  
Case Results**

[

[

]

**Table 9-2 Fast AOO Sample Case Comparing Chromia-Doped  $\text{UO}_2$   
Fuel and Non-Doped  $\text{UO}_2$  Fuel Analyses**

[

]



**Table 9-3 Fast AOO Sample Case Comparing Chromia-Doped GAD  
Fuel and Non-Doped GAD Fuel Analyses**

**[**

**Table 9-4 Impact of Chromia-Doping on BWR Sample Test Cases**

**[**

**]**

## 10.0 OPERATING EXPERIENCE

Since 1997, chromia-doped fuel rods and LFA's (Lead Fuel Assemblies) of various AREVA designs have been irradiated in commercial PWR and BWR reactors. No problems have been reported from the plants which are related to the doped fuel. Today, the experimental database covers chromia-doped  $\text{UO}_2$  fuel pellets enriched up to 4.95%  $\text{U}^{235}$  [ ]

1.

### 10.1 *Steady State Irradiation*

Chromia-doped fuel has been irradiated in PWR and BWR power reactors since 1997, as follows:

- A total of [ ] irradiation campaigns have hosted or are hosting chromia-doped fuel rods and LFAs equipped with chromia-doped pellets. Behavior has been as expected with a maximum rod burnup of approximately [ ].
- An LFA program in a U.S. BWR is nearing completion. The fuel will reach end-of-life exposures and be discharged after six years of operation in 2017.

The main characteristics of the irradiation campaigns outlined above are summarized in Table 10-1.

### 10.2 *Ramp Testing and Demonstrated PCI Benefit of Chromia-doped Fuel*

The PCI performance of the chromia-doped  $\text{UO}_2$  fuel was determined through dedicated and comprehensive power ramp test programs for both PWR and BWR applications (summarized in Section 6.2), which allowed the assessment of PCI performance gains relative to standard  $\text{UO}_2$ . In both PWR and BWR cases, the fuel and ramp test

parameters were selected such that the potential of failure risk is maximized with respect to the PCI mechanism involved.

To provide the most limiting conditions for the ramp tests, most of the power-ramped fuel rods were base-irradiated to an exposure in the [ ], which is the most critical for PCI failures. At higher exposures, the fuel has been shown to be less sensitive to the PCI type of failure mechanism. However hydrogen induced failure is a potential additional concern for very high exposure fuel. Therefore, in order to obtain a comprehensive assessment of chromia-doped  $\text{UO}_2$  fuel, the power ramp program also included very high burn-up fuel.

Studies were done to analyze the power ramp databases with doped and standard fuels in order to derive relevant PCI failure thresholds. Historically, thresholds were derived from power ramp data presented as ramp terminal level versus burn-up. However, this formulation does not capture the initial power effect which reflects the degree of fuel rod deconditioning that can occur in operation. No clear segregation between failed and non-failed rods is observed with this formulation (Reference 28).

In another approach, the power increment ( $\Delta P$ ) was shown (Reference 29) to be a determining parameter to derive a best-estimate failure threshold from the power ramp database, which is inversely proportional to initial power ( $P_i$ ). This  $\Delta P - P_i$  threshold has a burn-up dependency, which saturates in the mid-burnup range and can be conservatively applied for lower burn-up values. The  $\Delta P - P_i$  criterion was demonstrated on the historical power ramp database (Reference 29) and also on recent power ramp programs that use modern fuel. According to this  $\Delta P - P_i$  correlation, the chromia-doped fuel BWR ramp results are presented in Figure 10-1 together with the old non-liner standard fuel failure PCI threshold and the more recent liner rods. In the same figure, PWR data with chromia-doped fuel are included showing a consistent behavior with the BWR data. The fuel rod design and base irradiation conditions mainly affect the susceptibility of the test rod to fail by PCI. Assuming equivalent degree of conditioning of the tested BWR and PWR chromia-doped fuel rods, the failure threshold

and PCI resistance is mainly affected by ramp parameters controlling the cladding stress in the ramp.

The main conclusions that can be derived from the comparison of chromia-doped fuel with standard fuel power ramp data are as follows (Reference 30):

- For BWR applications, the chromia-doped PCI failure threshold brings benefits in comparison not only with the historical database, but more importantly with respect to modern liner fuel, especially in the range of medium high initial power levels. In that case, the benefit is a gain in margin of 7 to 10 kW/m (power increment) in comparison to the standard liner or non-liner fuel threshold (Reference 31).
- For PWR applications, the chromia-doped rods show a power increment failure that is 4 kW/m higher than for standard UO<sub>2</sub> M5™ fuel rods (Reference 32).

The chromia-doped fuel PCI failure threshold has been well defined by the PWR and BWR ramp programs. In particular, the degree to which the behavior of this fuel is enhanced with respect to standard UO<sub>2</sub> allows considering the chromia-doped fuel as an alternative to the present liner cladding in terms of PCI protection for BWR applications.

**Table 10-1 Operating Experience with Chromia-doped Fuel**

[

]

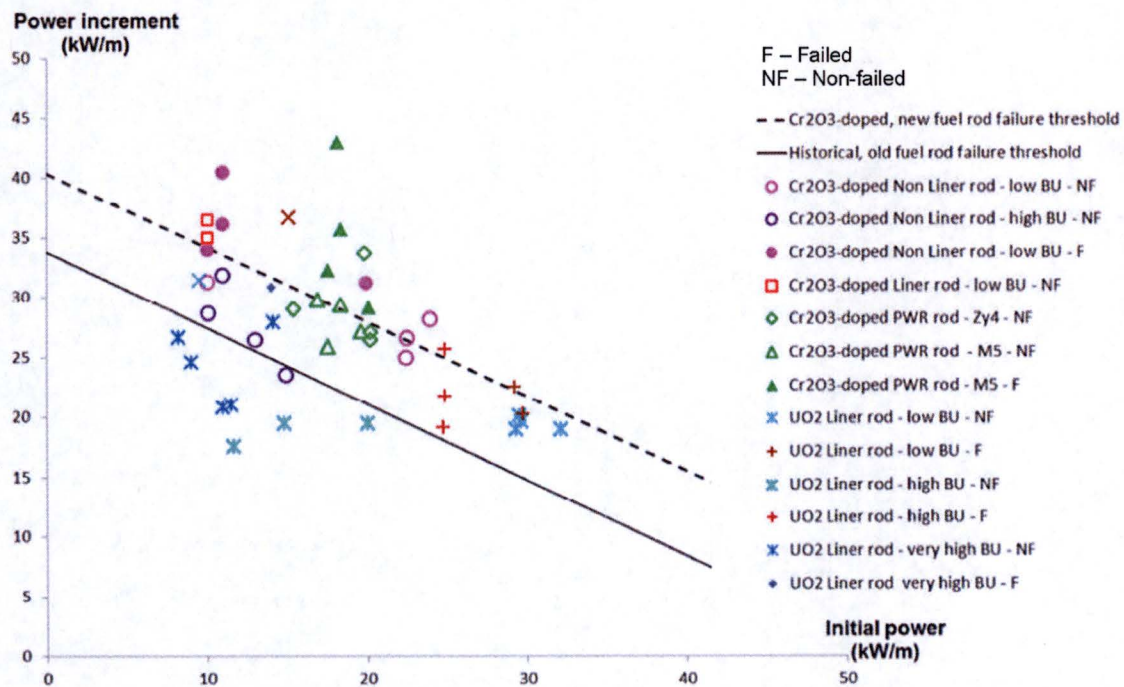


Figure 10-1 Ramp Test Data Showing Increased Fuel Failure Threshold for Chromia-Doped Fuel

## 11.0 REFERENCES

1. Standard Review Plan, NUREG-0800, Chapter 4, U.S. Nuclear Regulatory Commission, March 2007.
2. J. C. Killeen, "Fission gas release and swelling in  $\text{UO}_2$  doped with  $\text{Cr}_2\text{O}_3$ ", Journal of Nuclear Materials, Vol. 88 (1980), pp. 177-184.
3. A. Leenaers, L. de Tollenaere, Ch. Delafoy, S. Van den Berghe, "On the solubility of chromium sesquioxide in uranium dioxide fuel," Journal of Nuclear Materials 317 (2003) 62-68.
4. A.C. Momin et al, "High temperature X-ray diffractometric studies on the lattice thermal expansion behavior of  $\text{UO}_2$ ,  $\text{ThO}_2$  and  $(\text{U}_{0.2}\text{Th}_{0.8})\text{O}_2$  doped with fission product oxides," Journal of Nuclear Materials, Volume 185, (1991), Pages 308-310.
5. J. A. Cape, G. W. Lehman, "Temperature and finite pulse-time effects in the flash method for measuring thermal diffusivity," Journal of Applied Physics, Vol. 34, No. 7, 1963 pp. 1909-1913.
6. E 1461 – 01, "Standard test method for thermal diffusivity by the flash method," Annual Book of ASTM Standards, 2001.
7. C. Ronchi, M. Sheindlin, M. Musella and G.J. Hyland, "Thermal conductivity of uranium dioxide up to 2900 K from simultaneous measurement of the heat capacity and thermal diffusivity," Journal of Applied Physics, vol 85, number 2, 15 January 1999, p. 776.
8. MATPRO NUREG/CR-6150, Vol. 4, Rev. 2, INEL-96/0422  
SCDAP/RELAP5/MOD 3.3 Code Manual, MATPRO – A library of Material Properties for Light-Water-Reactor Accident Analysis.
9. D.G. Martin, "The elastic constants of polycrystalline  $\text{UO}_2$  and  $(\text{U,Pu})\text{O}_2$  mixed oxides – A Review," High Temperatures - High Pressures, Volume 21, 1989.
10. A. G. Evans and R.W. Davidge, "The strength and fracture of stoichiometric polycrystalline  $\text{UO}_2$ ," Journal of Nuclear Material, Volume 33, (1969), pp 249-260.



11. M. Oguma, "Microstructure effects on fracture strength of  $\text{UO}_2$  fuel pellets," Journal of Nuclear Science and Technology, Volume 19, Number 12, (1982) pp 1005-1014.
12. F. Lemoine, D. Baron and P. Blanpain, "Key parameters for the High Burnup Structure formation thresholds in oxide fuels," Proceedings of 2010 LWR Fuel Performance/TopFuel/WRFPM Orlando, Florida, September 26-29, (2010), Paper 062.
13. K. Nogita et al, "Effect of grain size on recrystallization in high burnup fuel pellets," Journal of Nuclear Materials, Vol. 248 (1997), pp. 196-203.
14. K. Une and S. Kashibe, "Corrosion behavior of irradiated oxide fuel pellets in high temperature water," Journal of Nuclear Materials, Vol. 232 Issues 2-3 (1996), pp. 240-247.
15. D. Manara et al, "Thermophysical measurements for AREVA Gd and Cr doped  $\text{UO}_2$ ," Report JRC96692, JRC-ITU, 2015.
16. D. Manara, M. Sheindlin, W. Heinz, and C. Ronchi, "New techniques for high-temperature melting measurements in volatile refractory materials via laser surface heating," Rev. Sci. Instrum., 79 (2008) p. 113901.
17. R. Böhler, M.J. Welland, D. Prieur, P. Cakir, T. Vitova, et al., "Recent advances in the study of the  $\text{UO}_2$ - $\text{PuO}_2$  phase diagram at high temperatures," J. Nucl. Mater. 448 (2014) pp 330-339.
18. A. Puranen et al. "Burnup effects on fine fuel fragmentation in simulated LOCA testing," Proceedings of the LWR Fuel Performance Meeting TopFuel 2013, Charlotte, NC, September 15-19, (2013).
19. F. Lemoine, "High burnup fuel behavior related to fission gas effects under reactivity-initiated accident (RIA) conditions," Journal of Nuclear Materials, Volume 248, (1997), Pages 238-248.
20. BAW-10247-PA Revision 0, "Realistic Thermal-Mechanical Fuel Rod Methodology for Boiling Water Reactors," AREVA NP, February 2008.

21. "Thermophysical properties database of materials for light water reactors and heavy water reactors," IAEA-TECDOC-1496, IAEA, June 2006.
22. J. K. Fink and M. C. Petri, "Thermophysical properties of Uranium Dioxide," ANL/RE-97/2, February 1997.
23. R. J. White, "The Growth of intra-granular bubbles in post-irradiation annealed  $\text{UO}_2$  Fuel," in "Nuclear fuel behavior modelling at high burnup and its experimental support" Proceedings of a Technical Committee meeting held in Windermere, United Kingdom, 19-23 June 2000.
24. R. J. White, "Fission Gas Release," HWR-632, Halden 2000.
25. ANP-10300P Revision 0, "AURORA-B: An Evaluation Model for Boiling Water Reactors; Application to Transient and Accident Scenarios," AREVA NP, December 2009.
26. ANP-10332P Revision 0, "AURORA-B: An Evaluation Model for Boiling Water Reactors; Application to Loss of Coolant Accident Scenarios," AREVA, February 2014.
27. ANP-10333P Revision 0, "AURORA-B: An Evaluation Model for Boiling Water Reactors; Application to Control Rod Drop Accident (CRDA)," AREVA, March 2014.
28. M. Billaux, "Modeling pellet-cladding mechanical interaction and application to BWR maneuvering," Proceedings of the 2004 International Meeting on LWR Fuel Performance. Orlando, Florida, September 19-22, 2004.
29. B. Cox. Pellet-clad interaction (PCI) failures of zirconium alloy fuel cladding – A review. Journal of Nuclear Materials Vol. 172, Issue 3 (1990), pp. 249 – 292.
30. C. Delafoy, V.I. Arimescu, R.M. Hengstler-Eger, H. Landskron, A. Moeckel, "AREVA  $\text{Cr}_2\text{O}_3$ -doped Fuel: Increase in Operational Flexibility and Licensing Margins," Topfuel, Zurich, September 13-17, 2015.

31. P. B. Hoffmann, P. Dewes. Post-irradiation examination and ramp testing of fuel rods with Fe-enhanced Zr liner cladding at high burnup. Proceedings of the 2004 International Meeting on LWR Fuel Performance. Orlando, Florida, September 19-22, 2004.
32. N. Teboul et al. AREVA optimized fuel rods for LWRs. Proceedings of the 2012 TopFuel Reactor Fuel Performance meeting, Manchester, United Kingdom, September 2-6, 2012.
33. C. Delafoy, P. Dewes, T. Miles, "AREVA NP Cr<sub>2</sub>O<sub>3</sub>-Doped Fuel Development for BWRs," Topfuel, San Francisco, September 30-October 3, 2007.

**The following pages changed relative to ANP-10340NP Revision 0:**

<b>Page Number</b>
13
14
16
49
92

**The original pages follow.**

on various microstructure types to identify how much  $\text{Cr}_2\text{O}_3$  is needed to achieve the enhanced viscoplastic behavior for chromia-doped fuel.

The  $\text{Cr}_2\text{O}_3$ -doped  $\text{UO}_2$  fuel grain morphology characteristics are specified to achieve the greatest improvement in enhanced fuel viscoplasticity. To that end, the optimum  $\text{Cr}_2\text{O}_3$  concentration of [ ] was identified, which leads to an average grain size of [ ] as shown in Figure 4-1, and significantly improves the fuel viscoplastic properties.

For the chosen chromia concentration, [ ]

].

#### 4.2 Theoretical Density

[ ]

]

The theoretical density of the oxide at 20 °C is equal to the average mass of four molecules composing the elementary cell that is divided by the volume of the elementary cell:

$$\rho_{th} = \frac{4M_{ox}}{N_{av}a_{ox}^3} \quad (4-1)$$

where:

$N_{av}$  Avogadro's number

$a_{ox}$  oxide lattice parameter

$M_{ox}$  oxide molecular mass

The average molecular weight of the doped oxide is by definition:

$$M_{ox\ doped} = (1 - E_{m\ Cr_2O_3})M_{UO_2} + E_{m\ Cr_2O_3}M_{Cr_2O_3} \quad (4-2)$$

Finally, the mole fraction of chromia in the oxide, which is needed in Equation 4-2, is given by the following:

$$E_{m\ Cr_2O_3} = \frac{\frac{E_w\ Cr_2O_3}{M_{Cr_2O_3}}}{\frac{E_w\ Cr_2O_3}{M_{Cr_2O_3}} + \frac{(1 - E_w\ Cr_2O_3)}{M_{UO_2}}} \quad (4-3)$$

where:

$E_w\ Cr_2O_3$  weight fraction of  $Cr_2O_3$  in the oxide

$M_{Cr_2O_3}$  molecular mass of  $Cr_2O_3$

$M_{UO_2}$  molecular mass of  $UO_2$

Therefore, the density of the chromia-doped  $UO_2$  follows from Equation 4-1 by dividing the formulas for doped and standard fuels:

$$\rho_{th\ doped} = \frac{M_{ox\ doped}}{M_{ox}} \quad (4-4)$$

In formulating Equation 4-4, the experimental finding that the lattice parameter suffers only a minor, negligible decrease was used (Reference 3). Therefore, the parameter  $a_{ox\ doped}$  is assumed equal to  $a_{ox}$ .



The specific heat of unirradiated  $\text{UO}_2$  and  $\text{Cr}_2\text{O}_3$ -doped  $\text{UO}_2$  fuel pellets was measured by differential scanning calorimetry at the Materials Research Unit of JRC-ITU using a cover gas of high-purity argon and a heating rate of 25 K/min (Reference 15). The relative uncertainty on the specific heat determined by this technique is estimated to be 7% (Reference 15). The JRC-ITU measured values for the specific heat of standard and chromia-doped  $\text{UO}_2$  fuel types is displayed in Figure 4-2, in which the high-temperature measurements from previous studies at JRC-ITU (Reference 7) are also shown.

A negligible effect of the chromia additive on the specific heat of  $\text{UO}_2$  is observed in Figure 4-2 for the low to medium (about 1500 K) temperature range. The slightly higher specific heat of chromia-doped fuel is in agreement with the law of mixtures and it is appropriate to ignore the negligible increase in specific heat due to chromia additive. The negligible effect of the chromia additive at high temperatures, where data are not available, is justified based on theoretical arguments, which apply over the full temperature domain. The same negligible effect of the chromia additive was also determined for chromia-doped gadolinia fuel.

It is shown in Reference 8 that in the low to medium temperature range the specific heat is well represented by the Debye and Einstein models, which describe the contribution of harmonic and anharmonic lattice vibrations; while at high temperatures (above 1500 K) the rapid increase in specific heat is attributed to point defect formation, especially Frenkel defects (pairs of uranium cation vacancies and interstitials). The chromium additive occupies mostly interstitial positions and has little impact on the uranium cation sub-lattice (although it can affect the oxygen sub-lattice) and thus it does not affect the formation of Frenkel defects at high temperatures. Consequently, the chromium additive has a negligible impact on the Chromia-doped  $\text{UO}_2$  specific heat in the high temperature range.

It is concluded that the addition of a small quantity of chromia dopant has a negligible effect on the specific heat of the urania matrix, [ ]. Therefore, chromia-doped fuel will be described with the same specific heat formulation as standard  $\text{UO}_2$ . Since specific heat and enthalpy are fully correlated variables (the



RIA is a fast rise of fuel power and temperature. The power excursion may lead to failure of the nuclear fuel rods and release of radioactive material in the primary reactor coolant.

Pulse irradiation tests show that fuel rod susceptibility to failure increases with increasing fuel burnup. It is also clear that the burnup dependent state of the rod and, in particular, the degree of waterside corrosion and related hydride induced embrittlement is very important for the survivability of fuel rods. Regarding fuel pellets, the factors of particular importance to the behavior include: heat-up rates, melting, fragmentation, fission gas induced transient swelling and transient fission gas release.

Under the initial phase of a RIA, the fuel pellet is heated almost adiabatically, i.e. without heat transfer taking place either inside the fuel pellets or across the pellet-clad gap. Due to the surface-peaked temperature distribution in combination with the burnup-induced depression of fuel melting temperature at the pellet periphery, peak temperature under rapid RIAs will first occur at a radial position of about 0.2 to 0.5 mm beneath the pellet surface. To extend the discussion on fuel temperature and the potential risk for fuel melting with a change from  $\text{UO}_2$  to chromia-doped fuel it is necessary to consider that:

[

]

All these elements indicate that the radial average fuel enthalpy threshold for incipient melting of chromia-doped fuel is not significantly different from the  $\text{UO}_2$  fuel enthalpy threshold.



transient when most of the initial stored energy has dissipated. The clad surface heat transfer rate and PCT are essentially determined by decay heat, minimizing the PCT impact of initial stored energy due to chromia-doping.

The large break case shows a larger increase in PCT because the PCT occurs earlier such that a portion of the initial stored energy still remains and contributes in a small way to the clad surface heat transfer rate, resulting in a slightly increased PCT when chromia-doping is used. For these LOCA test cases, the effect of chromia-doping on PCT is similar to the effect that occurs when gadolinium doping is used, also resulting in reduced fuel thermal conductivity and increased initial stored energy. Table 9-4 summarizes the LOCA evaluation results.

This CRDA test case shows the results of a BWR control rod drop accident. The increase in initial stored energy associated with chromia-doping resulted in an insignificant increase in both the peak channel enthalpy rise and the average enthalpy rise for all modeled channels. Table 9-4 summarizes the CRDA evaluation results.

### **9.3      *Impact on Nuclear Design Requirements***

There is no impact on reactor physics calculations because chromium and oxygen cross sections are included in the nuclear data library of the CASMO-4 lattice code. Additions of  $\text{Cr}_2\text{O}_3$  to the fuel will require no changes to existing neutronics codes or methodologies.

The absorption cross section of the chromium additive (3.1 barn) is very small in comparison to that of the fuel. Moreover, the chromium atoms occupy mostly interstitial position in the  $\text{UO}_2$  lattice, which is therefore practically not disturbed, resulting in the reactivity coefficients of the chromia-doped fuel being unchanged in comparison to standard fuel.

The requirements of both GDC 11 and GDC 26 regarding the reactivity coefficients of the fuel and the capability of the reactivity control system to maintain the reactor subcritical under cold conditions in situations that include equipment malfunctions, will be satisfied by the specific reload analyses that will be performed for chromia-doped